TECHNISCHE UNIVERSITÄT MÜNCHEN

Lehrstuhl für Siedlungswasserwirtschaft

MECHANICS AND SUBSTRATE TRANSPORT OF MOVING BIOFILM STRUCTURES

Danial Taherzadeh

Vollständiger Abdruck der von der Fakultät für Bauingenieur- und Vermessungswesen der Technischen Universität München zur Erlangung des akademischen Grades eines

Doktor-Ingenieurs

genehmigten Dissertation.

Vorsitzender: Univ.-Prof. Dr.-Ing. Peter Rutschmann

Prüfer der Dissertation:

1. Univ.-Prof. Dr. rer. nat. Harald Horn
2. Asst. Prof. Dr. ir. Cristian Picioreanu, Delft University of Technology/Niederlande
3. Univ.-Prof. Dr.-Ing. Wolfgang A. Wall

Die Dissertation wurde am 04.10.2011 bei der Technischen Universität München eingereicht und durch die Fakultät für Bauingenieur- und Vermessungswesen am 06.11.2011 angenommen.

Abstract

If there is a beauty of nature more fascinating than the vast variety of her species, it is the immense ability of them to adapt to the least likely livable environments. In this work, we look at the ways biofilms adapt to the harsh conditions of living in fast water flows by numerically studying the biophysical consequences of their special form and possible related function. As a special case, we look at the biofilm streamers, which are clusters of microbial aggregates connected to a tail elongated from the cluster in the direction of the flow. Streamers have a seemingly similar shape to streamlined bodies, a configuration intended to reduce the fluid drag force. Experimentally it is also observed that the streamers oscillate (flap) in the flow, which suggests that the form may provide higher mixing around the biofilm structure. The question that naturally arises is whether the streamer form is an adaptation mechanism providing a function or a passive formation? Obviously, every familiar form or behavior of an organism, e.g., the streamlined form of sperms, does not enforce an adaptation mechanism in that particular organism, e.g., drag reduction. Therefore, we take these hints and numerically construct a model of a single biofilm streamer to weigh the contribution of the fluid-induced oscillations and the special form on its physical and biological performance.

In the context of this work, a state-of-the-art two-dimensional fluid-structure interaction model of biofilm streamers, coupled with mass transfer of a dissolved substrate is developed. This model numerically calculates the transient deformation of the streamer with simultaneous substrate transport and uptake

using moving mesh finite element method.

We show that the streamlined form of the biofilm streamers reduces the fluid forces acting on the structure significantly. In addition, the periodic deformation (oscillation) of the flexible body increases the substrate transport into the biofilm compared to the static (immobile) case. Overall, we propose that the special morphology of the streamers, regardless of the formation process, is a successful strategy in reducing the fluid forces biofilms experience, and increases their overall biological fitness by providing relatively higher substrate transport especially in the tail section.

Kurzfassung

Wenn es etwas faszinierenderes, als die verschwenderische Vielfalt an Arten in unserer Natur gibt, so ist es die Fähigkeit der unterschiedlichen Spezies, sich an nahezu lebensfeindliche Umgebungen anzupassen. In dieser Arbeit betrachten wir, wie sich Biofilme, Aggregate von mikrobiologischen Lebewesen, eingebettet in einem, von ihnen produzierten Polymer, an die rauen Bedingungen in schnell strömendem Wasser anpassen. Dies geschieht durch mathematischen Modellierung in einem Reverse Engineering Prozess, der Ihre Form in Funktionsmodelle überführt. Insbesondere betrachten wir einen einen speziellen Fall, die sogenannten Biofilm-Streamer. Streamer sind Aggregate von Mikroorganismen, die sich zu einer fadenartigen Struktur verbinden, die sich ausgehend von der Mikrofilmstrukur in Richtung der Strömung ausbilden. Streamer bilden stromlinienförmige Körper, um den Widerstand in der vorbei strömenden Flüssigkeit so gering wie möglich zu halten. Experimente zeigen auch, dass Streamer in der Strömung oszillieren. Dies stützt die Vermutung, dass diese Struktur zu einer stärkeren Vermischung, der den Biofilm umgebenden Flüssigkeit führt. Die Frage, die sich daraus unmittelbar ergibt, ist ob die Ausbildung von Streamern ein aktiver Adaptionsmechanismus mit einer spezifischen Funktion ist oder nur eine passive Struktur ohne spezifischen Nutzen für den Biofilm. Es ist offensichtlich, dass nicht jede stromlinienförmige Struktur der Reduzierung des Strömungswiderstandes dient, ein bekanntes Beispiel dafür sind Spermien. Wir haben dies zum Anlass genommen, die Simulation eines Biofilm -Streamers, seiner Oszillation und seiner Form, auf ihren Beitrag

zur physischen und biologischen Performance hin zu untersuchen. Im Kontext dieser Arbeit wurde, ein “state-of-the-art” zweidimensionales Modell der Interaktion der Strömungsstruktur mit Biofilm-Streamern, sowie des zugehörigen Massentranfers entwickelt. Zur Berechnung des Zusammenhanges zwischen der Deformation des Streamers, dem Massentransport und der Stoffaufnahme, wurde die Finite-Element-Methode auf einem dynamischen Gitter verwendet.

Wir konnten zeigen, dass die Stromlinienform der Biofilm-Streamer die Strömungskräfte auf die gesamten Struktur signifikant reduzierten. Zusätzlich erhöhte die Deformation (Rekonfiguration) des flexiblen Körpers den Stofftransport in den Biofilm, verglichen mit einem statischen unbeweglichen Modell. Insgesamt lässt sich sagen, das dis spezielle Morphologie der Streamer, unabhängig von ihrem Entstehungsprozess, die Kräfte denen der Biofilm ausgesetzt ist reduzieren und ihre biologische Fitness durch höheren Stofftransport verbessern. Dies gilt insbesondere für den Bereich des Streamers selbst.

Contents

List of Figures

Acknowledgement

This thesis would never have been possible without the support, friendship, dedication and assistance of numerous people. First and foremost I wish to thank my advisor, Harald Horn. He has been supportive since the first day I met him, despite forgetting my the M.Sc. topic at the interview. With his broad knowledge on biofilms, specifically the real world biofilms compared to my modeled ones, he introduced me to the fundamental questions in the biofilm area, improved/polished my ideas and did more than I would expect to support me realizing them. He never gave up on me even when this work seemed impossible to achieve, and encouraged me to keep going. I feel enormously privileged to have him as my advisor.

Visiting the group of Mark van Loosdrecht in Delft University has been a huge milestone in my phd life. There we started working on some initial ideas together with Cristian Picioreanu including streamers, and I could not imagine working on any other topic than the challenge of many-physics life of streamers then. Cristian is an amazing scientist with deep understanding of biofilm modeling, and a great teacher. Each time we would start on a dead-end alley and end up with many open starts. He encouraged me to move on and has been with me on every stage of this work.

Another milestone in my work has been working closely with the group of Wolfgang A Wall at TUM. His group is packed with outstanding people. The discussions with him and his group were the life upgrades after game overs for me. The frequent short visits to Ulrich Küttler have been always very

confusing and yet eye-opening. I needed time to process the shear amount of the new knowledge after.

I am highly privileged to meet brilliant people on my way to here; people that have pieces of their knowledge contributed to this work throughout these years, which I would like to thank gratefully: Mark van Loosdrecht, Tom Battin, Angelo Simone, Thomas Neu and Michael Wagner.

Andrea Hille-Reichel has been a great source of inspiration both for my scientific and day-to-day life. I will always remember her sharp ideas, cold-hearted counter-arguments, emotional support and her trust in me. Several parts of the thesis are greatly improved with her comments. My dear friend Nika Dudkina helped me immensely by revising the language of the thesis. I am also very grateful to Konstantinos Athanasiadis for his recommendation to work on biofilms with Harald. Susanne Wießler and Marianne Lochner, thank you for helping me always so patiently; I know how bad I am at non-scientific tasks.

I would like to thank my friends Aliyar Firat and Edris Taher for being beside me at happy and less happy days. Words cannot describe their place in my life. David Martinez, my friend, the best decision was to hire you as my roommate during these years. Dear Oliver Kehl, you still owe me a beer. Yang Li, Ahmet Labena, Mateo Urena, Riccardo Matruglio, Bastian Herzog, and Eve Walters, you guys are awesome and I hope one day you will also become good in Kicker.

Most importantly, I thank my family, for their endless love and continuous encouragement. My parents, Lotfollah and Shamsi envisioned my life from beginning at where I am now, and supported me with their hard work so I can reach these days; I cannot imagine how difficult it must have been for them. It is impossible to record how grateful I am to them. Niousha and Soulmaz, my beautiful sisters, thank you for always being on my side and showing me what a warm family means. A very special thanks goes to my extended family Franz Baur and Anja Ivanova. Franz, despite being a *mere* mathematician, is a chaotic visionary self-taught scientist. He has a great role in my understanding of evolution and natural selection which inspired several parts of this work. He listened to me, encouraged me, and has been there whenever I needed a

shoulder. Anja, thank you for making our little family a warm cozy place and asking me when my works are published, constantly.

This work is build on the shoulders of many, friends and colleagues, yet one deserves my outmost appreciation. My wife, Maria Baur, has endured the burden of endless working hours and long frustrating periods of my work. She has been with me through every hardship and joyful “almost Dr.” days. I cannot imagine how I could have completed this thesis without her love, trust, and words of encouragement. Thank you, Mash!

Preface

This thesis is based, in part, on the following published and submitted articles:

- **Taherzadeh, D.**, Picioreanu, C., Küttler, U., Simone, A., Wall, W. A., and Horn, H. (2010) Computational study of the drag and oscillatory movement of biofilm streamers in fast flows. Biotechnology and Bioengineering, 105(3), 600-610.

- **Taherzadeh, D.**, Picioreanu, C. and Horn, H. (2011) Mass Transfer Enhancement in Moving Biofilm Structures. Biophysical Journal. (in revision).

Parts of the content and figures are based on the paper written together with my coauthors:

- Wagner, M., **Taherzadeh, D.**, Haisch, C., and Horn, H. (2010) Investigation of the mesoscale structure and volumetric features of biofilms using optical coherence tomography. Biotechnology and Bioengineering, 107(5), 844-853.

In preparation of this work several free and open source tools and resources have been used. I used Eureqa for finding emerging patterns in visually unrelated data points, Paraview for visualization of the drag related simulation results, Veusz for plotting, LyX for writing, Python for data post-processing, Git and GitX for source control, and last but not the least Oomph-lib website for Multiphysics finite element tutorials.

List of Symbols

Roman Symbols

$\hat{p}$	Kinematik pressure
$\overline{k}_m$	Spatially averaged external mass transfer coefficient
$\overline{Sh}$	Spatially average Sherwood number
$\overline{Sh}_0$	Spatially averaged, initial steady-state value of Sherwood number (t=0)
$\overline{Sh}_{tail}$	Spatially averaged Sherwood number evaluated at the tail section only
$\overline{Sh}_t$	Spatially averaged, quasi steady-state value of Sherwood number
$\mathbf{b}^F$	Vector of body forces
$\mathbf{d}$	Structural displacements vector
$\mathbf{d}_\Gamma$	Structural displacement of the interface Γ
$\mathbf{E}$	Green-Lagrangian strain tensor
$\mathbf{F}$	Deformation gradient tensor
$\mathbf{n}$	Outer normal vector to a surface
$\mathbf{S}$	Second Piola-Kirchhoff stress tensor

$\mathbf{u}$	Liquid velocity vector field
$\mathbf{u}_\Gamma$	Fluid velocity at the interface Γ
$\mathbf{X}$	Lagrangian or material system of reference
$\mathbf{x}$	Spatial system of reference
A	Area
A_B	Surface area of the biofilm
A_F	Frontal area of an object facing the flow
A_w	Outer area of the streamer — in 2-d cases equal to the perimeter of the object
c	Substrate concentration
C_D	Drag coefficient
C_L	Lift coefficient
c_0	Inlet substrate concentration
D	Substrate diffusion coefficient in water
E^S	Young's modulus of biofilm
E_{App}	Apparent elastic modulus
f	Vortex shedding frequency, as well as oscillation frequency of the streamer tip
F_L	Lift force
F_D	Drag force
$F_{V,x}$	x-component of the viscous force in the flow direction
FR	Fineness Ratio, defined as maximum length over maximum thickness

G	Speed-specific drag exponent
j	Net local solute flux
K	Half-saturation concentration of substrate
k	Reaction rate constant
k_m	Local external mass transfer coefficient
L	Biofilm streamer tail length defined from the tip to the intersection of the circular base and the tail. See Figure 4.1.
L^*	Biofilm tail length defined from the tip to the center of circular base.
L_x	Computational domain length
L_y	Computational domain height (width)
L_{ch}	Characteristic length
n_x, n_y	Components of the normal vector
p	Physical pressure within the fluid field
P_B	Wetted perimeter of biofilm structure
R	Substrate consumption rate inside biofilm
Re	Reynolds number
Re_D	Reynolds number based on the object diameter
s	Biofilm perimeter arc length
Sh	Sherwood number (local)
St	Strouhal number
t, T	Time
$u_{\infty,x}$, $u_{\infty,y}$	Relative velocities of the fluid in x- and y-directions, respectively.

u_∞ Bulk flow velocity

v Velocity

U_0 Inlet flow velocity

u_x, u_y Fluid velocity components in x- and y-directions, respectively.

Abbreviations

ALE Arbitrary Lagrangian-Eulerian method

AMR Adaptive Mesh Refinement

CA Cellular Automata

CLSM Confocal Laser Scanning Microscopy

CUDA Compute Unified Device Architecture

DOF Degree of freedom

FEM Finite Element Method

GPU Graphics Processing Unit

OCT Optical Coherence Tomography

SEM Scanning Electron Microscopy

SPH Smoothed-Particle Hydrodynamics

XFEM Extended Finite Element Method

Greek Symbols

Γ Biofilm-liquid interface

Γ_{CD} Mass transfer interface boundary

Γ_{FSI} Fluid-structure interaction interface boundary

λ^S Lamé's first parameter

μ^F Fluid dynamic viscosity

μ^S Shear modulus or Lamé's second parameter

ν^F Kinematic viscosity

ν^S Poisson's ratio of biofilm

Ω_F Fluid (sub-) domains

Ω_S Biofilm domain

Ω_H Biofilm head subdomain

ρ^F Liquid (water) density

ρ^S Biofilm density

ε Strain rate tensor

$\boldsymbol{\chi}$ Moving mesh (ALE) reference system

Superscripts

F Fluid

S Solid, here biofilm

Mathematical Symbols

∇ Gradient with respect to the spatial coordinates

1

Introduction

1.1. Motivation

Find a planktonic bacteria wandering in solitary, and you will be easily able to defeat the caused bacterial diseases. Find that same bacteria in biofilm mode of life, and it is much less likely that you can eliminate it. Bacterial biofilms are both dangerous and beneficial to humans. Biofilms are formed wherever there is a slight chance of access to nutrients not minding the harsh living conditions. This might be the way bacteria could have survived throughout millions of years of environmental and biological stresses on earth. What makes biofilms strong is that despite being tiny they are highly heterogenous and dynamic. Also, biofilms can communicate through various methods, eliminate their enemies, build strong shelters, cling to the ground when it is windy, and let go when it is a good time to go. Socially they also cooperate with each other and compete against other communities using communication channels. In contrast to larger organisms, microorganisms are armed with high metabolic flexibility and fast reproduction rates, which enable them to survive and overcome difficult conditions by adapting to almost every condition and environment.

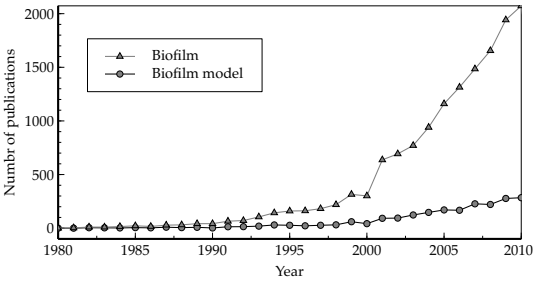

Figure 1.1.: Trends in biofilm research. The figure shows the total number of publications per year for the "biofilm" and "biofilm model" keywords through 1980 to date, demonstrating the rising trend in biofilm research, and biofilm modeling. Source: PubMed

For long biofilms were considered literally as a side issue in microbiology of very limited importance (Flemming (2011); see also Figure 1.1). Over the years, the role of biofilms became more clear and prominent through their significant presence in engineering problems, e.g., biofouling, water distribution systems and life-threatening diseases. Confocal Laser Scanning Microscopy (CLSM), micro-electrodes and genetic reporter systems were the breakthrough tools that further revealed the spatial and physiological heterogeneity of biofilms. For biofilms, the act of survival at the smallest scales seems to require relative complex machinery and size-specific methods to maintain the inner workings.

In multicellular organisms, the formation and development of structures depend on organisms' environmental conditions and genetic control, with various feedback mechanisms connecting two ends. The difficulty arises where, as scientists, we cannot distinguish whether a particular structure develops as a response to the surrounding physical conditions, or has a prescribed genetic agenda, or more likely a combination of both. One should try to grow biofilms in a flow-cell as close as possible to actual natural living conditions, apply several physical factors and measure the response of biofilms to these changing environmental conditions. Not that easy microbiologists say! Biological systems are, thanks to the chaotic and diverse world of natural selection, much more complicated and dynamic compared to purely physical systems. Two

identical systems, e.g., two biofilm experiments with the same initial conditions may show different local heterogeneities but yet demonstrate similar overall macroscopic properties. Apparently, physical world of organisms is not straightforward as well. With respect to this work, a comparable difficulty also arises when dealing with drag of structures in moving fluids and even more severe nonlinearities press when considering the interaction of liquid flow with a flexible structure such as flexible biofilms moving passively in liquid flow.

The lack of applicable experimental methods at very small scales to measure essential properties such as flow fields, material properties and concentration gradients, and the need to understand the basic processes in biofilms encouraged early modeling efforts in engineering field. The models in the last three decades have come from simple homogenous biofilm models to advanced multi-physics multi-dimensional multi-species models, which are able to solve several physical and biological processes of biofilms at the same time and interlinked.

We now know, qualitatively, that biofilms strongly interact with their environments, can form highly complex morphologies and adapt to wide variety of environmental conditions. The term biofilm even now embodies several biofilm structures including planar/patchy biofilms, dune/ripples/mushroom-like morphologies, streamers, filamentous and many more biofilm types uncategorized in between. With the help of advanced experiments and models deeper and more fundamental questions arise: Why do biofilms form such complex morphologies? How are the involved microorganisms benefiting from these forms? Why these particular forms? Do different biofilm types come to the same stable form under the same environmental conditions? Is a particular pattern, structure, community or morphology a converged one? How did it happen? How much is the influence of a morphology on the overall biofilm living cycle? And, how much is their influence on their living environment? What may be other benefits of this particular form? What are the triggers?

The focus of this work is not to answer all of the questions above, but to show how biofilm streamers (Figure 1.2), a particular form of biofilms develop, what biological and physical gains and losses of this form are, and finally quantitatively study the interaction of this particular form and its surrounding aquatic

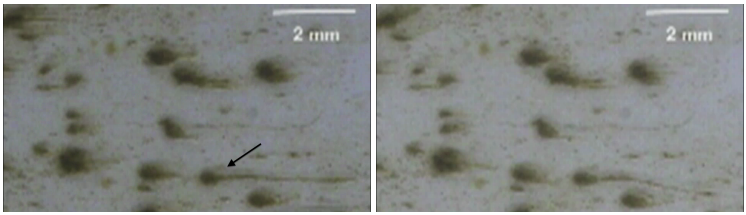

(a) (b)

Figure 1.2.: Diatoma biofilms in river forming streamers. (a) and (b) show two time snapshots of streamer motion in time. Screenshots credits: Iris Hoedl (WasserCluster, Lunz am See, Austria).

environment. At the end, biofilm streamers are only one of the interesting morphologies biofilms may develop, yet the fundamentals and tools presented in this work can be the cornerstone for future analogous studies.

1.2. Scope

In the context of this work we will look at the drag, mass transfer and fluid-structure interaction of oscillating biofilm streamers. Accordingly, the scope of this thesis is divided into three phases. Initially, a two-dimensional finite element model of biofilm-fluid interaction is developed, which tackles several challenges posed by close biofilm-liquid densities and large deformations of the biofilm streamer tail. Next, with the help of this model we try to find out why the streamers move in the first place, and calculate their drag in fast flows to verify whether such particular streamlined form helps to reduce the drag as expected or not. Finally, substrate transport and uptake processes are numerically coupled with the biofilm-fluid interaction model to find out whether the movement of the streamer tail and the resultant complex fluid dynamics enhance the mass transfer processes into the biofilms.

2

Background

In this chapter, we look at what biofilms are, how they grow and shape, and what factors affect their structure and morphology. Since this work focuses on biophysical modeling of biofilms, we also talk about the mechanical properties of biofilms. In addition, the current state of biofilm modeling is also introduced. Lastly, from the mechanical and transport point of view, the physical life of flexible biological structures and the interaction with their surrounding — that is what a biofilm streamer may experience — is briefly presented.

2.1. What are biofilms?

Biofilms are natural structures formed by microbial communities encapsulated inside a matrix of self- secreted extracellular polymeric substances (EPS), growing attached most commonly to a solid surface. Biofilms can be formed by single or many bacterial species (or fungi, algae and protozoa), where patterns of genes expressed differ significantly compared to the bacteria living in the planktonic mode (Sauer et al., 2002). Microbial cells and EPS constitutes the majority of the biofilm structure, where EPS composes more than half of the total organic carbon of biofilms (Flemming et al., 2000a) and is proposed to

directly influence the biofilm structure and cohesive strength (Flemming et al., 2000b; Pamp et al., 2007).

The abundant presence of biofilms has important implications in human life. Biofilms can attach to almost any surface, can grow at very low substrate conditions (e.g., drinking water systems) and are difficult to control and remove due to the protection provided by the EPS matrix. Biofilms are used in a wide variety of applications in e.g., wastewater treatment plants (Nicolella et al., 2000) and removal of pollutants (Singh et al., 2006). In health sector, biofilms cause infectious diseases, settle on implants, and cause water contamination when detached into the water systems (Costerton et al., 1987; Hall-Stoodley et al., 2004).

There are several (known) advantages for bacteria to live in biofilms. When biofilms are formed, a layer of EPS encloses the bacteria – which forms the basis for many physical properties of biofilms. Because of the polymeric nature of EPS matrix, diffusion becomes the dominating mass transfer mechanism. Thus, EPS can protect bacteria from toxins and UV by encapsulating and shadowing the inner parts, which usually would have had direct access to them in planktonic mode. Also, since they are protected in a shell, bacteria are sheltered from the fluid shear and other abrasive forces to some extent, and achieve longer retention times. Additionally, living in close proximity of adjacent neighbors, higher cell density provides them a higher possibility of cooperation and communication (Fux et al., 2005), e.g., through quorum sensing (De Kievit et al., 2001; Hammer and Bassler, 2003) and horizontal gene transfer (Li et al., 2002).

2.2. *Processes in biofilms*

The formation and development of biofilms occurs in a series of discrete and well regulated steps (Figure 2.1). Stages one and two are generally identified by a loose, reversible or transient association with the surface leading to a persistent adhesion. Next, bacterial cells come together to form microcolonies, grow and divide, and go toward maturation phase. Finally, parts of biofilm may detach and leave the structure, e.g., due to shear stress (and reattach else-

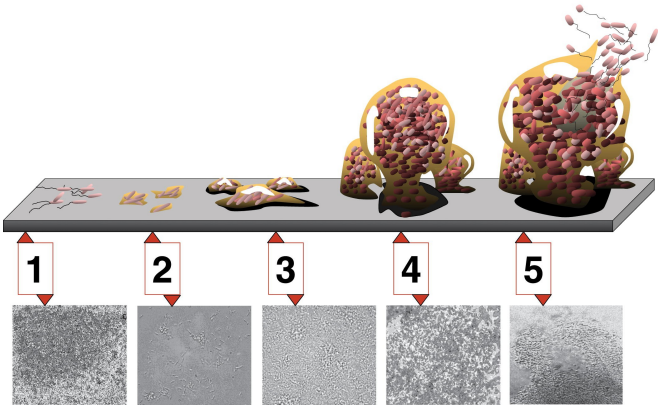

Figure 2.1.: 5 stages of biofilm development. Stage 1, initial attachment; stage 2, irreversible attachment; stage 3 and 4, maturation; stage 5, detachment and dispersion. Below, photomicrographs of a developing Pseudomonas aeruginosa biofilm related to each stage above (image credit: D. Davis).

where). It has been shown that the path that biofilms take toward maturation has significant impact on their quasi steady-state maturation characteristics including, but not limited to, the growth hydrodynamic condition, nutrient supply, and substrate transport limitations (Characklis, 1981; Horn et al., 2003; Klapper and Dockery, 2010).

Many processes in biofilms happen simultaneously, internally and externally, yet they happen at time scales with orders of magnitude difference between, schematically represented in Figure 2.2. Substrate is transported within bulk phase mainly by convection (advection), and through chains of diffusive transport processes reaches the biofilm structure. It has been reported that there is also a convective transport process inside the channels throughout the biofilm matrix (de Beer et al., 1994), however the contribution to the internal mass transfer is predicted to be not significant (see Picioreanu et al., 2000b).

Substrate is further used in bacterial growth and cell division processes, and finally part of the biomass can be eroded, detached, or migrate into the bulk fluid going out of the system or reattaching elsewhere.

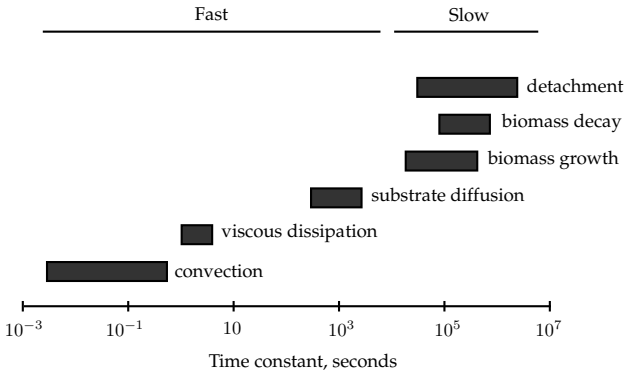

Figure 2.2.: Characteristic times for some processes occurring in biofilms. Reproduced from (Picioreanu et al., 1999).

2.3. *Factors influencing the structure and heterogeneity of biofilms*

Several biological and physicochemical factors influence the morphology and composition of the biofilms. There is a great body of research on the effects of nutrient availability (Xu et al., 1998; Horn et al., 2001; Stoodley et al., 2001) and hydrodynamics (van Loosdrecht et al., 1995; Stoodley et al., 1998, 1999d, 2002; Wäsche et al., 2002; Singer et al., 2010) on biofilms. Additionally, cell motility (O'Toole and Kolter, 1998; O'Toole et al., 2000; Klausen et al., 2003; Wood et al., 2006), quorum sensing (De Kievit et al., 2001; Hammer and Bassler, 2003; McLean et al., 2005), growth rate (Bakke et al., 1984), and community succession and growth history (Besemer et al., 2007, 2009) are also few other important factors that affect the heterogeneity and formation of biofilms. In this work, the first two factors, namely, hydrodynamics and nutrient availability will be the focus, and other factors will be neglected.

Spatial structure of biofilms

In contrast to the initial idea that biofilms were simply clumps of bacteria randomly stuck at surfaces, new research shows that biofilm systems are actually

dynamic and have their own agenda (Costerton et al., 1987; see Flemming, 2011 for a short history). The use, advancement, and combination of high-resolution three-dimensional imaging techniques, specific molecular fluorescent stains and genetic reporter systems have shown that biofilms are spatially and physiologically heterogenous (non-homogenous) structures (Hall-Stoodley et al., 2004). Figure 2.3 shows the biofilm internal structure at various spatial scales observed by respective widely recognized investigation methods.

Heterogeneity in biofilms may refer to the 3-dimensional (3-d) spatial structural and architectural dissimilarity and non-uniformity, and also may refer to the composition of the biocoenosis. Heterogeneity, of course, should be defined taking into account the relative scale; *microscale*: 10 to $<$100 µm, *mesoscale*: in the range of millimeters, and *macroscale*: in the dimension of river or reactor size (Figure 2.3). Generally, heterogeneity of the surrounding environments, that is the presence of strong substrate gradients, exposure to varying fluid forces, and transport limitations inside biofilms are some of the main drivers of heterogeneity in biofilms. In the following sections we take a look at the influence of some of these factors affecting the heterogeneity of biofilms.

Role of hydrodynamics

Morphology Leaving out the environmental conditions, biofilm structure and morphology are driven by biological factors. However, in presence of external constraints biofilms respond accordingly, developing into highly differentiated and complex morphologies. Liquid flow is one of these factors, which changes biofilms by influencing the colonization patterns (Augspurger et al., 2010), efficiency and extent of substrate transport, and most importantly hydrodynamic forces it exerts (Stoodley et al., 1999a).

In laminar flow, the cell clusters tend to be approximately hemispherical in shape, surrounded by a monolayer of singe cells (Stoodley et al., 1999b). However, in turbulent flows, the biofilms develop unique forms. The cell clusters become elongated in downstream direction forming filamentous biofilm *streamers* (Figure 2.4), where single cells sparsely attach in the void spaces between these streamers (Stoodley et al., 1999a, 1998). The relation between hydrodynamics and morphology becomes more evident knowing that, e.g., *P.*

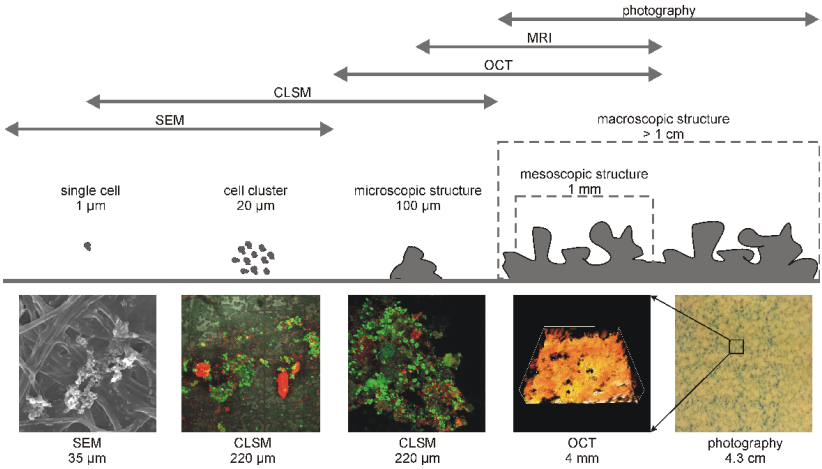

Figure 2.3.: Techniques to investigate biofilm structure at different scales. SEM, Scanning Electron Microscopy; CLSM, Confocal Laser Scanning Microscopy; OCT, Optical Coherence Tomography (Wagner et al., 2010).

aeruginosa, which grow as single cells in flask culture tend to form streamers in fast flows.

Laboratory observations indicate that biofilms are viscoelastic materials (see Section 2.4), similar to polymeric structures hinting toward the importance of EPS in founding the overall material properties of biofilms. From fluid dynamic point of view, this viscoelastic nature can lead to formation of various morphologies observed in flow-cells such as formation of wave-like ripples and dunes at high velocities that transverse slowly in the direction of flow (see Stoodley et al., 1999c and Gjaltema et al., 1994, Figure 7 there in).

To date, studies that investigate the processes behind formation of these complex morphologies are scarce. One of the first experimental attempts in understanding the formation of one of these mesoscale structures, biofilm streamers, has been conducted by Rusconi et al. (2010), and later extended (Salta et al., 2010). In their microfluidic setup, the group constructed channels with different corner shapes, and grew various strains of *P. aeruginosa PA14* in laminar flow. The team was expecting to see typical simple flat structures seen

Figure 2.4.: Schematic presentation of biofilm streamers in flow. The scale bar is $\approx 3 \times 10^{-4}$ m.

in laminar flows, but to their surprise threads of biomass formed in the middle of the channel, connected only to the lateral walls at the corners and the rest of the streamer structure laid suspended in the flow. Earlier, streamers were only reported in turbulent flows, and hence the group's findings suggested that probably more types of streamers could be found in nature. Also, they observed that the threads were surrounded by aggregates of EPS, both at the endings and also throughout the structure.

Motility and EPS formation were two other factors that affected the formation of the streamers significantly. Rusconi et al. (2010) cultivated three different mutants of *P. aeruginosa PA14*, where various features were different than in the wild-type strain. The mutants were (*pilC*) defective in the biogenesis of type IV pili, non-motile mutant (*flgK*) defective in the synthesis of a functional flagellum, and (Δ*pelA*) defective in the production of PEL, a glucose-rich polymer that is one of the main components of the EPS in *PA14* biofilms. The outcome of the experiment turned quite interesting. *pilC* and *flgK* mutants could form streamers, while Δ*pelA* could not, highlighting and confirming the important role of EPS in formation of streamers. In addition, the group could show that motility also has a significant role in formation of streamers. The streamers grown with the pili-deficient mutants appeared to be formed by multiple thin filaments rather than a more massive single thread. On the other hand, the flagellum-deficient bacteria made more clustered, clumpy streamers

compared to the smooth wild-type morphology. In their related work, Rusconi et al. (2011) showed that secondary flow, a relatively minor flow superimposed on the primary flow, around the corners directly influenced the formation of streamers. In the microfluidic channel setup studied therein, the group could show that by changing the angle of curvature in channels (with a zigzag pattern), thy could trigger the formation of thread-like biofilm structures. This quite interesting observation may also explain why the streamers observed in (Stoodley et al., 1998) formed behind the hemispherical bases, where also secondary flows are expected to exist (in form of circulating wakes).

Internal structure and material properties The flow characteristics determine the efficiency and magnitude of external mass transfer from fluid to biofilms and the other way around. The higher the liquid velocity, the higher the mass transfer rate attainable. The mass transfer, naturally, can have direct influence on the internal structure (and heterogeneity) of biofilms. Additionally, from mechanics point of view, biofilms show also strain hardening behaviour that can be related to stiffer and denser material, where the biofilm material gets harder by repeating application of forces (Hohne et al., 2009).

Figure 2.5 demonstrates the effect of hydrodynamics on the internal structure of biofilms observed using OCT microscopy (Wagner et al., 2010). It can be seen that the structure of the biofilm cultivated at $Re = 1000$ (Re calculated based on the channel width) consisted of aggregates and pores of varying sizes. Then again, biomass was more evenly distributed (more dense) within the biofilm cultivated in turbulent flow (see Figure 2.5, $Re = 2500$ and 4000). The biofilms cultivated in laminar and transient flow conditions (see Figure 2.5, $Re = 1000$ and 2500) were visually heterogeneous and porous in volume; they had a rough and open surface structure. On the other hand, the biofilm grown in turbulent flow was visually homogeneous in volume, but with variations in surface structure. Also, for the structures grown in turbulent flow cleft structures were present within the upper 600 µm of the biofilm, whereas the biomass between 600 and 1000 µm above the substratum was dense without significant porosity. These findings clearly demonstrate the role of hydrodynamics on the internal heterogeneity of the biofilms.

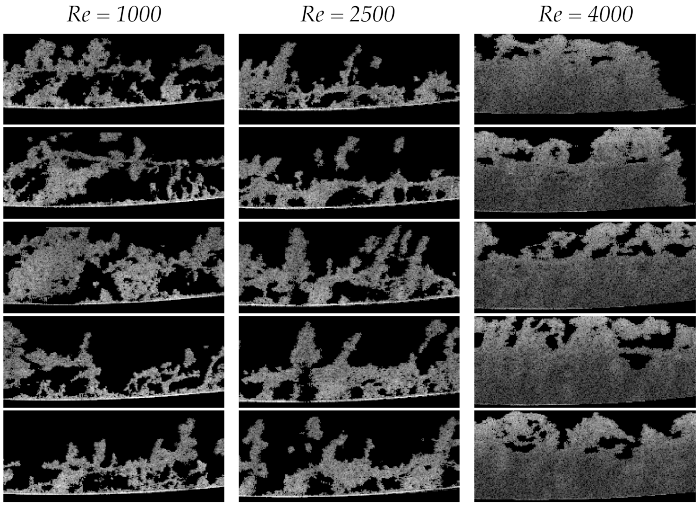

Figure 2.5.: Influence of hydrodynamics on the internal structure of biofilms observed with OCT microscopy at different positions and flow conditions (Wagner et al., 2010). The thickness of above biofilm layers were 1383 ± 97 µm, 1479 ± 110 µm, and 1602 ± 55 µm for Reynolds numbers of 1000, 2500 and 4000, respectively.

Role of nutrients

Initially, it has been shown that in addition to hydrodynamics, availability of nutrients also plays a key role in the development of biofilms at steady-state. Characklis (1990) showed that biofilm thickness increases with higher nutrient concentrations when shear is held constant. Otherwise, at constant substrate loading the biofilm thickness decreases with higher shear rate at faster flows Characklis (1981). Later, in another major study (Stoodley et al., 1999a) researchers observed an immediate response from biofilms when they increased the limiting nutrients tenfold (carbon and nitrogen). Beyond the obvious increase in thickness and surface coverage, biofilm also changed morphologically. The existing ripples disappeared, and clusters and streamers grew larger, where many of them merged together to form porous structures shadowing the influence of drag force on the structure.

Stoodley et al. (1999a) suggested that at high shear, where the influence of drag is high but mass transfer limitations are low, drag reducing planar structures are likely to form, their thickness depending on available nutrient concentration. However, at low shear rates, where the influence of mass transfer limitations are high but drag is low, highly porous structures with high surface exchange areas form (also visible in Figure 2.5). Because there is usually high heterogeneity in the spatial and temporal environmental conditions, intermediate structures may also occur, e.g., presence of ripples around streamers.

Combined effect of nutrient availability and hydrodynamics

Figure 2.6 demonstrates the observed trends between nutrient availability and fluid forces in biofilms (Stoodley et al., 1999a). The empirical diagram is divided into four zones, where different morphologies are expected to develop. Cells do not grow or stay attached when they cannot obtain enough substrate, or experience large shear forces (no-growth zone). Biofilm streamers and ripples are the dominant form where only low to moderate substrate concentrations are available, and fluid forces are high (Figure 2.6). In environments where fluid forces are low and high amount of substrate is available biofilms tend

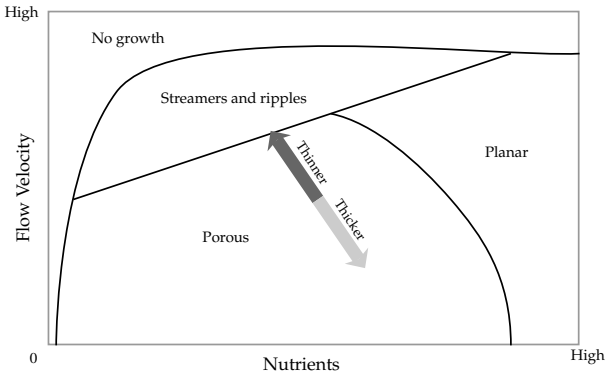

Figure 2.6.: Combined effects of nutrient availability and liquid shear diagram based on observational and hypothetical considerations of mass transfer and shear on biofilm morphotypes. The figure is reproduced from (Stoodley et al., 1999a).

to form planar structures, with lower densities and bulkier structure. Such diagrams are especially important in modeling studies, where experimental evidence is lacking, and help to select a more appropriate range of parameters, e.g., low substrate conditions for streamers.

2.4. Material properties of biofilms

Viscoelasticity is the property of materials that exhibit both viscous and linear or nonlinear elastic behavior when undergoing deformation. When biofilms are subjected to external forces they behave elastically over short periods of time (seconds) and there is a nonlinear relationship between applied force and resulting strain, while deformations are reversible. On the other hand, at longer time periods biofilms show viscoelastic behavior by resisting applied forces and displaying irreversible deformation (Stoodley et al., 1999d; Körstgens et al., 2001b; Stoodley et al., 2002; Shaw et al., 2004).

Modeling the mechanics of biofilms requires the knowledge regarding the mechanical properties of biofilms. Overall, material properties of biofilms have direct influence on how biofilms respond to external forces, type of detachment and dispersal mechanism, and three-dimensional matrix structures they form.

In literature, data regarding the material properties of biofilms are fairly sparse and fragmented, yet increasing in number. The problem is that the data have orders of magnitude difference in values. The reason can be partially attributed to large physiological heterogeneity of biofilms, and their successful adaptation to their environment. However, there is a more important issue. Currently, there is not a standard method to measure mechanical properties of all types of biofilms (Hohne et al., 2009). A summary of measurements of mechanical properties of biofilms related to this work is presented in Table 2.1.

Table 2.1.: Mechanical properties of biofilms

Subjects of study	Stressing Method	Viscoelastic Properties measured
Mixed culture and *Pseudomonas aeruginosa*	Increase of fluid shear induced deformation in flow cell	Apparent elastic modulus, $E_{App} = 17$ to 40 Pa (Stoodley et al., 1999d)
Pseudomonas aeruginosa	Compression test	$E_{App} = 6500 \pm 500$ Pa (Körstgens et al., 2001b)
Nano-filtration membrane biofilm	Rotational and oscillatory rheometry (shear)	$E_{App} = 3000$ to 3500 Pa (Houari et al., 2008)
Staphylococcus epidermidis and *Klebsiella pneumoniae*	Microfluidic device	Elastic modulus: *S. epidermidis* 3200 Pa, and *K. pneumoniae* 1100 Pa. Viscoelastic relaxation time: 15 s (Hohne et al., 2009)

2.5. *Physical life of flexible biological structures in flow*

Throughout this work, biofilm aggregates are assumed as flexible structures present in fast moving liquid flows, that consume nutrients available in the bulk liquid. Therefore, in this introductory chapter initially we look at the basic physical phenomena and principles which the flexible structures in flow experience without focusing specifically on biofilms. These phenomena include

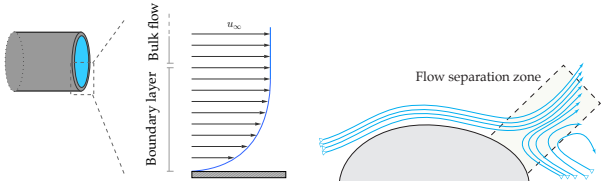

(a) Formation of the velocity gradients and boundary layer at a cross-section of a pipe flow

(b) Flow separation around a bluff body

Figure 2.7.: Velocity gradients and flow phenomena around bluff bodies

the formation of velocity gradients, fluid forces, unsteady flows, structure vibration, flow-flexible structure interactions and lastly substrate transport and concentration gradients.

Life in moving fluids[1]

Water is the source of life on earth and the majority of life forms live in aquatic environments. Through the evolution path, species living in water were selected for their highest adaptivity and fitness to a wide variety of conditions. The life forms are practically everywhere where the water is. Astonishingly, contrary to our perception of inhospitable environments, microorganisms can live even in extremely harsh environments, e.g., the *extremophiles* around the black-smokers of oceans at very high temperatures and high pH extremes of lakes in Yellowstone National Park (USA) (see (Rothschild and Mancinelli, 2001) for a thorough review), or very low nutrient conditions of drinking water pipes, to name a few — where there is liquid water there is life.

Flow and substrate gradients

The viscosity of the fluid leads to many interesting phenomena in the life of living species, including the formation of velocity gradients. The fluid flowing close to a solid surface comes to halt at the solid-liquid interface (or move with the same velocity as the wall), where a *no-slip* condition occurs. This

[1] With a glimpse to the extensive work of Steven Vogel (Vogel, 1994).

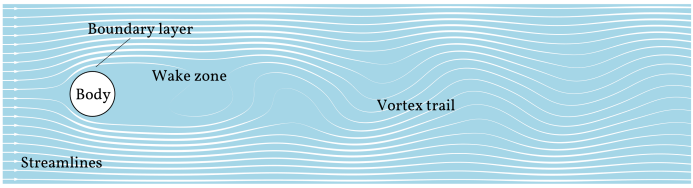

Figure 2.8.: Wake and boundary layer formation behind a circular cylinder in laminar flow.

phenomenon, together with the viscosity of the fluid, lead to the formation of velocity gradients (Figure 2.7a). The resultant velocity profile starts at zero at the solid interface and reaches the free stream velocity at a certain height. This layer of slowly moving liquid is called *hydraulic boundary layer,* where many extremely small sessile organisms live inside. Similar to hydraulic boundary layer formation, *concentration boundary layer* also forms around permeative and reactive objects such as biofilms. The concentration at the surface and vicinity of the object becomes lower than the concentration in the bulk phase due to the flux of the substrate into the object, and hence an analogous to no-slip condition occurs, where a physical region of concentration gradients forms around the object.

Figure 2.7b shows a hemispherical object fixed to the substratum in the flow. Close to the surface of the object, viscosity causes the fluid particles to slow down, and lose momentum. As the fluid gets closer to the object, due to viscosity and no-slip condition it goes around the object at a higher speed (along the streamlines), and meanwhile exerts a lower pressure on the body. On the other hand, the slower flow areas exert higher pressures. The decelerated fluid particles in the boundary layer do not stay attached to the surface, and in the case presented in Figure 2.8 these fluid particles get pushed back in the wide boundary layer formed, and create eddies behind the object. This region of strongly decelerated flow is called a *wake* which exhibits a different pressure profile than the main flow.

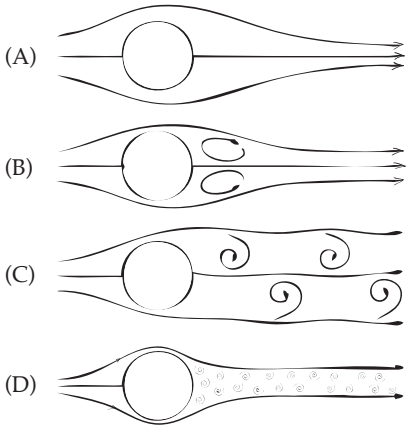

Figure 2.9.: Flow profile and pattern behind a circular cylinder. (A) Creeping flow, $Re_D < 10$; (B) Circulation zones form behind the cylinder at $10 < Re_D < 40$; (C) Trails of von Kármán vortices at $40 < Re_D < 2 \times 10^5$, and (D) Turbulent wake at $Re_D > 2 \times 10^5$, where a narrower wake forms. (Image reproduced from Vogel, 1994).

Unsteady flows and vortex shedding

Flow separation is the reason for many interesting flow structures at moderate Reynolds numbers, where both inertia and viscosity are at work. The typical picture of a laminar flow is a homogenous flow of the fluid bulk; a steady flow. In case there is an obstacle in the flow, we expect that the flow goes around the object and moves away along the streamlines. However, in reality, an interesting phenomenon occurs when an obstacle, e.g., a cylinder is immersed in a flow environment. A pattern of vortices, named *von Kármán vortex street*, starts forming behind the body, which are shed alternately from sides of the object, and transverse along the flow direction (Figure 2.9).

The frequency of vortex shedding is related to the non-dimensional Strouhal number (St) defined as

$$St = \frac{f \cdot L_{ch}}{u_\infty} \tag{2.1}$$

where f is the vortex shedding frequency, L_{ch} is the characteristic length of the object, e.g, hydraulic diameter, and u_∞ is the flow velocity. For a circular

cylinder or a sphere, it is found to be approximately equal to 0.2 over a wide range of Reynolds numbers (Williamson, 2003). If the Strouhal number is known, we can easily estimate the frequency of vortex shedding of a bluff body by using Equation (2.1).

Forces of fluids: drag and lift

Drag is the force that fluid exerts on the structure in the flow direction, and *lift* is the force perpendicular to the flow direction. Drag and lift forces have significant impact on the lives of the organisms on the surface of earth wherever a body comes into contact with a fluid, e.g. air or water. Throughout nature, there is much evidence hinting toward organisms attempting to reduce the drag force acting upon them (and eventually avoid breakage), e.g., streamlined form of fish body and wings, bending of trees in high winds, and drafting behavior in bird flocks.

The magnitude of the drag is directly proportional to the velocity of the fluid and the size of the object. The larger the body, the higher the drag it will experience. Furthermore, drag is made up of several components where the most prominent ones are *form (pressure) drag* and *skin friction*. As the name suggests, skin friction is due to the friction of fluid on the surface of the objects in the flow, and hence its magnitude is directly proportional to the wetted outer surface of the object exposed to the flow. On the other hand, at higher flow velocities, the wake formed behind an object creates a lower pressure field, and the pressure difference generated translates to a net force working on the object. This consequence of boundary layer separation (and loss of momentum) is called the form drag (also pressure drag). The general size and shape of the body is the most important factor in form drag, since they determine the characteristic of the boundary layer separation and the consequent dimension of the wake.

Reynolds number (Re)[2] is a dimensionless quantitative measure that weighs the relative magnitude of inertial forces to viscous forces, and hence indicates

[2]The Reynolds number can be defined in two ways: based on the channel or pipe diameter in internal flows, denoted by Re, and based on diameter of the diameter of an object (or hydraulic diameter) which flow goes around it, e.g. a cylinder in flow, denoted by Re_D.

whether any of these forces are dominating. At low flow velocities ($Re_D \ll 1$) viscous forces dominate, while at high flow velocities ($Re_D > 100$) the inertial forces prevail. In the intermediate region between ($0.1 < Re_D < 100$) both viscous and inertial forces become important. Therefore, based on the definition of the two forms of the drag, at low velocities (low Re_D) skin friction is the dominant form of the drag, while in fast flows (high Re_D) the form drag dominates.

The problem with the measurements of drag and lift is that the value of the measured force does not differentiate between different shapes and geometries, and cannot be used for comparison. Hence, in fluid dynamics, two dimensionless coefficients are defined, termed the drag coefficient (C_D) and lift coefficient (C_L), which are used to quantify the drag or resistance of a body placed in a fluid environment. C_D and C_L are not constant but vary as a function of relative flow speed, flow direction, object position and size:

$$c_D = \frac{2F_D}{\rho^F u_{x,\infty}^2 A} \qquad c_L = \frac{2F_L}{\rho^F u_{y,\infty}^2 A} \tag{2.2}$$

where F_D and F_L are the drag and lift forces, ρ^F the density of the fluid, $u_{x,\infty}$ and $u_{y,\infty}$ are the relative velocities of the fluid in x- and y-directions, and A the reference area. Consequently, the drag and lift forces depend on the drag and lift coefficients (which are measured experimentally), the area and also the square of relative flow velocity. So, e.g., with two times higher velocity, a fixed object will experience four times higher drag; this is one of the main fitness costs which defines the upper limit for the size of animals in moving fluids.

Looking at Equation (2.2), we can see the direct relation of the drag and the area. Notably, the area mentioned in the drag calculations itself is very crucial, and depends on the type of drag coefficient being measured. The area can be defined in many ways, but generally two ways are often used in literature: (i) *projected (frontal) area*; the maximum area confronting the flow, perpendicular to the flow direction, (2) *wetted area*; the total surface area exposed to the flow.

For the sake of convenience and staying related to the context of this work in the next section only the drag of fixed objects in moving fluids will be covered.

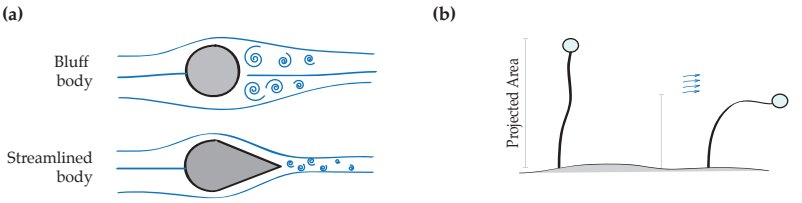

Figure 2.10.: Drag reduction mechanisms. (a) streamlining: drag is reduced when the size of the wake zone is reduced, (b) drag reduction by reconfiguration.

Drag reduction: streamlining and reconfiguration

For the species living in fast moving fluids or moving at high speeds the challenge is whether there is a way to reduce the dominant form drag. Not surprisingly, nature usually finds a way to optimize and reduce costs, in this case, since millions of years. The exposed area and shape (in relation to size of the wake) are two main factors that living organisms can modify to reduce the fluid forces in fast flows.

An often encountered method to reduce the drag in nature (and also man-made structures) is *streamlining*. The shape of the body in wings of birds, sessile aquatic organisms, and fish are examples of such an adaptation to reduce the fluid forces. The streamlined profile of their structures is characterized by a rounded front and a slowly tapering tail (Figure 2.10). This way, separation which occurs closer to the trailing edge is delayed, resulting in a smaller wake, reduced fluid momentum loss, and hence, reduced form drag, although the increased area raises skin friction.

In addition, another less apparent method of reducing the drag is to manipulate the area exposed to the flow. Plants depend on sunlight to survive – usually the higher exposure the better – and one way to achieve higher sunlight exposure is to expand and increase the surface area. Nevertheless, the higher area also increases their chance of breakage in high winds or fast water flows. As often seen in nature, the plants are flexible, and make use of their flexibility by passively changing their shape through bending and twisting when experiencing high fluid forces (Koehl, 1977; Vogel, 1984, 1989; Harder et al., 2004). Hence, flexibility is a required property for this type of modification of

geometry and shape to reduce drag, more appropriately termed *reconfiguration* (Vogel, 1984, 1994).

Different from static immobile structures (bluff bodies), drag of flexible structures does not correlate with the square of the velocity any longer, and requires an additional measure than the drag coefficient alone. Vogel (1984) proposed such measure, called *speed specific drag* factor (see Section 4.1 for more details). For example, for the case presented by Alben et al. (2002), the self-similar bending of the filament reduced the drag significantly. Koehl (1996) also mentions a similar observation, that the flexible sessile organisms experience lower drag forces compared to the rigid ones of the same shape because the deformable organisms are "passively blown into more streamlined shapes". There are several other methods of drag reduction in nature, e.g., manipulating surface roughness, where a review of these methods can be found elsewhere (Vogel, 1994; Koehl, 1996; Vogel, 2003).

In engineering terms, reconfiguration, and overall, deformation of flexible bodies in flow belong to the category of the problems called fluid-structure interaction, which will be described in the following section.

Vortex induced vibrations (VIV)

At fast enough flows, when the trail of von Kármán vortices are shed, in addition to the formation of patterns behind the object, another interesting phenomenon occurs. The magnitude of drag and lift forces on the object also starts to periodically vary in time; drag has the same frequency of the vortex shedding and lift oscillates at two times the vortex shedding frequency. If the object is moveable or flexible, the exerted forces will cause the object to also oscillate leading to the phenomenon of vortex induced vibration.

In biological systems, vortex induced vibration may cause severe damages to the survival of the organism. Resonance, or in our case, mechanical resonance is the tendency of a mechanical system to absorb more energy when the frequency of its oscillations matches the system's natural frequency of vibration than it does at other frequencies. At these frequencies, even small periodic driving forces can produce large amplitude oscillations. These *natural frequencies*, are the frequencies at which a system naturally vibrates once it has been set into

motion. To visualize better, consider a beam fixed at one end, having a weight attached to its other end. Once pulled downward, then released, the beam will oscillate at its natural frequency in the absence of any other forces. If the exerted forces periodically bring the object close to their natural frequencies, the object will start to move drastically at the *amplitudes* that may lead to the failure of its structure.

What if a flexible structure is put behind a cylinder? Will it dampen the vortex shedding or will it start to move with the similar frequency of oscillations?

Fluid-structure interaction: mechanics of flexible structures in flow

Throughout the literature there are thousands of research papers on vortex formation, vortex induced vibrations and vortical instabilities in wakes, demonstrating that an understanding of a typical, geometrically simple flow behind a bluff body poses a great challenge to scientists and engineers (Figure 2.11a). Wakes behind bluff bodies are complex; they involve the interactions of three shear layers in the same problem, namely a boundary layer, a separating free shear layer, and a wake (Williamson, 2003). In fluid-structure interaction the problem domain is extended to include also the nonlinearities arising from the interaction of the structure with the fluid. Detailed experiments, state-of-the-art models, and accurate numerical methods have improved our understanding of typical problems in fluid-structure interactions. Therefore, it does not come as a surprise that until recently researchers did not know the mechanism behind the flags flapping in the wind (Zhang et al., 2000). With a better understanding of the process, come also novel applications, e.g., energy harvesting in oceans by placing a piezoelectric eel-like membrane in the wake of a bluff body and using the von Kármán vortex street forming behind the bluff body to induce oscillations in the membrane (Allen and Smits, 2001) and piezoelectric wind energy harvesting (Sivadas and Wickenheiser, 2011) similarly, to name a few.

Due to their (visco)elastic nature, biofilms in flow also belong to general class of fluid-flexible structure interaction problems, where flexible structures (or bodies, flexible sheets of e.g. textile) interact with fast flows. As schematically shown in Figure 2.11, there are also other cases in nature with similar mechanisms to the flag-in-the-wind problems, such as the fish locomotion (Beal et al.,

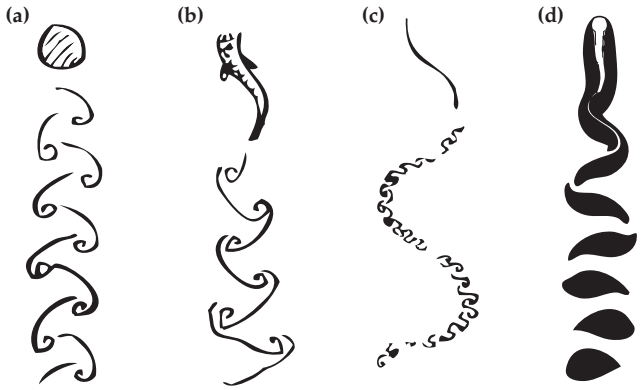

Figure 2.11.: Natural fluid-structure interaction type of problems. This figure schematically shows the classical von Kármán vortex street behind a (a) rigid cylinder; (b) swimming fish; (c) flapping filament (or flag); and (d) a biofilm streamer, showing both large- and small-scale vortical structures. Image inspired and partly reproduced from (Shelley and Zhang, 2011)

2006; Drucker and Lauder, 2001) or even snorting (Huang et al., 1995).

What is causing flags to flutter so playfully? Is it that the flag follows the fluid pattern around it (going with the flow), or does the motion of the flag affect the wind flow, and there is a coupled dynamics behind it? Initially, Taneda (1968) performed the first experimental work on the dynamics of flags in the wind tunnel. Similarly, Zhang et al. (2000) placed a filament held at its upstream end in a 2-d like flow of soap film. They showed that a single flag can experience three states of immobility (still generating trailing vortices behind the filament end), regular stable sinusoidal undulatory deformation, and bistability. Later, Zhu and Peskin (2002) numerically studied the flapping flexible filament in a flowing soap film using the immersed boundary method, in which they showed that the bistability of the filament observed (Zhang et al., 2000) is related to the length of the filament. Below a critical length the filament is always immobile, while above the threshold the filament becomes bistable. Using a method, close to the method in the current work, Sawada and Hisada (2007) analyzed the effect of representative parameters, e.g., length, mass density and bending rigidity of the filament, inflow velocity, and soap

film viscosity on the flapping of the filament. They showed that the length of the filament and the state of resonance between the filament and the flowing soap film largely determines the stability of the filament. The outcome of varying the velocity in their problem showed that the stability of the filament depends on whether large amplitude (resonance) occurs or not. When the resonance occurred the state became most stable, whereas at a bifurcation point either an unstable flapping state or a stretched-straight state appeared. Thereafter, numerous studies have investigated the dynamics of thin filaments in the flow, which due to the scope of this thesis will not be discussed further (see Shelley and Zhang (2011) for an engaging review).

2.6. State of the art in mathematical modeling of biofilms

Once researchers and engineers noticed the importance of biofilms in natural systems and health, the need for predicting and controlling the behaviour of biofilms encouraged them to seek a deeper understanding of biofilms. Thus, a set of guiding principles were needed to understand the distribution and diversity of microorganisms in the context of their micro- and macro-environments as a step toward the ultimate goal of constructing descriptions of full microbial ecosystems (Klapper and Dockery, 2010).

The area of biofilm modeling has changed dramatically in the last three decades driven by the advancement of computational methods, but more importantly by much lower computational costs. Nowadays steady-state simulation of flow that lasted two days to compute on a supercomputer in the 1980s can be performed on a small laptop in a matter of seconds. So, how did the first biofilm models look like?

One-dimensional multispecies models

One of the most prominent mathematical model of biofilms was introduced by WANNER AND GUJER (Gujer and Wanner, 1984; Wanner and Gujer, 1986), which described the biofilm dynamics using a one-dimensional multi-substrate and multi-species biofilm model employing a continuum approach and a moving boundary. This way, the model was able to predict changes in biofilm

thickness, transient behavior and spatial distribution of microbial species and substrates in the biofilm. The so called WANNER & GUJER model was later implemented in the very popular AQUASIM software by Wanner and Reichert (1996). Since AQUASIM was very easy to use and could be extended to include more advanced submodels it was (and still is) used extensively throughout the field of biofilm research to quantitively describe the overall macroscopic conversions and processes in biofilm systems (e.g., see Horn and Hempel (1997); Horn et al. (2003); Elenter et al. (2007)). This model calculates gradients in z-direction (perpendicular to the substratum). The height of biofilm also changes in time using a moving boundary method. The WANNER & GUJER model assumes a physical continuum model, where arbitrary chemical processes are considered, and the mechanical processes can be introduced using various empirical detachment functions (velocities). Nevertheless, not surprisingly, the 1-d models produce non-homogenous results in one direction, lacking spatial and heterogeneity information in other directions.

Multi-dimensional multi-species models

With the advance of new imaging techniques, specially confocal microscopy, soon it became evident that biofilms are quite heterogenous, both in microbial composition and structure. In the meantime, a new class of biofilm models were introduced, which could visually replicate this spatial heterogeneity in two or three dimensions using a discrete formulation (Wimpenny and Colasanti, 1997; Picioreanu et al., 1998).

The underlying processes of the discrete models are very similar to 1-d models, with the difference that microbial cells are allowed to grow and divide in more than one direction. This category of models, generally called Cellular Automata (CA) models, uses simple rules for distribution of the daughter cells and elimination of the detached cells. Cellular automata models are capable of replicating observed trends in structural heterogeneity seen in biofilms. Later, these models were extended to include simplified mechanical analysis (Picioreanu et al., 2001). Apart from the CA models, the continuum approach of 1-d models was also extended later on to more dimensions (Alpkvist and Klapper, 2007b; Duddu et al., 2008).

The models cited above had a common view on biofilms, that chemical and mechanical processes control the biofilm formation. It was a view that, despite being work-in-progress, most biologists and microbiologists would argue against. Biofilms consist of aggregates of individual microbial entities that interact with each other and their surroundings in both biological and physical ways. Individual-based models (IbM) (Kreft et al., 1998, 2001) were the new class of models to address this shortcoming of continuum models (lack of interaction and individual representation view of microbial life), where biofilm bulk was represented as a collection of discrete separate individual particles growing, dividing, interacting and eventually decaying and disappearing.

The first generation of individual-based models, unlike the CA models (Picioreanu et al., 1998, 1999, 2000b), neglect the hydrodynamics. Later, simple liquid flow (e.g., assuming hydraulic boundary layers), detachment and transport sub-models were included in the models (Xavier et al., 2005a). Xavier et al. (2005b) introduced the LEVEL-SET interface tracking method in IbM models to track the outer boundaries of the biofilm domain in time. There was also a successful combination of the IbM and continuum models by using an individual-based description of the bacteria and a continuum representation of the biofilm matrix (Alpkvist et al., 2006). A more advanced and general implementation of IbM was recently introduced in an open-source code IDYNOMICS, which seeks to bring different approaches in IbM modeling into a single standard framework (Lardon et al., 2011). Complementary to and inspired (Alpkvist et al., 2006) previous models, IDYNOMICS introduces several enhancements, e.g., the biofilm pressure field (similar to Alpkvist et al., 2006; Alpkvist and Klapper, 2007b) and the continuous-in-time EPS excretion leading to more realistic fluid behaviour of the EPS, to name a few.

The biofilm models presented so far considered a simple physical environment where biofilm could not mutually interact with the surrounding fluid. The influence of flow on biofilm was modeled indirectly using assumptions such as empirical detachment functions, hydraulic boundary layers, and external mass transfer coefficients. Most of the parameters describing these assumptions were either measured experimentally or transferred from similar non-biofilm systems, which affected the reliability and accuracy of the results.

Therefore, a new generation of models was proposed, where the physics of the system was modeled using coupled mechanical, chemical and biological sub-models employing advanced numerical techniques.

Mechanical and multiphysics models

Biofilms usually are found in flowing aquatic environments, and hence are facing liquid shear forces. Since they are composed of cells, water and EPS similar to other viscoelastic polymers they deform under the application of shear forces. If the amount of applied force exceeds the internal cohesiveness biofilms experience fracture and eventual failure (detachment). The majority of the biofilm models neglect the mechanics of biofilms, or include it (e.g., in detachment) by employing simple empirical correlations of erosion (Gujer and Wanner, 1984; Wanner and Gujer, 1986; Wanner and Reichert, 1996; Horn et al., 2001, 2003; Xavier et al., 2005a,b; Alpkvist and Klapper, 2007b) or decay through stochastic rule-based assumptions (Pizarro et al., 2001; Bohn et al., 2007).

Notably, Dillon and Fauci (2000) considered a microscale model of biofilm formation using Immersed Boundary Method, originally developed by Peskin et al. (Peskin, 1977, 2003). Later, Alpkvist and Klapper (2007a) developed a ball-spring model of biofilms, which used Immersed Boundary Method as well to simulate the mechanical response and detachment of biofilms in flow, neglecting the biomass growth. With their model, they could show qualitatively how a sloughing event occurs, and also how biofilm patches may roll by forming temporary bonds in the presence of fluid shear.

Multiphase mixtures belong to a sophisticated class of methods, which assume biofilms as viscoelastic fluids inside another fluid with lower viscosity (e.g., water). Cogan (2004) used this method, combined with an osmotic pressure related to polymer solution theory, to study the disinfection mechanism in biofilms. This model was later extended to study the role of cohesion in long-time biological life and mechanics of biofilms (Klapper and Dockery, 2006). Winstanley et al. (2011) also modeled the biofilm growth assuming the EPS as a polymer solution, whose viscoelastic rheology is described by the classical Flory–Huggins theory.

Another generation of the mechanical models incorporates general finite element method (FEM) or eXtended finite element methods (XFEM) to model the continuum growth and mechanics, especially the fluid-structure interaction of biofilms. To evaluate the effect of detachment on biofilm structures Picioreanu et al. (2001) developed a two-dimensional finite-element model assuming an elastic model for the solid biofilm, Lattice Boltzmann Method (LBM) for laminar flow, solute transport with reaction, and cellular automata for growth and bi-directional spreading. Their model applied a one-directional (fluid on biofilm) fluid stress loading on the elastic biofilm structures, assuming a steady-state flow field and no influence of structure movement on the flow (one-way coupling). In another study, Laspidou and colleagues (Laspidou and Rittmann, 2002; Laspidou et al., 2005) developed a unified multi-component cellular automata model (UMCCA) using finite element analysis to model mechanical properties of biofilms reproduce the laboratory observations such as breakage. Towler et al. (2007) used a finite element software (ANSYS) and modeled the steady-state FSI of a hemispherical biofilm cluster in turbulent flow using a linear viscoelastic Burger constitutive relation for the biofilm material. The 2-d model of Duddu and co-workers (Duddu et al., 2008, 2009) included the mass transfer and growth of biofilms using XFEM and level-set interface tracking method. Böl et al. (2009) also used FEM with two different material models and realistic structures from CLSM to study the biofilm detachment with basics similar to the work of (Picioreanu et al., 2001).

To conclude, the models developed so far are able to capture the dynamics of biofilm development qualitatively and but not in a quantitatively reliable way. One obvious reason can be the lack of experimental data and the related accuracy, e.g., material properties and local flow and concentration conditions. Another reason could be that due to the complexity of the biofilm processes and their far range of time scales we are not yet able to incorporate them in a unified model. Overall, the general modeling trends seem to be going towards the use of finite element family of multiphysics models. In addition, also the recent developments in GPU hardware makes IbM models, or hybrid of both, quite promising.

3

Biofilm streamers: study plan

3.1. Streamers and drag

The forces on a *living* object in a flow depend on its shape, and its shape also depends on the forces it experiences (Vogel, 1994). The formation of streamers is generally linked to two factors: the fluid shear and the viscoelastic nature of the biofilm clusters (Shaw et al., 2004). However, up to now the interaction of local flow with biofilm could hardly be investigated due to, e.g., difficulties in micro-scale *in situ* flow and force measurements. Hence, in search for alternatives, modeling studies could be of a great assistance. A literature survey shows that the interaction of fluid with deformable biological structures (such as biofilms) is becoming an increasingly active field of research both in biology and numerical methods (Zhang et al., 2000; Zhu and Peskin, 2007; Alpkvist and Klapper, 2007a; Duddu et al., 2009; Böl et al., 2009).
Stoodley et al. (1998) grew mixed population biofilms consisting of *Pseudomonas aeruginosa*, *Pseudomonas fluorescens*, and *Klebsiella pneumoniae* in a flow cell under turbulent flow conditions. The formed streamers oscillated rapidly, with frequencies proportional to the flow velocity, suggesting that the vortex shedding from the cell clusters was the cause of the oscillations. Why do biofilms

exhibit a streamlined shape in fast flows? Streamlining in high Reynolds number (*Re*) flow acts to reduce the costs of fluid forces on the structure by delaying separation of the flow from the surface of the object in fast flows. In contrast, streamlining at low Reynolds numbers is not effective, as streamline separation only occurs when inertia becomes the dominant force at work at high Reynolds numbers. The Fineness Ratio (*FR*) defined as the ratio of maximum length to the maximum thickness is an indicator of streamlining. Bodies of revolution, symmetrical about their long axis, demonstrate minimum drag in the range of *FR* of 3 to 7 (Fish, 1998). In airship (e.g., Zepellin) design an optimal *FR* is 4.5, which provides the minimum drag for the maximum volume von Mises (1959). The streamer Stoodley et al. (1998) studied had a *FR* of 4.48.
Therefore, based on this preliminary evidence, formation of biofilm streamers may be one possibility for the aggregated microorganisms, amongst others, to reduce the fluid forces acting on the biofilm structure. The first part of this work investigates the local environment of flexible biofilm streamers in fast flows and presents results that support the above hypothesis.

3.2. Streamers and substrate transport

Biofilm cells can get their nutrients either from the bulk liquid or from the support material on which they grow attached. When the soluble nutrients (called substrates) are provided by the liquid, a transport chain forms from the bulk liquid to the biofilm cells. Although in the bulk flow convection is the dominant transport mechanism for substrates, around the biofilm surface a mass transfer boundary layer develops, where diffusion dominates. Diffusion is by far the main transport mechanism of solutes to/from microbial cells also in the biofilm since the gel-like biofilm matrix largely prevents convection.

In terms of mass transfer, a fast fluid flow can be beneficial to microbial inhabitants of biofilms as it will assure more solute transport through a thinner boundary layer, thus providing better solute exchange between biofilm and bulk liquid. However, faster flows also exert larger forces on the biofilm, which lead to larger stresses in the biofilm structure and eventually to biomass detachment. One way biofilms cope with these stresses, similar to sessile marine

organisms (Vogel, 2003), is by developing (visco-)elastic flexible bodies, easily deformable under forces exerted upon them by the flow. Biofilm streamers are one of the complex microbial architectures which are believed to employ the viscoelastic material properties to their benefit. It has been initially reported that biofilm streamers can grow preferably in flow-cells under turbulent hydrodynamic conditions (Stoodley et al., 1998) and in extreme acidic environments (Edwards et al., 2000). Biofilm streamers are therefore commonly observed in rivers (Besemer et al., 2007), where the flow is generally turbulent. However, there are reports of streamers developing behind spacer filaments from the feed channels of reverse osmosis membrane devices (Vrouwenvelder et al., 2010), supposedly operated in laminar but unsteady flow conditions. Recently, Rusconi and colleagues (Rusconi et al., 2010) also reported the formation of filamentous streamers in microfluidic devices under laminar flow conditions, and showed that formation of thread-like streamers is proportional to the intensity of the secondary flow around the corners in their microfluidic setup Rusconi et al. (2011).

In addition to the flow conditions, nutrient availability also plays a significant role in shaping the biofilm structure. Stoodley and co-workers (Stoodley et al., 1999a) reported that at high shear rates the existence and the thickness of biofilm streamers were related to the nutrient availability. The distinguishable streamer structures and ripples developed at low substrate concentrations, whereas in more concentrated substrate environments they were overgrown and merged to form heterogeneous porous structures thus shadowing the influence of liquid shear.

On the engineering side, it has been reported that the substrate transfer rate can be increased by irregularly shaped or filamentous biofilms (Siegrist and Gujer, 1985; Zhang et al., 1994). As a result of these studies, it has been proposed that the increased mass transfer is caused by biofilm protuberances penetrating the boundary layer into the convection-dominated bulk fluid (Siegrist and Gujer, 1985; Zhang et al., 1994; Nagaoka and Sanda, 2005; Wäsche et al., 2002). However, if the biofilm structure is rigid (i.e., not allowing oscillatory movement) theoretical models both in 2-d (Picioreanu et al., 2000b) and 3-d (Eberl et al., 2000) clearly showed that, by contrary, a decrease in mass transfer will be

expected in immobile finger-like, dendritic or mushroom-like biofilm structures compared to planar and smooth biofilms. Therefore, it has been hypothesized that the periodical movement of elastic biofilm structures induced by the flow may be the real cause of increased mass transfer in finger-like or streamer biofilms.

Since, to our knowledge, the problem of coupled fluid-flexible structure interaction with unsteady mass transfer has not been studied before another important aim of this work is to introduce in detail the newly developed computational methods. Next, we characterized quantitatively the increase of mass transfer coefficients for the oscillating biofilm relative to a rigid immobile structure. From the multiple factors that may influence the magnitude of mass transfer to the moving body, we studied here the dependency of mass transfer coefficients on (i) liquid velocity and (ii) biofilm flexibility.

4

Model implementation of biofilm streamers in flow

4.1. Drag and fluid-structure interaction of moving biofilm streamers

Modeling the oscillation of biofilm streamers is a fluid-structure interaction problem, where two tightly coupled phenomena must be taken into account: the biofilm structural motion and the fluid flow. The structural motion can be safely described by large deformation elastodynamics, neglecting viscoelastic contributions to the streamer deformation due to very short motion time-scales compared to viscoelastic deformation time-scales (Shaw et al., 2004). The fluid flow is modeled by the incompressible Navier-Stokes equations. In this study, the Arbitrary Lagrangian-Eulerian (ALE) formulation for fluid domain is employed to account for the common deformation of fluid and solid at their interface. From a solid mechanics point of view, the deformed shape of the streamer is determined by pressure load and shear stresses exerted by the fluid on the streamer boundaries. From a fluid dynamics perspective, the motion of the streamer is imposed on the fluid as a moving boundary condition.

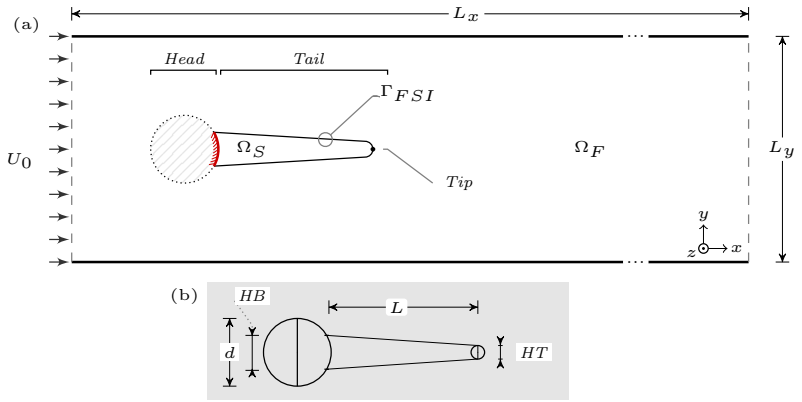

Figure 4.1.: Two-dimensional biofilm streamer model description. (a) Water flows from left to right and view is from the top of the flow channel. The streamer length is $L = 1.492 \times 10^{-3}$ m, and its base diameter is $d = 3.33 \times 10^{-4}$ m (corresponding to $L/d \approx 4.5$). The domain length is $L_x = 12 \times 10^{-3}$ m and height $L_y = 3.2 \times 10^{-3}$ m. (b) Geometric construction of the biofilm streamer showing the streamer dimensions where $HT = 6.6 \times 10^{-5}$ m and $HB = 1.44 \times 10^{-4}$ m.

Model domain

To model the oscillation of the biofilm streamers, a two-dimensional streamer, shown in Figure 4.1, is subjected to a range of flow conditions similar to those considered in the experimental settings of Stoodley et al. (1998) and with the same dimensions as the streamer studied therein. The domain is a rectangular channel, with length L_x in the main stream direction, x, and width (height) L_y in the side stream direction, y.

Besides avoiding extreme computational difficulties, there are also physical reasons to start with a 2-d approximation. Stoodley et al. (1998) found out that the streamer had no significant vertical motion (z-direction). This finding ensures the assumption that the flow has an x-y plane transient variation, which can be captured by a 2-d model.

To replicate the formation of the streamer and study the various transient streamer lengths, several streamers of different tail lengths from the limit case $L/d = 0$ (only the circular base) to $L/d = 11$ were simulated — d is the

diameter of the circular biofilm base and L is the streamer tail length. The streamer studied by Stoodley et al. (1998) is represented by $L/d = 4.5$.
The problem domain is divided into two non-overlapping computational sub-domains Ω_F and Ω_S. Ω_F is the deforming fluid sub-domain, where the Navier-Stokes equations are solved to obtain both pressure and velocity field; Ω_S is the biofilm streamer tail sub-domain, where the structural elastodynamic equation is solved for the displacement field. Both sub-domains share a common interface Γ_{FSI}.
Three different systems of reference are used within this work. Structural deformations are described in the Lagrangian or material formulation. The corresponding Lagrangian coordinate system denoted by $\mathbf{X}$ is associated with the particular material points. The Eulerian or spatial system of reference denoted by $\mathbf{x}$, in which the observer is fixed in space and looks at the fluid passing. In the ALE description of the motion (see Donea and Huerta (2003)), a third reference system, denoted by $\boldsymbol{\chi}$, is required to identify the grid points. In the following sections the velocity $\mathbf{u}$ and the pressure p are chosen for the unknowns of the fluid field, whereas the structural field unknown is the displacement $\mathbf{d}$.

Fluid mechanics

The laminar fluid flow in the deforming sub-domain Ω_F is described by ALE version of the incompressible Navier-Stokes equations, consisting of momentum equation

$$\left.\frac{\partial \mathbf{u}}{\partial t}\right|_{\boldsymbol{\chi}} + (\mathbf{u} - \mathbf{u}_G)\cdot\nabla\mathbf{u} - 2\nu^F \nabla\cdot\varepsilon(\mathbf{u}) + \nabla\hat{p} = \mathbf{b}^F \qquad \text{in } \Omega_F \times (0,T), \tag{4.1}$$

and continuity condition

$$\nabla\cdot\mathbf{u} = 0 \qquad \text{in } \Omega_F \times (0,T), \tag{4.2}$$

These time-dependent equations are solved for the velocity field $\mathbf{u}$ and the kinematic pressure $\hat{p}$ in the fluid sub-domain Ω_F. In these equations, $\boldsymbol{\varepsilon}(\mathbf{u})$ denotes the strain rate tensor, $\mathbf{b}^F$ represents vector of body forces, $\nu^F = \mu^F/\rho^F$,

is the kinematic viscosity with dynamic viscosity μ^F and fluid density ρ^F, and ∇ denotes the gradient with respect to the spatial coordinates $\mathbf{x}$. Here we assume that no gravitation or other volume forces affect the fluid, so that $\mathbf{b}^F = \mathbf{0}$. The term $(\mathbf{u} - \mathbf{u}_G)$ in Equation (4.1) defines the ALE-convective velocity, that is, the relative velocity of the fluid flow inside a moving mesh (see Donea and Huerta (2003) for the details of implementation), where the geometrical location of a mesh point is obtained from the unique mapping $\mathbf{x} = \varphi(\boldsymbol{\chi}, t)$. The ALE-convective velocity can be determined by

$$\mathbf{u}_G = \left.\frac{\partial \varphi}{\partial t}\right|_{\boldsymbol{\chi}} \tag{4.3}$$

The constitutive equation for a Newtonian fluid reads

$$\boldsymbol{\sigma}^F = -p\mathbf{I} + 2\mu^F \boldsymbol{\varepsilon}(\mathbf{u})$$

whereby $p = \hat{p}\rho^F$ denotes the physical pressure within the fluid field. The strain rate tensor $\boldsymbol{\varepsilon}(\mathbf{u})$ can be written as:

$$\boldsymbol{\varepsilon}(\mathbf{u}) = \frac{1}{2}(\nabla \mathbf{u} + \nabla \mathbf{u}^T) \tag{4.4}$$

Structural Mechanics

The structural deformations of the biofilm streamer (sub-domain Ω_S) are obtained using an elastic material model together with a geometrically nonlinear formulation to allow for large structural deformations. The equations for the structure are formulated in a Lagrangian frame of reference. The coordinates in the current and reference configurations are denoted by $\mathbf{x}$ and $\mathbf{X}$, respectively. Initially, the current coordinates are taken to equal the reference coordinates (i.e. $\mathbf{x} = \mathbf{X}$ at $t = 0$).

The displacement $\mathbf{d}$ is the difference between the initial position of a material point and its current position:

$$\mathbf{d} = \mathbf{x} - \mathbf{X} \tag{4.5}$$

Table 4.1.: Model parameters used in fluid-structure interaction simulations of biofilm streamers.

Name	Description	Value	Unit
μ^F	Water dynamic viscosity	1×10^{-3}	$\mathrm{kg \cdot m^{-1} \cdot s^{-1}}$
ρ^F	Water density	1000	$\mathrm{kg \cdot m^{-3}}$
U_0	Water inlet velocity	0.1 ,0.2 ,...,0.5	$\mathrm{m \cdot s^{-1}}$
ρ^S	Biofilm density	1000	$\mathrm{kg \cdot m^{-3}}$
E^S	Young's modulus	5000	$\mathrm{kg \cdot m^{-1} \cdot s^{-2}}$
L/d	Tail to head ratio	0 ,1 ,2.5 ,4.5 ,11	-
ν^S	Poisson's ratio	0.4	-

The structural field Ω_S is governed by the nonlinear elastodynamics equation

$$\rho^S \frac{\mathrm{d}^2 \mathbf{d}}{\mathrm{d}^2 t} = \nabla \cdot (\mathbf{F} \cdot \mathbf{S}) + \rho^S \mathbf{b}^S \qquad \text{in } \Omega_S \times (0, T), \tag{4.6}$$

that determines the structural displacements $\mathbf{d}$ by prescribing equilibrium between the body forces $\mathbf{b}^S$, the internal forces determined from the second Piola-Kirchhoff stress tensor $\mathbf{S}$, the deformation gradient $\mathbf{F}^S = \partial \mathbf{x} / \partial \mathbf{X}$ and forces of inertia.

For the employed ST. VENANT-KIRCHHOFF type of material used in this work, the second Piola-Kirchhoff stress tensor $\mathbf{S}$ is related to the Green-Lagrangian strains $\mathbf{E}$ via:

$$\mathbf{S} = \lambda^S \operatorname{tr}(\mathbf{E})\, \mathbf{I} + 2\mu^S \mathbf{E} \tag{4.7}$$

with

$$\mathbf{E} = \frac{1}{2}(\mathbf{F}^T \cdot \mathbf{F} - \mathbf{I}) \tag{4.8}$$

The Lame constants λ^S and μ^S are related to the Young's modulus E^S and Poisson's ratio ν^S via:

$$\lambda^S = \frac{E^S \nu^S}{(1+\nu^S)(1-2\nu^S)}, \quad \mu^S = \frac{E^S}{2(1+\nu^S)} \tag{4.9}$$

The biofilm density ρ^S, Young's modulus E^S, and Poisson's ratio ν^S are reported in Table 4.1.

Boundary conditions

Because the streamer position changes continuously in time, the finite element mesh will be continuously deformed. The boundary conditions control the displacement of the moving fluid mesh with respect to the initial geometry. The boundary connecting the tail to the streamer base is fixed and the rest of tail boundaries are free to move. At the moving boundaries of the streamer, the fluid-structure interaction interface boundary Γ_{FSI}, the mesh velocities, representing the fluid, equal the deformation rate, representing the biofilm:

$$\mathbf{u}_{\Gamma,FSI} = \frac{\mathrm{d}\mathbf{d}_\Gamma}{\mathrm{d}t} \tag{4.10}$$

where $\mathbf{d}_\Gamma$ is the structural displacement of the interface Γ_{FSI}, $\mathbf{u}_\Gamma$ is the fluid velocity at the interface Γ_{FSI}. At all other boundaries of the domain except the FSI boundaries the mesh movement is set to zero in all directions.
At the interface Γ_{FSI} the dynamic continuity states:

$$\sigma^S \cdot \mathbf{n} = \sigma^F \cdot \mathbf{n} \tag{4.11}$$

where $\mathbf{n}$ is the unit vector normal to the boundary, and σ^F and σ^S are the Cauchy stresses of fluid and structure, respectively. Equation (4.10) and Equation (4.11) form the coupling conditions on the FSI interface Γ_{FSI}.
The inlet flow boundary condition (at $x = 0$) is defined as a uniform velocity profile with horizontal velocity component $u_x = U_0$ and transverse velocity component $u_y = 0$. The velocity U_0 is set from 0.1 to 0.5 $\mathrm{m \cdot s^{-1}}$, corresponding to Reynolds numbers of up to 167 with respect to the diameter d of the base of the streamer (Re_D). To improve the convergence of the numerical procedure at the beginning of the simulations, the inlet flow velocity is smoothly increased from zero to the target velocity during the initial 0.1 s. The slip condition is applied to the upper and lower domain walls, at $y = 0$ and $y = L_y$. This condition assumes that there are no tangential forces on the boundary and that $u_y = 0$; this implies that no boundary layer develops. Due to this boundary condition, both the inlet flow velocity and the average channel velocity before the streamer are identical and equal to U_0. The slip boundary condition is

selected to reduce the domain size, which is necessary to avoid the adjacent wall interferences in calculating the forces. At the outflow ($x = L_x$), the zero pressure and no viscous forces boundary condition is applied. In addition, the no-slip condition is imposed on the circular base of the streamer: $u_x = 0$, $u_y = 0$.

Drag force and drag coefficients

When a fluid flows past a body, forces that occur at the body-fluid interface are (i) tangential (shear) stresses and (ii) normal stresses, which are a function of position. If we integrate the forces over the surface of the body, the resultant in the direction of the upstream flow is called drag. The force exerted depends on the object shape (and its possible deformations), fluid velocity and fluid properties. In water, drag can be decomposed into two different forms: skin friction (viscous drag) and pressure drag. Skin friction exists due to the interaction of the surface of an object with fluid; pressure drag is due to the difference in pressure between the front and the rear side of a body. The dimensionless drag coefficient C_D is used to compare the drag of objects with different sizes, defined similar to Equation (2.2) as:

$$C_D = \frac{2F_D}{\rho^F U_0^2 A_F} \tag{4.12}$$

where F_D is the drag force, ρ^F is the fluid density, U_0 is the mean flow velocity (equal to inlet velocity due slip boundary condition on the walls) and A_F is the frontal area facing the flow, in this case the diameter d of the streamer base. In our simulations, the drag force is calculated as follows:

$$F_D = \oint_{A_W} (-F_{V,x} + p \cdot n_x)\, \mathrm{d}A \tag{4.13}$$

where, $F_{V,x}$ is the x-component of the viscous force, p is the pressure, n_x is the x-component of the outer normal vector $\mathbf{n}$, and A_w is the outer area of the streamer.

Speed-specific drag

In contrast with rigid bodies, flexible bodies may deform or reconfigure to reduce (or increase) the forces of the fluid acting on them. Besides, the flexible and rigid bodies may have different shapes and sizes, which make it difficult to compare them by drag coefficients only. Hence, a new parameter is needed to emphasize the importance of flexibility (vs. stiffness) regardless of the shape and size, and have a measure for reconfiguration. We call this factor G factor (refer to Vogel, 1994, pp. 116-120; therein termed "E").

For cases of a bluff bodies (e.g., cylinder and sphere) at moderate to high Reynolds numbers the drag varies with the square of velocity, that is $F_D \propto U_0^2$, and therefore, $C_D \propto U_0^0 \propto Re^0$. As a result, if we plot the curve of C_D versus the Re will give us a horizontal line parallel to x-axis; that is the exponent G in Equation (4.14) is zero.

$$C_D \propto \frac{F_D}{U_0^2} \propto U_0^G \propto Re_D^G \tag{4.14}$$

Any deviation from this horizontal line can be a sign indication an unusual behavior of a bluff body, e.g., as a result of reconfiguration. If the line in this plot ascends, that is if G is greater than zero, it means that the structure is deforming (reconfiguring) in a way that makes the drag become relatively higher compared to typical bluff bodies. For example, a G value of +1.0 means that the drag is proportional to the cube of velocity, rather than to the square. However, a line with negative slope (a negative G value) indicates that the drag will be less for the structure at faster flows, compared to bluff bodies. Hence, by plotting F_D/U_0^2, termed "speed-specific drag", versus the flow velocity U_0 and measuring the slope of the curve, we can predict the drag performance of the body in fast flows (Vogel, 1994, pp. 116-120).

4.2. Mass transfer enhancement in moving biofilm structures

Substrate transport model description

Many physical, chemical and biological processes act simultaneously in biofilms with orders of magnitude difference in time and spatial scales. The biofilm is,

for example, exposed to different forces by the liquid flow, internal mechanical stress develops leading to deformations and eventually to biofilm detachment, solutes are transported by convection and diffusion, solutes are converted in multiple reactions with very different rates, then microbial cells can grow, divide and be transported in the biofilm, while extracellular polymers are excreted. This model assumes only the very fast processes with relaxation times in the order of seconds or less (Picioreanu et al., 2000a), characteristic for a relatively thin biofilm streamer ($\sim$100 µm). Therefore, although the very fast fluid dynamics, biofilm deformations and substrate transport with reaction are calculated from time-dependent equations, the slow biofilm development processes are ignored and the biofilm neither grows nor do biomass patches detach.

Drag and lift forces deform the flexible structure and in return the structure also changes the flow conditions, since the walls bounding the fluid domain are moving. This fluid-structure interaction is modeled by coupling the Navier-Stokes equations of fluid motion with the structural dynamics of the biofilm and solving the equations simultaneously. In nature, biofilms behave as viscoelastic materials (Shaw et al., 2004) (i.e., they show elastic solid-like response in short time-scales and viscous fluid-like response in long time-scales). However, due to the very small time scales studied in this work (<2 s), we assume an elastic material model for the biofilm streamers. Further, the mass transfer is modeled by solving the dynamic convection-diffusion-reaction equations using the actual flow velocities calculated from Navier-Stokes equations. The arbitrary Lagrangian–Eulerian formulation for fluid domain is employed to account for the mutual deformation of fluid and solid at their interface (Section 4.1). The following sections will describe the model details and its numerical implementation.

Substrate transport model domain

The two-dimensional (2-d) biofilm streamer shown in Figure 4.2, with geometrical and mechanical specifications analogous to the model developed in Section 4.1, is subjected to a range of flow conditions similar to those consid-

ered in the experimental settings of (Stoodley et al., 1998)[1] . We considered this 2-d model simplification because an accurate solution of the equivalent three-dimensional (3-d) problem is intractable with our current computational resources. Nevertheless, we believe that also the obtained 2-d results provided very significant insight and could guide the development of much more computationally intensive 3-d models in future.

The flow domain is a rectangular channel, with length L_x in the main stream direction, x, and width L_y in the side stream direction, y (Figure 4.2).

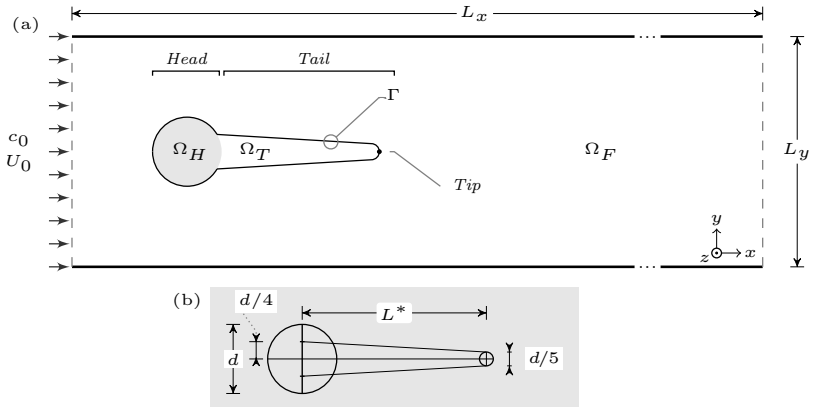

Figure 4.2.: (a) Schematic representation of the two-dimensional sub-domains and boundary conditions: Ω_H, biofilm head sub-domain; Ω_T, biofilm streamer tail sub-domain; Ω_F, fluid sub-domain; Γ, interface between biofilm and fluid. At the inlet boundary c_0 is the constant inlet substrate concentration and U_0 the fluid velocity. The center of Ω_H is located at $x = y = 1.5 \times 10^{-3}$ m. (b) Geometric construction of the biofilm streamer.

Similar to Section 4.1, depending on the physics equations solved, the computational domain is partitioned in a few sub-domains, in which different sets of equations are applied. For the fluid-structure interaction, the domain consists of three non-overlapping computational sub-domains: the circular

[1]The main difference between the model domain in mass transfer simulations (current section) and the drag simulation ones described in Section 4.1 is that the previous domain geometry does not include the biofilm head section Ω_H in the description of the model, and is removed from the geometry, while the current one does include the head section. Also the tail is defined differently; that is L^* and L are not identical.

biofilm colony head Ω_H, the biofilm streamer tail Ω_T and fluid Ω_F. The whole biofilm domain is the union $\Omega_B = \Omega_H \cup \Omega_T$. We define the whole interface Γ between the biofilm and the fluid as $\Gamma = \Gamma_{FSI} \cup \Gamma_{CD}$, where $\Gamma_{FSI} = \Omega_F \cap \Omega_T$ and $\Gamma_{CD} = \Omega_F \cap \Omega_B = \Gamma_H \cup \Gamma_{FSI}$ (with Γ_H the head surface). Γ_{FSI} is the fluid-structure interaction interface (because only the biofilm tail is mobile) and Γ_{CD} the mass flux continuity interface (because the whole biofilm consumes soluble substrate). The parameters used in current work are listed in Table 4.2.

Table 4.2.: Model parameters used in simulations of substrate transport and uptake in moving biofilm streamers.

Parameter	Symbol	Value
Fluid-structure interaction		
Liquid density*	ρ^F	$1000\ \mathrm{kg \cdot m^{-3}}$
Liquid dynamic viscosity*	μ^F	$10^{-3}\ \mathrm{kg \cdot m^{-1} \cdot s^{-1}}$
Biofilm density†	ρ^S	$1000\ \mathrm{kg \cdot m^{-3}}$
Biofilm Young's modulus‡	E^S	1000 and $4000\ \mathrm{kg \cdot m^{-1} \cdot s^{-2}}$
Biofilm Poisson's ratio¶	ν^S	0.4
Mass transfer with reaction		
Substrate diffusion coefficient§	D	$2.5 \times 10^{-9}\ \mathrm{m^2 \cdot s^{-1}}$
Substrate uptake rate coefficient‖	k	$0.03\ \mathrm{mol \cdot m^{-3} \cdot s^{-1}}$
Substrate saturation coefficient**	K	$0.003\ \mathrm{mol \cdot m^{-3}}$
System properties		
Domain length	L_x	1.2×10^{-2} m
Domain height (width)	L_y	3×10^{-3} m
Streamer head diameter††	d	3.33×10^{-4} m
Streamer tail length††	L^*	$4.5 \times d$
Inlet substrate concentration‡‡	c_0	$0.025\ \mathrm{mol \cdot m^{-3}}$
Inlet fluid velocity††	U_0	$0.1, 0.15, \ldots, 0.45\ \mathrm{m \cdot s^{-1}}$

* water, 20 °C; † assumed close to water because biofilms consist of >90 % water; ‡ see section Mass transfer enhancement as a function of flow velocity and biofilm flexibility; ¶ assumed close to rubber; § dissolved oxygen in water at 20 °C, ‖ assumed for oxygen uptake by heterotrophic microorganisms (cf. (Henze, 2000)), with a microbial concentration in the biofilm of $20\ \mathrm{g \cdot L^{-1}}$; ** affinity of heterotrophic microorganisms for oxygen (cf. (Henze, 2000)); †† estimated from (Stoodley et al., 1998); ‡‡ relatively low dissolved substrate concentration, here 10 % of oxygen saturation in water in contact with air.

Fluid-structure interaction

The formulation and implementation of fluid-structure interaction is described in detail in Section 4.1. Unlike Section 4.1 where the sub-domain Ω_H was excluded from the FSI calculations, here fixed constraints are applied to Ω_H whereas Ω_T is free to move. Γ_{FSI} is the boundary where the effective coupling of fluid-structure interaction is enforced (see Figure 4.2) so that the fluid at Γ_{FSI} moves with the same velocity as the walls of the biofilm structure. In addition, the dynamic continuity of stresses also applies on Γ_{FSI}. At all other boundaries of the domain the mesh movement is set to zero in all directions.

The transient solution of the FSI sub-model describes the unsteady liquid flow and the movement of the biofilm streamer boundaries in time. The FSI model provides the basis for the unsteady solute mass transfer sub-model presented in the following section.

Substrate transport: convection-diffusion

The mass transfer model couples the convection-diffusion transport of solute in the liquid sub-domain Ω_F, solved on moving mesh frame (spatial coordinates), and the diffusion-reaction solute mass balance in the biofilm sub-domain Ω_B, solved on material coordinate frame (fixed coordinates) in order to minimize the numerical interference of the stabilization algorithm.

Assuming transport of diluted chemical species through diffusion and convection in the fluid sub-domain, the mass balance equation on Ω_F states:

$$\left.\frac{\partial c}{\partial t}\right|_{\boldsymbol{\chi}} = -(\mathbf{u}-\mathbf{u_G})\cdot\nabla c + \nabla\cdot(D\nabla c) \tag{4.15}$$

where c is the solute (here substrate) concentration, D the diffusion coefficient, $\mathbf{u}$ the liquid velocity field vector and $\mathbf{u_G}$ the moving mesh velocity. The velocity term $\mathbf{u}$ is obtained from the solution of Navier-Stokes equations and $\mathbf{u_G}$ from the solution of ALE equations, both solved in FSI sub-model (see Section 4.1 for details).

In the biofilm sub-domain Ω_B the diffusion-reaction equation reads:

$$\left.\frac{\partial c}{\partial t}\right|_{\mathbf{X}} = \nabla \cdot (D \nabla c) + R \tag{4.16}$$

The substrate consumption (reaction rate R) is assumed to follow a simple Monod kinetics:

$$R = k \frac{c}{K + c} \tag{4.17}$$

where k is the reaction rate constant and K is the half-saturation concentration of substrate. Certainly, other reaction schemes and rates as well as multiple solute components can be easily included to describe more complex systems. We also assumed here for simplicity of the model analysis that the diffusion coefficient in biofilm is equal to that in the liquid.

The inlet boundary is set to $c = c_0$ assuming a constant substrate inlet concentration. The outlet boundary imposes a zero diffusion flux, assuming that convection is the dominating process carrying the substrate outside the domain, so that $\mathbf{n} \cdot (D \nabla c) = 0$. On the Γ_{CD} boundary continuity conditions were set both for concentrations and also for fluxes. The rest of the boundaries are insulated so that there is no flux of solute (no-flux boundary condition).

In the present study, the time-dependent calculations were started from the converged steady-state solutions of flow field and substrate concentration in the immobile biofilm configuration (Figure 4.2).

Mass transfer enhancement and Sherwood number

In order to quantify the mass transfer enhancement of oscillating biofilms, the dimensionless Sherwood number (*Sh*) is used. The local Sherwood number *Sh* is calculated in each point at the biofilm surface Γ_{CD} as (Deen, 1998):

$$Sh = \frac{k_m \cdot L_{ch}}{D} = \frac{L_{ch} \cdot \left.\frac{\partial c}{\partial n}\right|_{\Gamma_{CD}}}{(c - c_0)} \tag{4.18}$$

where L_{ch} is a characteristic length, k_m is the local external mass transfer coefficient, c is the local concentration of solute, c_0 is the concentration of solute in the bulk fluid (i.e., far away from the biofilm, here equal to the inlet concentration) and n is the normal direction to the biofilm surface. The characteristic

length for the mass transfer could be defined as $L_{ch} = 4A_B/P_B$ similar to the hydraulic diameter of the structure, where A_B and P_B are the surface area and wetted perimeter of the 2-d biofilm structure, respectively. Within the finite element model solution, the gradient of concentration normal to the biofilm surface was calculated from the value of net local solute flux j at the interface Γ_{CD}:

$$\left.\frac{\partial c}{\partial n}\right|_{\Gamma_{CD}} = \frac{j|_{\Gamma_{CD}}}{-D} \tag{4.19}$$

In order to compare the mass transfer in different system configurations a spatially averaged Sherwood number, $\overline{Sh}$, is calculated around the perimeter of the whole biofilm structure (Γ_{CD}):

$$\overline{Sh} = \frac{\int_{\Gamma_{CD}} Sh \, \mathrm{d}s}{\int_{\Gamma_{CD}} \mathrm{d}s} = \frac{\bar{k}_m L_{ch}}{D} \tag{4.20}$$

where $\bar{k}_m$ is the spatially averaged external mass transfer coefficient, and ds is differential length on the streamer-liquid interface Γ_{CD}. In the same way, an average $\overline{Sh}_{tail}$ can be calculated for the tail section only (Γ_{FSI}).

The mass transfer enhancement $\Delta\overline{Sh}$ is expressed by the relative increase of $\overline{Sh}$ in the oscillating streamer case (transient calculations), when a quasi steady-state has been reached (denoted by $\overline{Sh}_t$) relative to the Sherwood number in static conditions $\overline{Sh}_0$ (stationary calculations), thus $\Delta\overline{Sh} = (\overline{Sh}_t - \overline{Sh}_0)/\overline{Sh}_0$. $\overline{Sh}_t$ is calculated by averaging the $\overline{Sh}$ in time using a sufficiently large time interval once the $\overline{Sh}$ has reached a quasi steady-state oscillation.

4.3. Model solution

Fluid-structure interaction

The equations governing the flow and the displacement of the biofilm structure are solved with a monolithic FSI approach, where the equations governing the fluid flow and the displacement of the structure are solved simultaneously using a single solver. BACI, a finite element code developed by INSTITUTE

FOR COMPUTATIONAL MECHANICS at TECHNISCHE UNIVERSITÄT MÜNCHEN (Küttler et al., 2010) is used to simulate the FSI aspects of biofilm mechanics. The computations are done on an ALE mesh using 9560 triangular mesh elements, yielding 83702 degrees of freedom. The maximum time step used by the solvers was $10^{-4}\,s$. For details regarding the FSI implementation and solution procedure refer to Küttler and Wall (2008), and Küttler et al. (2010).
The simulations were performed on AMAZON EC2 cloud servers (High-CPU Extra Large Instance, 8 virtual cores, 3GHz each). The simulation times were up to 15 hours per second of simulations for high frequency oscillations.

Mass transfer

Solution strategy The model equations governing the unsteady two-dimensional flow, the displacement of the biofilm structure and the solute concentration fields were solved based on a stabilized Galerkin finite element method, implemented in COMSOL MULTIPHYSICS v4.1 (COMSOL, Burlington, MA).

We used a sequentially coupled solver arrangement for both the steady-state (static biofilm) and the transient (moving biofilm) problems. In one time step of the transient solution, first the FSI fields (liquid flow velocity $\mathbf{u}$, pressure p, and the biofilm deformation) are solved monolithically until the tolerances are satisfied (see Section 4.3). Second, the solute concentration field c is solved using the calculated flow field of the first step.

The simulations were performed on a workstation with 4 AMD Opteron 6174 processors (48 cores) and 256 GB RAM. The simulation times were up to 6 days per second of each simulation at the optimal mesh size, when the numerical code was running on 4 cores with $\sim 4.6 \times 10^5$ degrees of freedom for the standard case. For stability, the time steps were restricted to maximum 5×10^{-4} s. Additionally, the solver took the necessary smaller time steps where required to resolve the fast system changes. The relative tolerance was set to 10^{-3}, and the scaled absolute tolerance to 10^{-5} for all variables, where each field variable was scaled to its representative value (e.g., displacements were scaled by a factor of 10^{-5}).

Mesh convergence studies In order to obtain reliable and accurate results, we found that it is important to choose very carefully the size and distribution of finite element mesh, as well as the length and width of the computational domain. In the present study detailed mesh studies were carried out, where different mesh sizes for the domain Ω_F and biofilm-liquid boundary Γ_{CD} were investigated. The goal was to achieve mesh-size independence, while keeping some optimal simulation costs in terms of run times and memory requirements. Also, special care had to be taken with meshes around the moving parts because due to large structure deformations extremely small mesh sizes would lead to early mesh quality depreciation (and even to fatal mesh element inversions).

As the scope of this work was to investigate the enhancement of mass transfer caused by biofilm movement, the overall Sherwood number $\overline{Sh}$ was chosen as one of the criterion for mesh convergence. Based on the results presented in Figure 4.3a, we concluded that a maximum mesh size of 5×10^{-6} m on the biofilm-liquid boundary Γ_{CD} is sufficiently fine to resolve the flow and mass transfer fields. In addition, maximum mesh size of 6.67×10^{-5} m was selected for the rest of the domain following a similar analysis. These mesh sizes have been used in all computations reported in this work.

The streamer lays in a non-homogenous concentration and flow gradients. Hence, in addition to the global mesh study we performed the local mesh studies based on the local sherwood number, *Sh*. Figure 4.4a demonstrates the magnitude of *Sh* on the perimeter of the streamer (arc length) using different mesh sizes. The highest variation is on the edge region of the plot corresponding to the left side of the circular head (Ω_H) which faces the flow directly, and thus the thinnest boundary layer forms around it. Figure 4.4b shows a close-up of this region, where the maximum mesh size selected also conforms to the selected mesh based on the overall Sherwood number, $\overline{Sh}$.

In order to optimize the minimum number of mesh elements that can produce a reliable result we used a hybrid mesh, which is a combination of boundary layer mesh around the boundaries with very high substrate and flow gradients (around the streamer body) and triangular mesh in the remaining parts of the domain (Figure 4.3b). Boundary layer mesh elements, i.e., the highly anisotropic linear elements along the boundaries, were generated around the

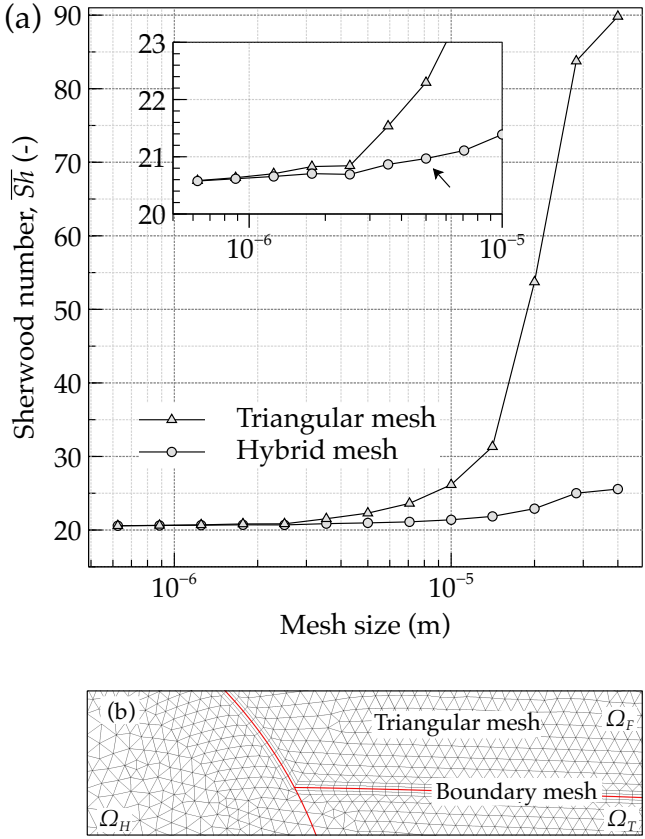

Figure 4.3.: (a) Mesh size convergence studies for the boundary Γ_{CD} with respect to the *overall* mass transport number $\overline{Sh}$ over the whole biofilm. The arrow shows the maximum boundary mesh size selected throughout the simulations: 5×10^{-6} m. (b) Example of the hybrid mesh around the biofilm-liquid boundary Γ_{CD}.

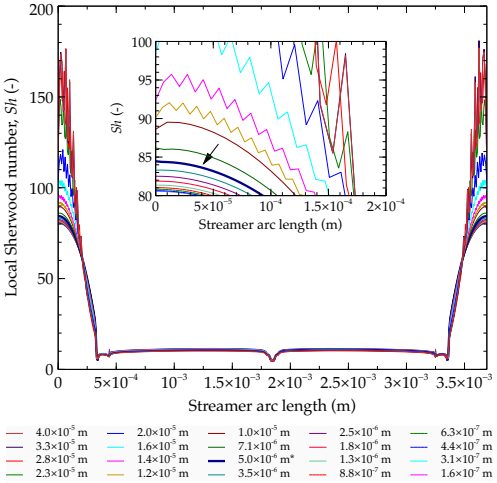

(a) Local profile of *Sh* along the streamer arc length. The arrow shows the maximum boundary mesh size selected throughout the simulations.

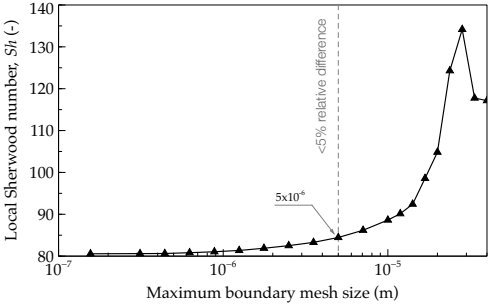

(b) Close-up of the region with the highest variance of *local* Sherwood number, *Sh*, with respect to different mesh sizes. The bold line highlights the maximum boundary mesh size selected throughout the simulations.

Figure 4.4.: Mesh size convergence studies for the boundary Γ_{CD} with respect to the local mass transport number *Sh* along the perimeter of the biofilm.

interface Γ_{CD}. A first order free triangular mesh (constructed using advancing front technique) is used for the rest of the sub-domains.

5

Results and discussions

Table 4.1 and 4.2 summarize the parameters used in the simulations and the characteristics of the streamer studied throughout this work. The Young modulus, the measure for streamer elasticity, is chosen in the range of the values reported by (Stoodley et al., 1999d; Aravas and Laspidou, 2008) and (Körstgens et al., 2001a) (see Table 2.1).

Initially, the model simulation results are analyzed from two perspectives: (i) the effect of the streamer on the flow characteristics and vice-versa, as well as (ii) the influence of the flow-induced vibrations on the stress inside the streamer.

Next, we address the initial hypothesis proposing possible enhancement of substrate transfer to oscillating biofilm streamers. Therein, three aspects are discussed : (i) the general characteristics of a flexible structure oscillating in the liquid flow in relation to solute mass transfer, (ii) the overall effect of the biofilm flexibility on the enhancement of mass transfer at different flow rates, and (iii) comparison of two biofilms having different elasticities to evaluate the relative contribution of structural flexibility on substrate transport.

5.1. Oscillation mechanism of biofilm streamers

When flow past the streamer generates a pattern of swirling vortices in the wake region (the well-known von Kármán vortex street), periodic shedding of these vortices from the surface of the streamer body induces periodic pressure variations on the structure (Figure 5.1). Despite using a laminar flow model, our simulations show that the streamers begin to oscillate due to formation of these vortices in a specific range of Reynolds numbers between 60 and 80 (see Lewandowski and Stoodley, 1995 for a discussion on the validity of laminar flow assumption).

A series of snapshots showing the transient movement of the ALE mesh is shown in Figure 5.2A. Starting from the rest configuration ($t = 0$), the flow develops and finally reaches a periodic stage with regular oscillations in the flow pattern. Vortex shedding makes the streamer vibrate, as it can be seen from Figure 5.2B. Figure 5.3A shows the amplitude and frequency of the oscillations in the streamer tip position, starting after a certain time and reaching a steady oscillatory pattern. Vortex shedding causes the drag force F_D to oscillate as well (Figure 5.3B). The streamer reaches a quasi steady-state oscillation pattern, in which the amplitudes, frequencies and average drag remain periodically unchanged.

5.2. Oscillation characteristics of biofilm streamers

Stoodley et al. (1998) investigated the behavior of streamers in high flow velocities of up to 50.5 $\mathrm{cm} \cdot \mathrm{s}^{-1}$ ($Re \approx 3351$). The path of motion of the streamers was visualized by staining the biofilm with neutral density fluorescent latex spheres and time exposed fluorescent images were taken to show the range of streamer motion. Amplitude and frequency of streamer oscillations are the two most important characteristics studied in this section.
Figure 5.4 compares the maximum amplitudes of the streamer vibration calculated numerically with those experimentally measured. Similar to the experimental results, the streamer started to oscillate only for Re_D larger than a specific value, and the amplitude of oscillations reached a plateau value.

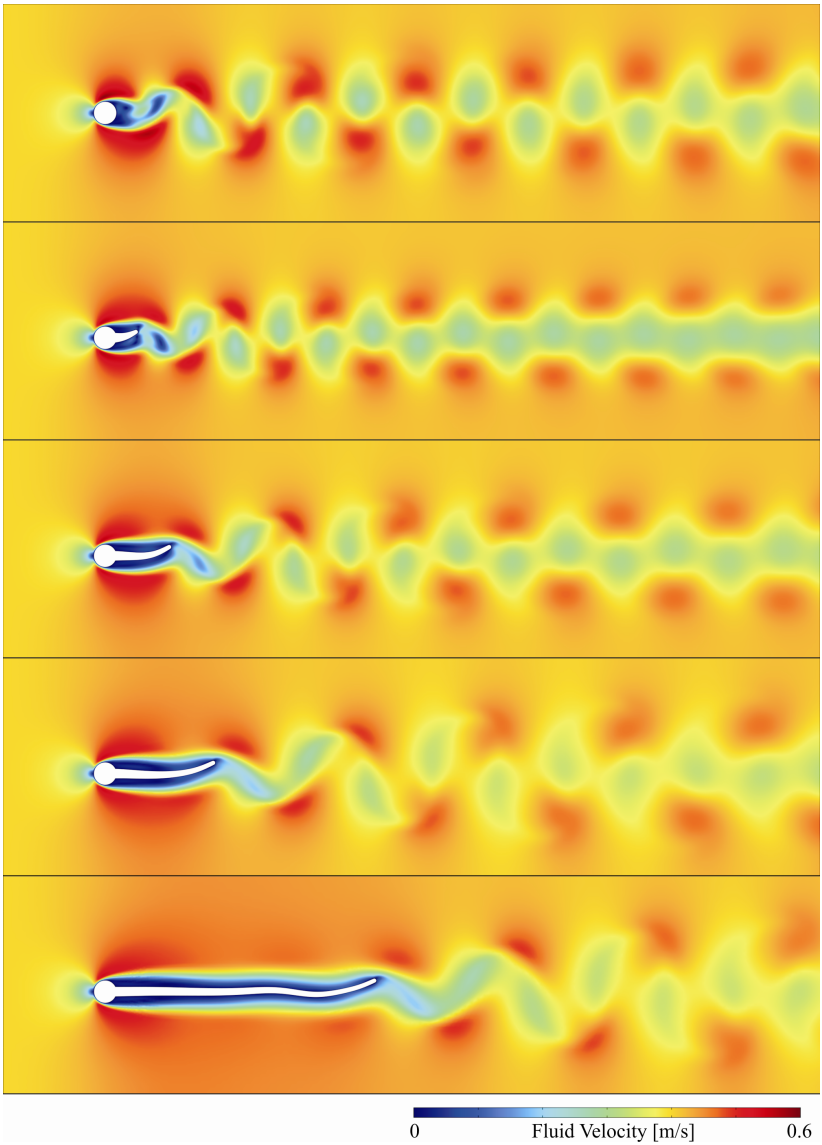

Figure 5.1.: Flow patterns behind biofilm streamers of different lengths. The motion of the tail is upward. L/d ratios are 0, 1, 2.5, 4.5 and 11, ordered descending. Inlet velocity is $0.4\,\mathrm{m}\cdot\mathrm{s}^{-1}$ ($Re_D = 133$).

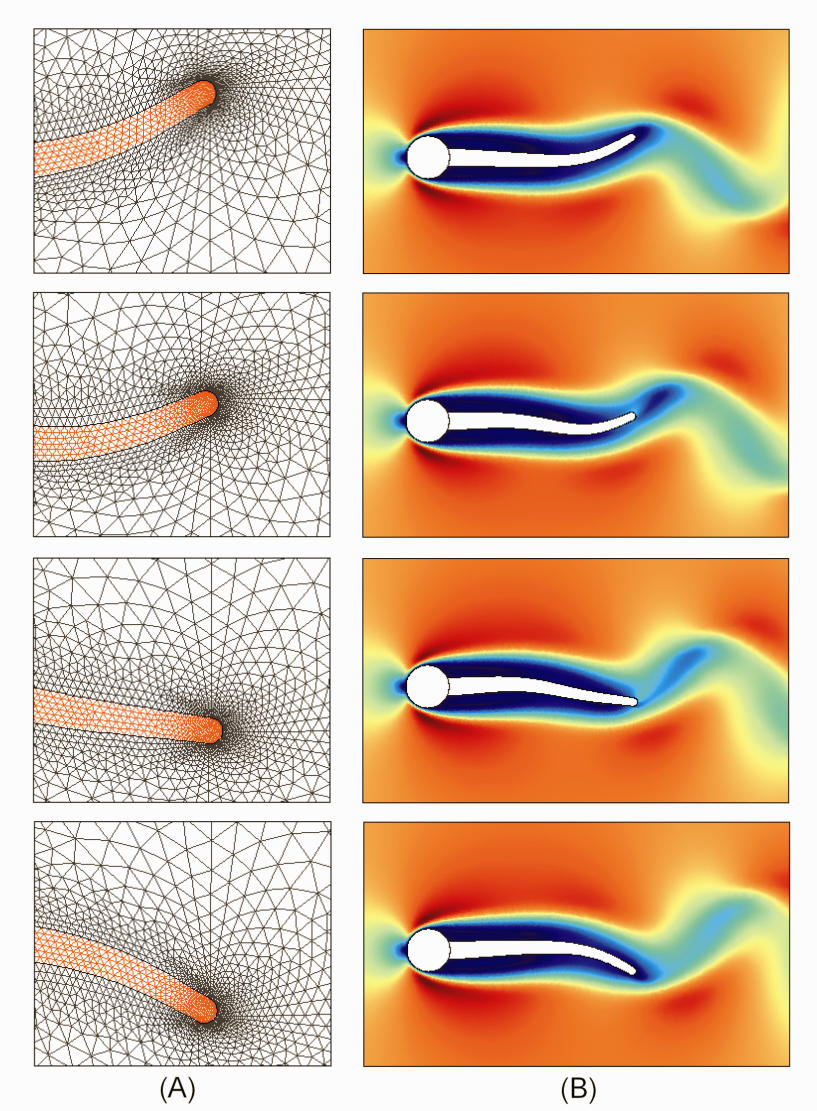

Figure 5.2.: (A) Snapshots of the ALE mesh movement, (B) Snapshots of the velocity field and the streamer oscillation in half a period. The highest velocity is $0.546\ \mathrm{m \cdot s^{-1}}$ (red) and the lowest is $0\ \mathrm{m \cdot s^{-1}}$ (blue). Here $L/d = 4.5$, $U_0 = 0.4\ \mathrm{m \cdot s^{-1}}$ ($Re_D = 133$) and the time between each snapshot is 1×10^{-4} s.

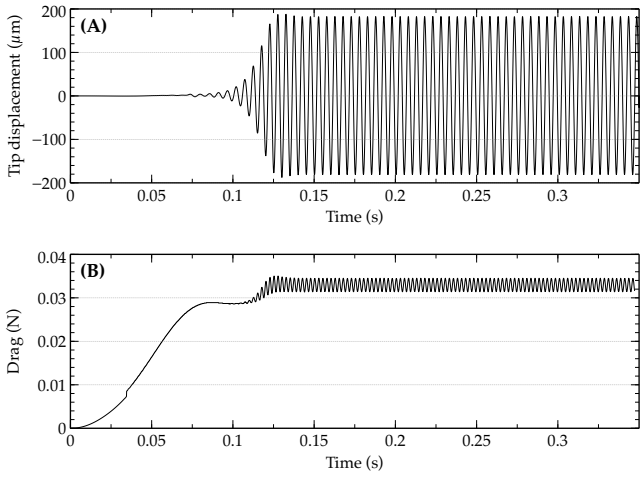

Figure 5.3.: (A) Transient displacement of the streamer tip in y-direction, (B) Drag force in time. Parameters used: $L/d = 4.5$, $U_0 = 0.4\,\mathrm{m \cdot s^{-1}}$ ($Re_D = 133$)

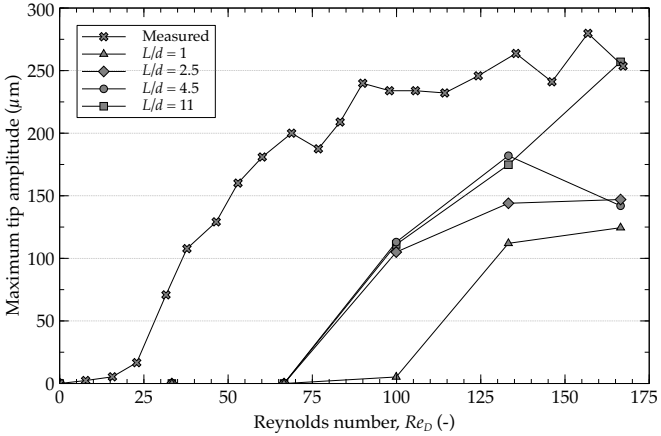

Figure 5.4.: Maximum amplitudes are plotted versus Reynolds number. The measurement data are reproduced from the experiment by Stoodley et al. (1998). Here, the diameter of the streamer, d, is used as the characteristic length in calculating the Reynolds numbers.

The value of the critical velocity at which vortex shedding begins depends on the shape as well as the size of the biofilm cluster. A larger biofilm characteristic length, here the diameter d of the circular head, translates to a higher Re_D number, which implies that the onset of oscillatory behavior shifts to slower flows. Slowly increasing the velocity, the larger biofilm clusters start to shed vortices earlier.

To obtain the frequencies of streamer oscillation, the displacements of the streamer tips were used for time-domain analysis using Fast Fourier Transform method (FFT, refer to Section A.6 for the algorithms used). For the circular base without tail, the frequencies were extracted from the drag force oscillations measured on boundaries of the circular base. Figure 5.5A shows the frequencies of vortex shedding for a circular base and various streamer lengths. It can be observed that when the flow velocity is increased (larger Re_D), the frequency of streamer oscillation and vortex shedding increases as well, which is in agreement with the experimental observations.

The periodic flow is characterized by the Strouhal number, that is, the dimensionless frequency of the oscillations, defined in Equation (2.1) as follows:

$$St = \frac{f \cdot L_{ch}}{U_0} \tag{5.1}$$

where f is the frequency of flow oscillations, L_{ch} is the characteristic length (here the base diameter d), and U_0 is the mean velocity of fluid passing the body (here equal to the inlet velocity). Figure 5.5B presents the calculated Strouhal number versus Re_D derived from our simulations. The Strouhal number can be used together with the object size and fluid velocity to predict the frequency of vortex shedding.

The oscillation of an object induced by vortex shedding might have considerable consequences, e.g., breakage, when the object is flexible and the rate of shedding is close to some natural oscillatory frequency of the object (Vogel, 1994). In our simulations, the natural frequency of the biofilm streamer was occasionally in the vicinity of vortex shedding frequencies which, together with complex wake interactions, can partly account for the irregular behavior of the streamer in some simulations and also the sloughing events in the ex-

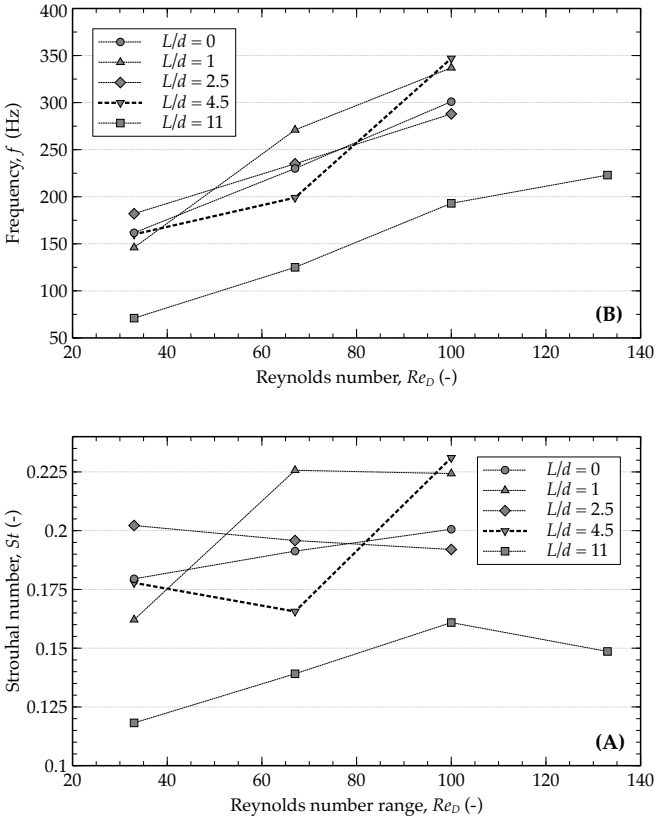

Figure 5.5.: (A) Frequencies of vortex shedding and oscillation of the streamers, with and without tail. (B) Strouhal numbers. $L/d = 0$ represents the circular base without a tail.

periment. The natural frequencies calculated using eigenfrequency analysis of the streamer tail for L/d ratio of 4.5 were approximately 28.8, 129.4, 317.2, 484.7 Hz.
Several factors have strong effects on the deviation of the simulation results from the experimental results, apart from measurement errors. The assumed material properties, local turbulence effects, outlet boundary condition and 2-d assumption are few of these factors. In addition, our simulations were focused on a single streamer, while flexible bodies in the actual environment may interact with each other (Ristroph and Zhang, 2008). Nevertheless, the case of biofilm streamers in flow is a three-dimensional problem and a 3-d model is required to investigate further aspects such as presence of the substratum in future.

5.3. Effect of streamer length on drag

Furthermore, this work investigated the effect of the special streamer form, here correlated to length, on the overall biofilm drag. Figure 5.6A shows the drag coefficients for various streamer lengths and flow velocities. At low flow velocities ($Re_D = 33$), the drag increased with the tail length. However, at high flow velocities, where the pressure drag becomes more significant, the streamer tail helped to streamline the body and reduce the drag. Remarkably, there was a maximum 23 % drag reduction by a streamer tail ($L/d = 4.5$) compared to the circular biofilm base without a tail, at the highest flow velocity used for simulations ($Re_D = 167$).
In addition, to measure the effect of the streamer flexibility and reconfiguration on drag at higher flow velocities, the G parameter related to speed-specific drag was calculated. For the circular base, the value of the calculated G ($G = -0.24$) is close to the experimental value reported in literature for cylinders in Re_D range of 10 to 120 ($G = -0.29$; Vogel, 1994, Table 6.1 therein). Figure 5.6B shows that at Re_D larger than 133, the circular shape ($L/d = 0$) has a G value close to zero, as expected from the rigid bodies. The lowest G value corresponds to $L/d = 4.5$, where it experiences the lowest drag scaling compared to rigid bodies. To be specific, the drag of a streamer with $L/d = 4.5$ ($G = -0.46$, $Re_D = 133 - 167$)

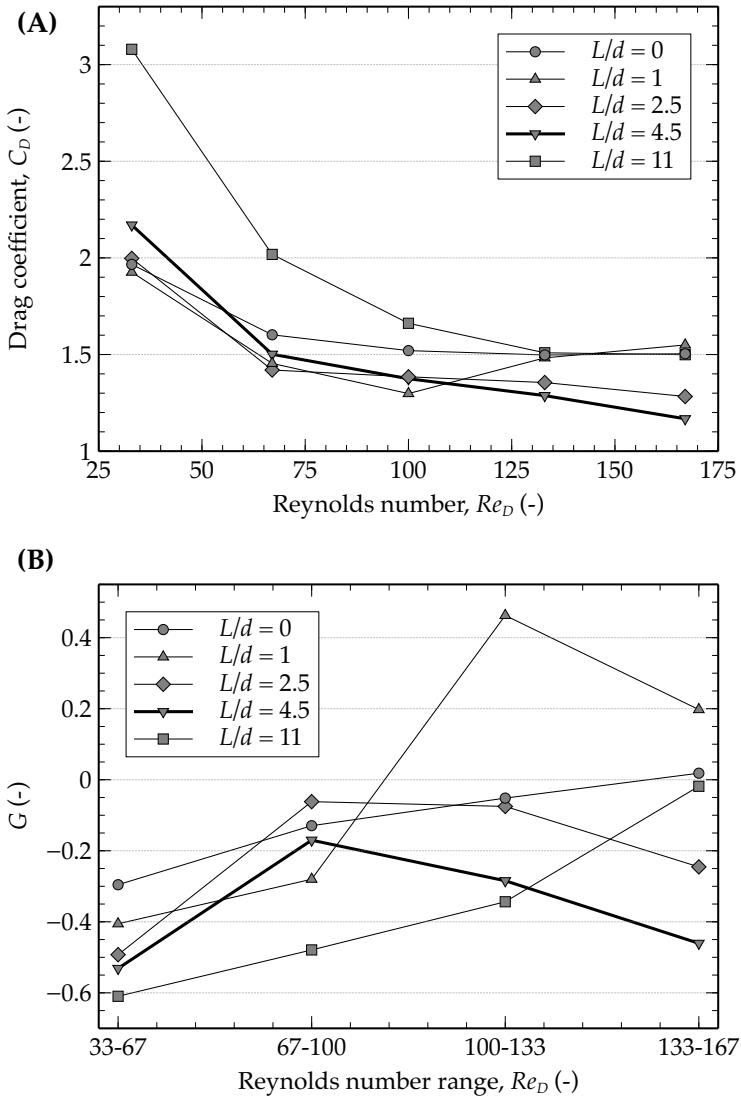

Figure 5.6.: (A) Drag coefficient of streamers versus Reynolds number. (B) G values related to speed-specific drag versus the Reynolds number ranges. Here $L/d = 0$ represents the circular base without a tail.

increases by the power of 1.54 with respect to the flow velocity, in contrast to the power of 2 for the circular case ($L/d = 0$). Hence, it is expected that at higher flow velocities ($Re_D > 133$), the streamer with L/d ratio of 4.5 will experience the lowest drag with the increase of flow velocity amongst others. The drag coefficient of the streamer with L/d ratio of 11 is found to be close to the drag coefficient of the circular base ($L/d = 0$) at the highest flow velocity studied. This shape also exhibits a G value close to zero at high flow velocities ($Re_D > 133$). Thus, there is an optimum streamer length to minimize the drag, which in our case is $L/d = 4.5$.

5.4. Effect of streamer elasticity on drag

It has been proposed that the biofilms may actively alter their mechanical properties through modifications to EPS to adapt better to various stress conditions in flow (Hall-Stoodley et al., 2004; Salta et al., 2010). Considering the range of properties considered in this model, the question that arises is how much the mechanical properties of biofilms would affect their living conditions, e.g., on the drag that biofilm streamers experience. To answer this, several simulations with wide range of elasticities and tail to head ratios are numerically simulated (Figure 5.7). As seen in Section 5.3, the streamer growth and formation positively reduces the drag up to an optimum length. Nevertheless, compared to immobile streamers (fixed), the drag of oscillating biofilms are higher at all the flow velocities in contrary to the concept of *going with the flow*. How can a structure that moves with the flow experience higher drag compared to the one that is fixed and does not move? One theory can be that since the structure is moving there is a higher frontal area blocking the flow, and hence there is higher resistance to flow; the less the body moves the less the flow disturbances and as a result less fluid momentum is dissipated at the walls.

Figure 5.8 shows the relative increase of the drag compared to an immobile case, where there are increases of up to 60%. So, the oscillating streamers have significantly higher drags compared to the immobile ones, so why is the benefit then to form streamers? Looking closer to Figure 5.7, the drag coefficients of oscillating streamers are mostly in the region between an immobile streamer

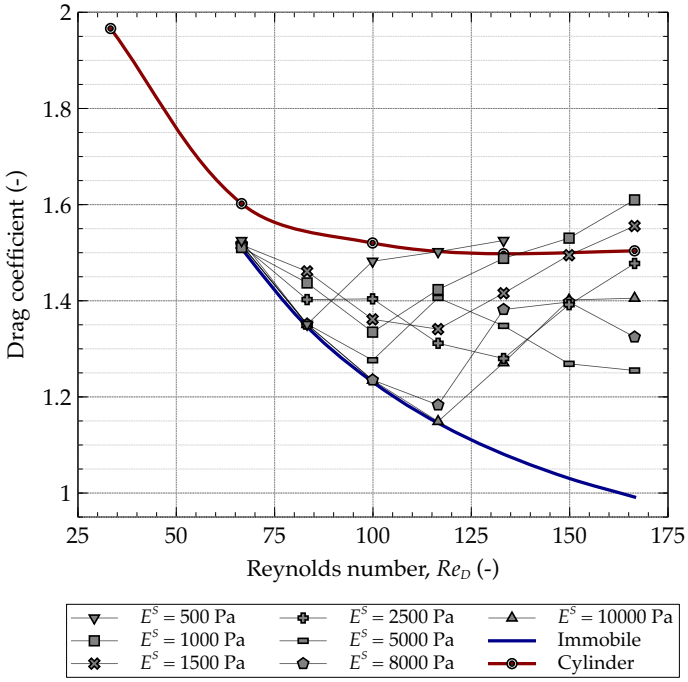

Figure 5.7.: Influence of flexibility of biofilm streamers on drag for the case of $L^*/d = 4.5$.

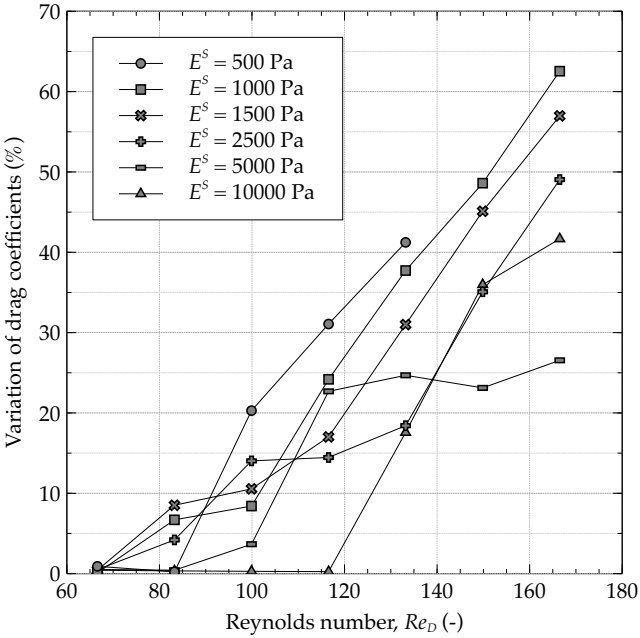

Figure 5.8.: Increase of drag coefficients of biofilm streamer with $L^*/d = 4.5$ caused by the oscillations compared to the immobile case.

and cylinder. Hence, the outcome is that the streamer formation reduces the drag, but the drag reduction is more significant if the material is less flexible.

5.5. *Effect of streamer density on drag*

The effect of density on drag was also investigated. However, it was found (see Table 5.1) that the density does not have a significant effect on the oscillating characteristics of the streamer and the drag in the range of common biofilm densities.

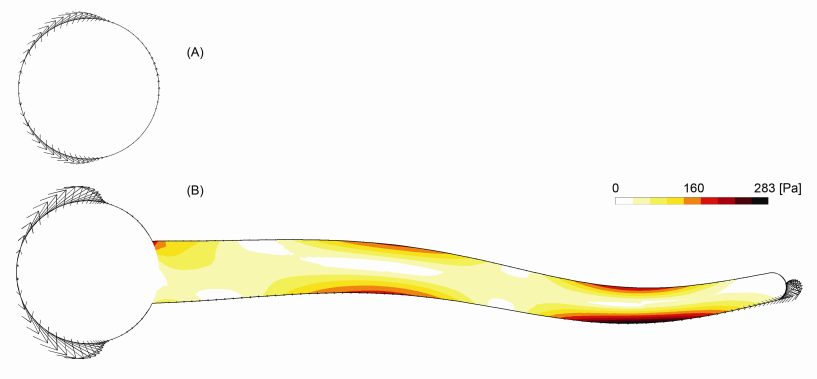

Figure 5.9.: (A) Vectors of nodal fluid shear on the biofilm with $L/d = 0$. (B) Vectors of nodal shear, and contours of Von Mises stresses inside the streamer tail with L/d ratio of 4.5. The inlet velocity is 0.4 $\mathrm{m \cdot s^{-1}}$ ($Re_D = 133$) for both the snapshots. The maximum value of shear for $L/d = 0$ is 33.9 Pa, and 30.9 Pa for $L/d = 4.5$.

Table 5.1.: Effect of biofilm density on the drag and oscillation behavior. The parameters used in the simulation are: $L/d = 4.5$, $U_0 = 0.4\ \mathrm{m \cdot s^{-1}}$ ($Re_D = 133$).

Density ($\mathrm{kg \cdot m^{-3}}$)	C_D (-)	Oscillation Frequency (Hz)	Amplitude (µm)	Strouhal Number (-)
950	1.2838	199.6	169	0.1662
1000	1.2913	199.0	181	0.1658
1100	1.2950	196.9	177	0.1639
1200	1.2988	195.2	182	0.1625

5.6. *Closer look at the forces, stresses and growth conditions*

Besides evaluating the effect of streamer oscillations on the drag, the reverse analysis is also interesting: what could be the effect of flow-induced oscillations on the biofilm streamer itself? Figure 5.9 shows the fluid viscous (shear) forces acting on the body and the stress conditions inside the tail. For the streamers, the highest shear force is experienced at the tip of the streamer and the front side of the base facing the flow. Other sections of the streamer are protected from the fluid shear forces, as seen by force vectors acting on the boundaries. Similarly, the circular clusters without tail ($L/d = 0$) experience the shear force only on the front side downstream of the flow.

Especially, the simulation result presented in Figure 5.9 gives an idea on how hydrodynamic conditions and growth/development of biofilm streamers may interact. As long as substrate is available, the microorganisms will divide and grow. Therefore, they will need space. Growth in the lateral direction (y-direction, and also z-direction in 3-d) will somehow be limited due to exposure to high shear forces and thereby forced detachment (Picioreanu et al., 2001; Horn et al., 2003; Böl et al., 2009). Growth in the y-direction will also decrease the availability of substrate as the diffusion distance will increase with increasing size of the aggregate. Hence, a favorable direction to propagate would be in x-direction behind the base, as it is protected from the shear forces. Moreover, biofilm growth in streamers may also benefit from the enhanced mass transfer due to the flapping movement of the streamer and also the mixing in the wake behind the base. The development of a streamer-like structure oscillating in the flow seems to be a very good strategy for microorganisms to obtain the highest possible supply of substrates out of the bulk phase, while reducing the detachment probability. The increasing stress in the y- (and z-) direction will force the microorganisms to grow in the flow direction and, by doing so, streamer-like structures will develop. This "shear stress induced growth of streamers" hypothesis can be proved using fluid-structure interaction models adapted for biofilm growth (Küttler et al., 2010).

High values of the Von Mises equivalent stress are shown in Figure 5.9 at the bent segments of the streamer as well as where the tail is attached to the base. These regions with stress concentrations are likely to detach, similar to the streamers experimentally observed by Stoodley et al. (1998). As mentioned earlier, streamer structures will have a benefit compared to larger circular structures. But this will only be valid up to a certain ratio of L/d, depending on the internal strength developed by the microorganisms and other factors present such as fluid forces, gravity and flapping space available.

As a final point, achieving the lowest drag itself may not be the foremost reason to form streamers, but can be a strong factor when considering detachment. The simulations presented provide an idea on how the biofilm structures behave in the flow field. Future work should couple fluid-structure interaction, time-dependent material models, mass transfer and biofilm development to

provide better insight into the transient nature of the biofilm lifecycle seen in the experiments. In this respect, numerical tools may help to increase the knowledge, since the lack of methods for reliable measurement of local biofilm dynamics and physical properties is still a challenging problem to date.

5.7. *Effect of oscillatory movement of streamer on substrate transport*

In Section 5.1 we showed that the flag-like flexible biofilm streamers vibrate in the flow due to formation of von Kármán vortices behind the structure. The streamlined shape of biofilms helps reducing the drag when the structure is immobile (see Section 5.4). Conversely, model results suggested that, unfavorably, the streamer oscillation increased the drag compared to the immobile structure. Hence, the question that arises is what biofilm streamers may gain from the oscillations?

To study the effect of the flow-induced vibration (oscillatory movement) on the mass transfer of substrate (i.e., any solute consumed by the biofilm cells) from bulk liquid to the biofilm structure, a biofilm streamer with length to width ratio $L^*/d = 4.5$ was placed in the middle of a rectangular channel subjected to liquid flow. In this standard model case the inlet flow velocity was $U_0 = 0.4$ m/s and the biofilm's Young modulus $E^S = 4000$ Pa.

The steady-state flow and substrate concentration fields were first calculated, keeping the biofilm streamer immobile. For this stationary problem the substrate concentration is presented in Figure 5.10a, the velocity magnitude in Figure 5.10e and a zoomed concentration field in Figure 5.10f. The decrease of substrate concentration in the biofilm is characteristic for diffusion-reaction systems with reactant consumption. The lowest concentrations are in the middle of the streamer along its long axis. Typically, the lowest overall concentration values are present inside the streamer base and gradually concentrations increase towards the narrowing streamer tail.

The steady-state solution was also chosen as initial condition for the time-dependent simulations with unsteady flow and oscillating structure. In the time-dependent (transient) simulation, the streamer started to vibrate after

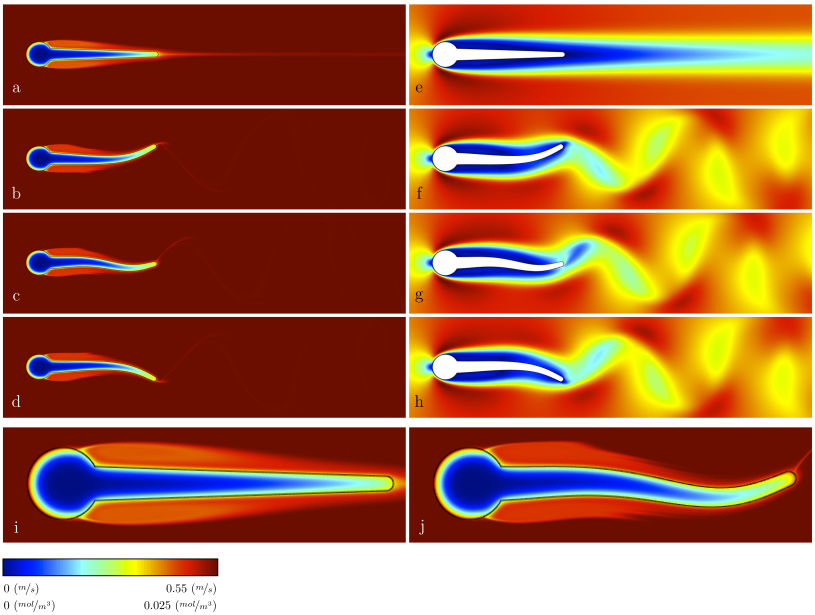

Figure 5.10.: Spatial distributions of soluble substrate concentration and the liquid velocity magnitude: (a) concentration and (e) velocity for immobile streamer; (b-d) concentration and (f-h) velocity in transient conditions, when the streamer tip is moving downwards for half of an oscillation period (0.8137, 0.8149 and 0.8159 s, respectively); (i) and (j) magnified substrate concentration fields for static and moving streamer, respectively, showing the formation of concentration boundary layer.

about 0.08 s. This can be seen in the recorded y position of the streamer tip (Figure 5.11c). The velocity field reveals the formation of a von Kármán alley of vortices (Figure 5.10e-h). Corresponding to these vortices, a dynamic wake of lower solute concentration spreads behind the streamer in a wave-like shape (Figure 5.10b-d and Figure 5.10j). As a consequence of the increasingly stronger streamer oscillations, the mass transfer also gradually increases until an oscillatory quasi steady-state is reached after approximately one second (Figure 5.11a). Typically, the relaxation time of mass transfer towards reaching a stable state in moving conditions is longer ($\sim$1 s, Figure 5.11a, b) than that for reaching stable streamer oscillations ($\sim$0.1 s, Figure 5.11c). The enhancement in mass transfer is quantified by the evolution of the overall Sherwood number in time, shown in Figure 5.11a. The streamer vibration makes the steady-state mass transfer rate to have an oscillatory behavior as well.

The overall mass transfer is enhanced during oscillations compared with the immobile structure case. Initially, when the streamer tail is not moving, $\overline{Sh}_0 = 25.7$. Once vibrating, the $\overline{Sh}$ reaches a maximum of 28.5, which is 11 % increase in the mass transfer for the whole structure due to the movement of the streamer tail. Calculated along the tail section only, the streamer movement can induce an even larger mass transport enhancement of 27 % (Figure 5.11b).

A closer look at the patterns from Figure 5.12 during a few oscillation periods reveals that the mass transfer at different moments in time is directly correlated to the position of the points on Γ and their transverse speed, e.g., streamer tip position and tip movement speed, as shown in Figure 5.12. The maximum mass transfer enhancement (Figure 5.12c) occurs close to the moment when the tip speed is the largest (in absolute value, Figure 5.12b). Consequently, the frequency of Sherwood number oscillations is exactly two times the oscillation frequency of the tip. These observations strongly point to the main cause of mass transfer enhancement when the streamer is moving: the increased relative velocity between liquid and the biofilm structure. In fact, this conclusion is not surprising because a faster fluid velocity (i.e., a higher Reynolds number Re_D) is normally correlated to thinner boundary layers and increased mass transfer coefficients (i.e., higher Sh numbers).

Although it can be expected that the streamer tip will benefit from the move-

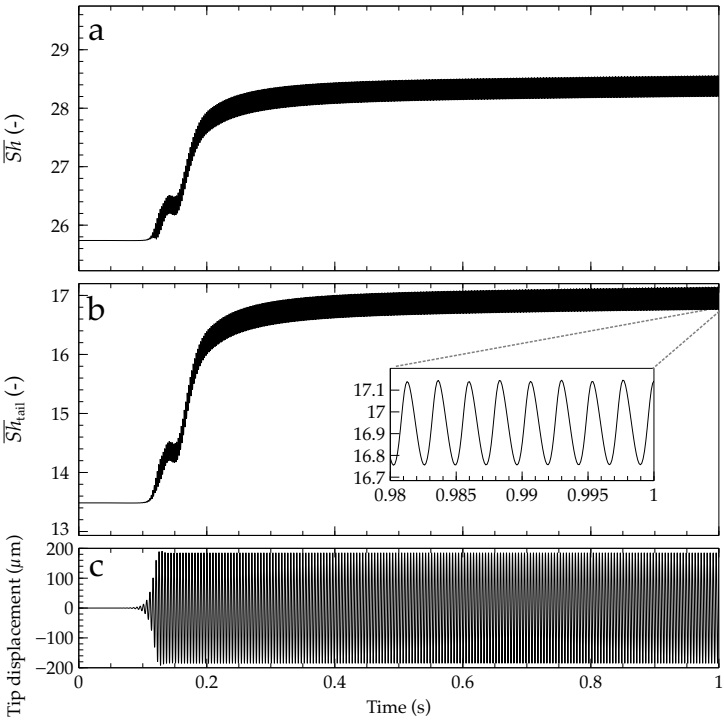

Figure 5.11.: Increase of overall mass transfer when the streamer tail begins to vibrate. (a) Overall Sherwood number, $\overline{Sh}$, increasing from an immobile steady-state ($t = 0$) to the oscillatory quasi steady-state ($t \approx 1$ s). (b) Evolution of the $\overline{Sh}_{tail}$ evaluated only over the streamer tail, from the immobile to oscillatory steady-state. (c) Displacement of the streamer tip in time. Simulation conditions: $E^S = 4000$ Pa, $U_0 = 0.4$ m/s.

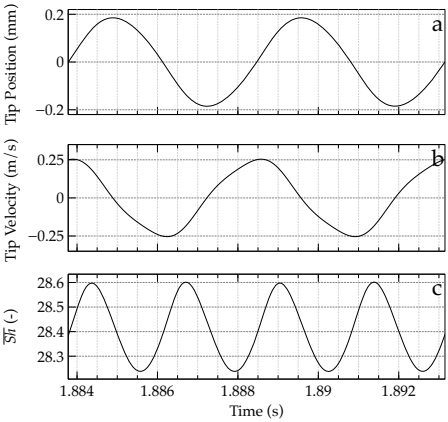

Figure 5.12.: Detailed representation of the streamer oscillation characteristics over a short period of time. (a) Streamer tip displacement; (b) streamer tip velocity and (c) overall Sherwood number, $\overline{Sh}$, during two oscillation periods. The mass transfer number reaches a maximum close to the middle point between the extreme positions of the tip — when also the speed of the tip is at maximum. Simulation conditions: $E^S = 4000$ Pa, $U_0 = 0.4$ m/s.

ment, the question is also how much is the mass transfer enhanced at other positions on the streamer surface. Figure 5.13 shows the local profiles of the concentration, the Sherwood number for the whole streamer body and a detailed *Sh* distribution along the tail section, in static and moving conditions. The maximum local mass transfer ($Sh = 110$) occurs at the streamer base, which is exposed frontally to the flow (sections I-II and VIII-I on Figure 5.13a), however, this value cannot be improved by the tail movement. The mass transfer quickly falls towards a minimum at the fluid boundary layer separation zone (point II on Figure 5.13, visible also in Figure 5.10i, j), where the fluid flow becomes detached from the surface of the streamer head. The mass transfer then starts to increase toward the tip (point V), where along the tail it reaches a relatively stable value of *Sh* between 13 to 14 and 17 to 18 for the static and moving cases, respectively. Figure 5.13c shows the relative enhancement of *Sh* compared to the static case along the streamer perimeter, which demonstrates that the regions close to the tip of the moving structure can experience very

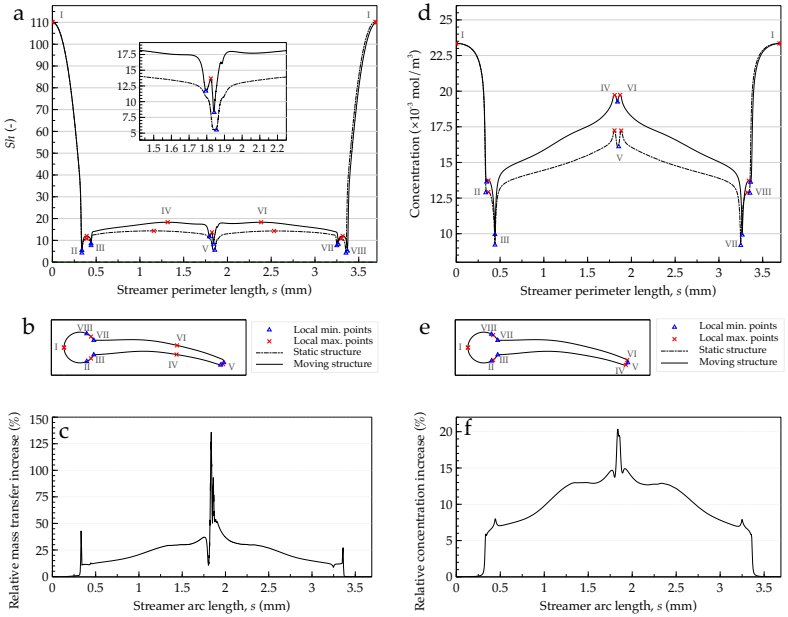

Figure 5.13.: Distributions of local mass transfer (represented by *Sh*) and concentrations over the whole biofilm-liquid boundary and their relative increase in oscillatory conditions with respect to the static case. Values for the static case (dashed lines) are compared along the biofilm outer perimeter, *s*, with those obtained in moving conditions: (a) and (d) Local Sherwood number, *Sh*, and concentration; (b) and (e) places on the biofilm-liquid boundary where the local *Sh* maxima and minima occurred and corresponding locations for concentration extremes; (c) relative increase in the local mass transfer; (f) relative increase in the concentration at the biofilm surface.

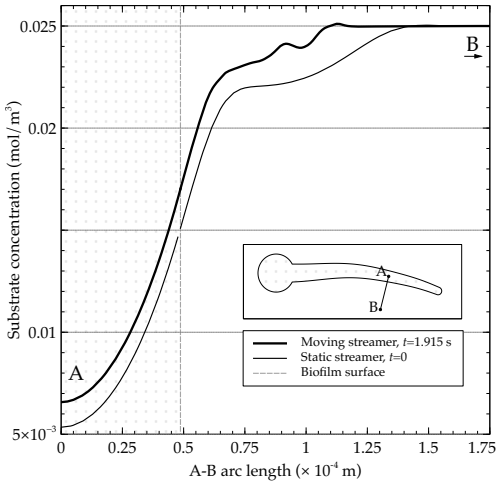

Figure 5.14.: Increase of substrate concentration in the biofilm in moving conditions. Concentration profiles are computed along the line segment A-B, perpendicular to the biofilm surface, as shown in the inset streamer. The tail is moving downward.

significant mass transfer increase of 50 to 135 %. The concentration profile on the biofilm surface (Figure 5.13d), the associated concentration maxima points (Figure 5.13e), and the relative increase in concentration (Figure 5.13f) also exhibit similar trends, with maxima locations even closer to the streamer tip (point V). Hence, it can be concluded that the main contribution to the overall mass transfer enhancement comes from the regions on the streamer tail closer to the tip, along the points IV, V and VI. Moreover, the strongly increased mass transfer near the streamer tip can cause a greater microbial growth in that region. This enhanced growth could lead to a faster elongation of the streamer tail and may constitute one of the causes why streamers actually exist.

The mass transfer increase is also visible from the reduced thickness of the boundary layer near the tail tip in oscillatory conditions (compare Figures Figure 5.10i and j). Figure 5.10j shows a tip which is far better supplied with substrate than it is for the static case. This is further underlined in Figure 5.14, where the boundary layer thickness can be seen clearly for the concentration profiles constructed at the point IV in the direction normal to the biofilm surface.

Although starting from the same c_0 value in bulk liquid, the concentrations for the moving structure are higher in the boundary layer compared with a static streamer. Consequently, also the concentration inside the biofilm remains higher for the moving streamer and could lead to more microbial growth.

5.8. *Mass transfer enhancement as a function of flow velocity and biofilm flexibility*

The effect of flow velocity on mass transfer in oscillating streamers was studied by setting various inlet flow velocities U_0 ranging from 0.1 to 0.45 m/s while keeping other model parameters unchanged. These conditions correspond to Reynolds numbers (Re_D, relative to the streamer head diameter d) between 33 and 150 , calculated as $Re_D = U_0 \cdot d \cdot \rho^F / \mu^F$.

It is well-known that at faster flows the mass transfer is higher due to the thinner concentration boundary layer formed around the structure. For simplified configurations, e.g., forced convection past a cylinder in laminar flow regime, Sh can be approximated as $Sh = f(Re^{0.5}, Sc^{0.33})$, where Sc is the Schmidt number (Khan et al., 2005). For the more complex geometrical structure analyzed in this study, the increase in mass transfer with increased Re_D in static cases deviates from this dependency. Figure 5.15 shows the effect of different flow velocities and movement on mass transfer, with and without the streamer motion. As expected, the Sherwood number of static streamers, i.e., steady-state simulations without movement, increases by increasing the flow velocity, and scales with $Re_D^{0.42}$. However, the oscillating streamers exhibit a different behavior. The higher the velocity the higher the mass transfer increase compared to a static streamer, a 15 to 20 % increase for the whole structure. For $E^S = 4000$ Pa, for example, Sh scales with $Re_D^{0.63}$ and for the more flexible structure having $E^S = 1000$ Pa with $Re_D^{0.74}$ in the interval from $Re_D = 80$ to 150. The mass transfer enhancement is even more pronounced for the tail section (see Figure 5.11b).

Several measurements of mechanical properties of biofilms have produced various results for the elastic modulus E^S (see Lau et al. (2009), Table S2 therein, for a summary). As a result, it has been proposed (Hall-Stoodley et al., 2004;

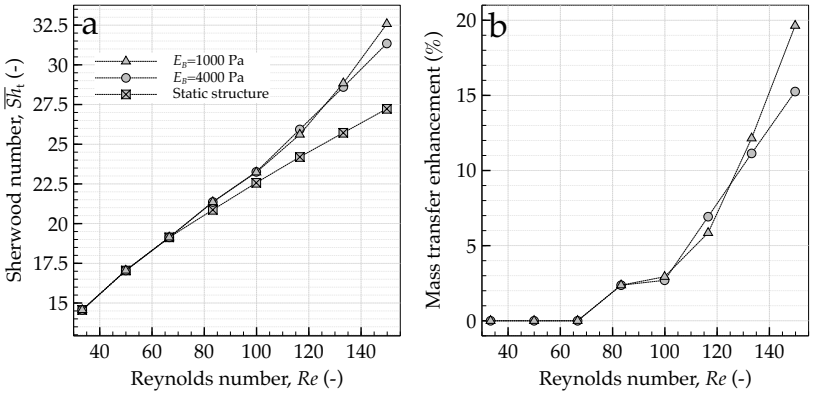

Figure 5.15.: Increase of overall mass transport for faster flows, and for the oscillating streamers with different elasticities. (a) Effect of fluid velocity, represented by Re_D, on mass transfer, represented by time-averaged overall Sherwood number, $\overline{Sh}_t$; (b) mass transfer enhancement of oscillating biofilm streamers with different flexibilities relative to the static structure. The more flexible structure with Young's modulus of $E^S = 1000$ Pa permits more substrate transfer than the stiffer one with $E^S = 4000$ Pa

Salta et al., 2010) that this variety in the biofilm elasticity might be an adaptive response to different shear environments (e.g., through the modification of extracellular polymeric substances, EPS) and that biofilms may benefit from having viscoelastic properties. Hence, the question that arises is whether the alteration of the mechanical properties of the biofilm (here the elasticity) has also a profound effect on the substrate uptake of the biofilm. We therefore investigated numerically two flexible biofilm streamers with different elasticities of $E^S = 1000$ Pa and $E^S = 4000$ Pa, values which are in the range of reported biofilm elasticity in the literature (Stoodley et al., 1999d; Körstgens et al., 2001b; Aravas and Laspidou, 2008). Lower values of elasticity are also reported in the literature, however, these values could not be used in our model because the numerical methods employed in this work fail at very high flexibilities due to very high mesh deformation. For higher values of the elasticity modulus E_B the biofilm is too stiff to begin oscillation and there would be no movement.

Figure 5.15a,b shows that at lower flow velocities the contribution of a higher biofilm flexibility to mass transfer is minimal. For velocities higher

than 0.4 m/s ($Re_D = 133$), however, the mass transfer enhancement becomes relatively higher for more flexible structures ($E^S = 1000$ Pa). Hence, from the substrate uptake point of view a more flexible (more elastic) streamer structure is favorable. On the other hand, from the drag point of view a more flexible structure in the flow also experiences a higher drag and stress on the body (Zhu et al., 2010), and hence it would develop a higher chance of breakage and detachment. This latter balancing between favorable substrate uptake and unfavorable drag should put a theoretical constraint on how flexible a biofilm can become.

5.9. *The interplay of fluid flow, drag, substrate transport and biofilm growth*

In Sections 5.3 and 5.4 we showed that due to the streamlined form the drag on a streamer with $L/d \approx 4.5$ (that is $L^*/d \approx 5$) at $U_0 = 0.4$ m/s ($Re_D = 133$) can be 14 % lower than on a biofilm with circular base having the same projected area to the flow. If we consider a static streamer, this relative drag reduction by the streamlined shape considered is even higher (39 %). Despite constituting a drawback with respect to the fluid forces that the biofilm experiences, these oscillations also increase the substrate uptake of the biofilm by as high as 20 % for the whole structure (see Figure 5.15) and even significantly higher at the tail area closer to the tip. It should also be noted that a static and rigid biofilm is also more vulnerable to changes of local flow directions, very common in rivers, whereas a flexible streamer aligns better and moves with the flow.

Overall, the development of the streamer's teardrop shape might be a result of the viscoelastic nature of the biofilm matrix exposed to fluid forces. The initial patchy biofilm structure elongates being pulled by the flow and could follow a simultaneous transient self-similar bending (Alben et al., 2002, 2004), where also the newly produced microbial cells are pushed downstream (Stoodley et al., 1999a). Nevertheless, the present study shows that the flexible elongated biofilm shape may create an opportunity for bacteria to benefit from higher substrate availability that the oscillations provide and therefore form highly competitive niches in nature (Besemer et al., 2009). Higher substrate

availability towards the tip also facilitates higher growth at the tail section, while being shielded from fluid forces in the wake of the head section is also possible (the blue area in Figure 5.10e-h). Especially under high shear and substrate limitation the streamer will mainly grow at the tip and thereby self-sustain the streamer formation. Eventually, there must be a trade-off between faster growth rate due to more substrate and detachment induced by the larger forces present when the biofilm streamers oscillate.

The results presented here demonstrate that the main contribution to the increase of mass transfer comes from the flow-induced movement of the biofilm tail, in spite of the fact that the tail resides in the diffusion-dominated wake of the head section (Figure 5.10). Accordingly, on a broader view, we propose that the relative movement of any extension of biofilms, e.g., due to filamentous strains or heterogeneous surface structures that vibrate due to local flow instabilities, should contribute to the increase of substrate uptake.

6

Conclusions

Biofilm streamers are one of biofilm morphologies consisting of a head and tail; the head fixed to the substratum, and the tail moving (oscillating) freely in the direction of the flow. In this work, a numerical model of biofilm streamers is developed, which focuses on the drag and substrate transport of these flexible structures in aquatic flows. This model is able to capture the transient deformation of the streamers, and at the same time calculate the substrate uptake by solving the coupled physics of fluid flow, solid deformation, and substrate transport simultaneously. The fluid-structure interaction problems, especially with mass transfer, are quite challenging, since *coupled* physics of non-linear solid mechanics and highly non-linear convective flow and mass transfer problems are solved at every time-step.

In nature, the relationship between the biological form and functional performance is complex and non-linear (Koehl, 1996). Hence, it is necessary to quantitatively estimate how differences in morphological characteristics affect biological performance (Shiino and Kuwazuru, 2011). By replicating the experimental setup of (Stoodley et al., 1998) and using realistic simulation parameters, we show that the streamlined form of the streamers reduces the drag significantly compared to circular clusters. The length of the tail has also

a very important effect on the drag reduction. Streamers with a length to base diameter ratio of ~ 4.5 provided the optimum form to reduce the drag, while the shorter or longer ones experience larger drag. Contrary to the intuitive expectation that *going with the flow* would help to reduce fluid forces, the drag reduction was mostly caused by the streamlined form of the structures and not by their flexibility in the range of material properties simulated. Compared to the immobile streamers, oscillating streamers showed actually higher drags, which might be ascribed to the higher projected area facing the flow caused by oscillations. Ultimately, some preconditions seem to be necessary so that going with the flow would reduce the drag (e.g., minimum length and very low elasticity, see Koehl (1996)).

From the biological point of view, this work considers the substrate transport into the biofilm and further consumption, but neglects microbial growth. When the biofilm streamers start to oscillate, the movement profoundly increases the external substrate transport into the biofilm. The more flexible structures benefit from this movement to a greater extent. In comparison to the head section the streamer tail experiences lower external mass transfer (lower *Sh*). However, once oscillating, the highest solute transport *enhancement* is located towards the tip of the streamers. The tail of the streamer is in the wake of the head section, which shields the tail from the fluid shear. It is likely that the growth in size would be rather restricted in the head section due to high shear forces. Instead, possibly due to much higher external mass transfer and higher internal stresses, microbial growth would result into a higher biomass compactness and density in the head region. Once reaching a critical head size, the alternative growth path should be toward the flow direction, into the wake zone. This could be one of the possible mechanisms for the formation of biofilm streamer morphology.

Results and methodology from this work can also be applied to other fields of research, e.g., encouraging the development of novel micro-mixing modules in microfluidic systems and flexible artificial biofilm supports that benefit from the enhanced mass transfer while having lower susceptibility to breakage of the flexible tails.

7

Outlook

7.1. Morphological convergence

Through the last three decades, extensive experiments have been conducted which show that "biofilms" exhibit numerous morphologies and adaptation mechanisms to ever changing conditions. Generally, these experiments have concentrated largely on either ends of biological mechanisms or physical ones. There are several references (Lewandowski and Stoodley, 1995; Stoodley et al., 1998, 1999a) that mention biofilms form special structures, e.g., streamers when they are in turbulent flows. In reality, the generalization to biofilms may not be in fact justified. The experiments have been conducted on a very selected group of biofilm forming bacteria, mostly *P. aeruginosa*, which belong to a group of bacteria known for their versatile metabolic capacity and broad potential for adaptation to fluctuating environmental conditions (Sauer et al., 2002; Silby et al., 2011). The first question is whether other types of bacteria also form such morphologies?

Numerous studies have suggested that biofilms are more than mere aggregates of cells, but that the organisms involved can communicate with each other, cooperate and compete, and modify their way of life depending on the

environmental conditions and selection pressures. Investigation of the biomechanics of biofilms can be a way to shed light on the level of organization in biofilms, whether they are a passive result of the environment they live in, or they actively modify their living conditions (Hall-Stoodley et al., 2004). Does a required function (e.g., drag reduction) lead to a specific structure (e.g., biofilm streamer shape), or is the streamlined shape formed by passive (de)formation of the structure in flow?

One of the methods to tackle the questions above that we propose is to study the convergence of various types of model biofilms, starting from monocultures. The occurrence of *convergence* in morphology of various biofilm models into a single form (or category of forms) can be a strong suggestion toward the domination of the physical factors in that particular environment. A challenging question would be to what extent is the contribution of each of biological and physical factors to the overall fitness and formation of particular morphology. To date, the studies that focus on the biological diversity in different biofilm morphologies and the connection of diversity-form are scarce. Considering the biofilm streamers, we still do not know in a diverse community what a role each member plays in formation of such structure, or what particular property or mechanism of a member increases its fitness within certain environment. Succession path of organisms is also a very important evidence that can help to explain the transient exchange and trade-off between biological and physical aspects (Besemer et al., 2007, 2009; Singer et al., 2010).

We showed that the streamer shape reduces drag and increases external mass transfer. What are the genetic mechanisms that are triggered, which lead to formation of a particular morphology? Determination of the connections, at genetic level, between fundamental processes, e.g., EPS secretion and presence of pili or flagella, to morphology, and the events triggering them are crucial and necessary.

7.2. Multiple interacting streamers

Performance of an organism can depend on the morphology of its neighbors (Koehl, 1996). To date, our knowledge on single biofilm streamers is limited,

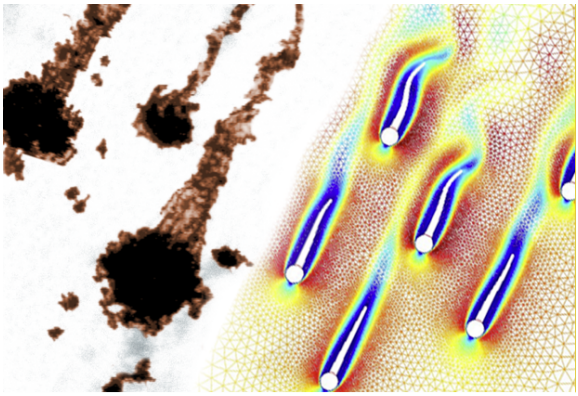

Figure 7.1.: Multiple streamers in flow. (left) Snapshot of streamers oscillating in flow (Stoodley et al., 1998), (right) a modeling experiment with several streamers in flow. The background is the moving mesh, and the colors indicate the flow velocity, red being the highest, and blue the lowest.

while at multiple streamer (community) level there is none. In this work, we also focused on a single streamer. Logically, the presence of other streamer bodies in the vicinity of a single streamer should also alter its drag and nutrient uptake. It has been shown experimentally that the morphology and special arrangement of aquatic sessile animals (Vogel, 1994) or macrophytes (see Koehl (1996) and references therein) changes the environmental conditions that each member of the group encounters. In similar direction, recent studies on two flexible filaments interacting with demonstrate the importance of studying the tandem configurations and interactions (Zhang et al., 2000; Zhu and Peskin, 2003; Jia et al., 2007; Jia and Yin, 2008).

7.3. The third dimension

The current rwo dimensional (2-d) model implemented in this work successfully captures the 2-d von Kármán vortices and formation of the concentration and hydraulic boundary layers. The 2-d assumption is not too far from the reality. Indeed, up to $Re = 188.5$ von Kármán vortices have 2-d symmetry planes and at higher velocities the vortex street becomes unstable due to formation of

3-d perturbations, which would require a 3-d model to capture it. Nevertheless, since the fluid-structure interaction of flexible structures is a very dynamic system, 2-d assumption can not capture some of interesting effects, like buoyancy while flapping, formation of vertical boundary layers, and formation of recirculation zones out of the plane of the 2-d model. Secondary flows have been shown to have critical importance in formation of streamers (Rusconi et al., 2010, 2011). The works of (Vo and Heys, 2011; Alben, 2011) showed that dynamic recirculation immediately downstream of the flexible (biofilm) structures pulls the structure (and extensions) upward, and helps the nutrient transport where it is limited by diffusion.

7.4. Numerical methods suitable for biofilm modeling

Biofilm modeling poses special challenges apart from the computational power compared to a non-biological traditional finite element problem. When biomass grows, parts of the growing domains come close to each other, and may even contact, which is a very big problem for current ALE finite element methods. Biofilm detachment is another challenge to modeling. Processes happen at very large time-scale differences (multi-scale problem). Listed below are some of the methods proposed to tackle the challenges, or still needing an attack plan.

Biofilm detachment

Biofilm detachment has been a problem for both numerical modeling and experiments for a long time. Experimentally, the only methods currently employed to measure the extent of detachment is to make macroscopic mass balances around the biofilm reactors, and conclude the amount detached by subtracting the amount of biomass collected in the effluent from the amount present in the influent. Hence, very little is known about the microscopic detachment mechanism, and the processes that lead to detachment.

On the modeling side, there is an additional challenge for the current models and methods. One part of the challenge concerns the numerical procedure of detachment. How should a part of the structure detach? A physically accurate calculation will require stress failure and crack propagation analysis, which

Figure 7.2.: Biofilm streamer detachment. Flow is from left to right.

are quite complex topics themselves. Hence, one way would be to simplify the process by defining a stress threshold for failure (e.g. similar to Picioreanu et al., 2001 and Böl et al., 2009), and mark the elements that are above this threshold as detached. For transient FSI studies using finite element with ALE, it is not a trivial solution though. Last but not least, the detachment may not even be only caused by detachment but induced by organisms, which requires additional two-way couplings between biology and mechanics.

Arbitrary Lagrangian-Eulerian (ALE) methods

Arbitrary Lagrangian-Eulerian methods have the problem that they are strictly mesh dependent, and fail when mesh nodes are not in the order they were initially (hence very large displacements are to be avoided). Detachment requires parts of the domain elements to *disappear* and therefore change the domain topology. This puts a large constraint on the ALE-based methods, as they are continuum based and have problems when the mesh is stretched too much. Also, there will be missing elements in the biofilm domain, which will require numerical guess-work to fill them with either fluid elements or extend the solid domain. Also, adaptive mesh refinement can be an (expensive) option, and needs to be investigated. Are there any better methods than ALE biophysical biofilm modeling?

Mesh-free methods

The mesh- (grid-) independent methods, such as smoothed-particle hydrodynamics (SPH), do not have the problems mentioned related to ALE. The SPH method is suitable for treating large deformations, complex morphologies and complex material models, to name a few. SPH method works by dividing the fluid into a set of discrete elements, referred to as particles, which have a spatial distance, over which their properties are *smoothed* by a kernel function. With the development of new methods and advances in parallel computing (specially CUDA and GPUs[1]), the previous problems of speed and cost with mesh free problems seem solved these days. Hence, mesh-free methods look quite promising. Still, in comparison to wide availability of multi-physics finite element tools, the lack of an available toolset for mesh-free methods can be quite hindering in research.

Extended finite element method (XFEM)

The fixed-grid methods are very suitable for the cases where steep gradients are known prior to simulation. In particular, when very strong and localized gradients develop, for instance due to substrate consumption in biofilms, both fixed-grid methods and classic finite element methods fail to provide an accurate solution or the number of degrees of freedom to be solved (DOF) becomes quite high to resolve spatial gradients. Adaptive Mesh Refinement (AMR) is a solution that can refine the grid around these problematic areas. However, AMR methods are technically very complex, costly if they are called very frequently (e.g., FSI), and not very robust for complex geometries. In addition, mesh generation algorithms usually do not employ parallel methods, and are quite cumbersome for very large problems (many DOFs).

The extended finite element method is one of the methods developed to ease difficulties in solving problems with localized features that are not efficiently resolved by mesh refinement. XFEM allows the overlapping of discontinuities not aligned with the finite element mesh. In this method pre-processing in terms of mesh generation and construction of equation systems are implemented on the

[1]CUDA stands for Compute Unified Device Architecture, and is a parallel computing architecture developed by Nvidia to be used on their graphics processing units (GPUs).

node level, and can be highly parallelized along with the solution of resulting equation systems (main-processing). These advantages make this method very suitable for large problems on parallel environments, allowing high levels of complexity in initial and transient geometries and physics. Hence, XFEM is highly recommended for the future studies of biomechanics of biofilms.

7.5. Biofilm growth and FSI: a multi-scale problem

To date, only two works (Kissel et al., 1984; Picioreanu et al., 1999) acknowledge the large temporal scale differences of biofilm development. Their methods separate the natural time-scale in biofilm systems to achieve a realistic calculation speed. To do so, three time scales are defined: (1) microbial growth, in the order of hours or days, (2) mass transport of solutes, in the order of minutes and (3) hydrodynamic processes, in the order of seconds. Initially, step 2 and 3 are solved, and the results are used in a new iteration to solve for step 1. If the domain geometry is modified, then the algorithm cycle start over with the new settings.

Although being an effective workaround, more robust methods are required that can handle the multi-scale interaction of each of the main processes in biofilms with an acceptable level of abstraction and accuracy at each level.

Bibliography

Alben, S., 2011. Interactions between vortices and flexible walls. International Journal of Non-Linear Mechanics 46 (4), 586–591.

Alben, S., Shelley, M., Zhang, J., 2002. Drag reduction through self-similar bending of a flexible body. Nature 420 (6915), 479–481.

Alben, S., Shelley, M., Zhang, J., 2004. How flexibility induces streamlining in a two-dimensional flows. Physics of Fluids 16 (5), 1694.

Allen, J. J., Smits, A. J., 2001. Energy harvesting eel. Journal of Fluids and Structures 15 (3-4), 629–640.

Alpkvist, E., Klapper, I., 2007a. Description of mechanical response including detachment using a novel particle model of biofilm/flow interaction. Water Science and Technology 55 (8-9), 265–273.

Alpkvist, E., Klapper, I., 2007b. A multidimensional multispecies continuum model for heterogeneous biofilm development. Bulletin of Mathematical Biology 69 (2), 765–789.

Alpkvist, E., Picioreanu, C., van Loosdrecht, M. C. M., Heyden, A., 2006. Three-dimensional biofilm model with individual cells and continuum EPS matrix. Biotechnology and Bioengineering 94 (5), 961–979.

Aravas, N., Laspidou, C., 2008. On the calculation of the elastic modulus of a biofilm streamer. Biotechnology and Bioengineering 101 (1), 196–200.

Augspurger, C., Karwautz, C., Mußmann, M., Daims, H., Battin, T. J., 2010. Drivers of bacterial colonization patterns in stream biofilms. FEMS Microbiology Ecology 72 (1), 47–57.

Bakke, R., Trulear, M. G., Robinson, J. A., Characklis, W. G., 1984. Activity of *Pseudomonas aeruginosa* in biofilms: Steady state. Biotechnology and Bioengineering 26 (12), 1418–1424.

Beal, D. N., Hover, F. S., Triantafyllou, M. S., Liao, J. C., Lauder, G. V., 2006. Passive propulsion in vortex wakes. Journal of Fluid Mechanics 549, 385–402.

Besemer, K., Hödl, I., Singer, G., Battin, T. J., 2009. Architectural differentiation reflects bacterial community structure in stream biofilms. The ISME Journal: Multidisciplinary Journal of Microbial Ecology 3 (11), 1318–1324.

Besemer, K., Singer, G., Limberger, R., Chlup, A., Hochedlinger, G., Hödl, I., Baranyi, C., Battin, T. J., 2007. Biophysical controls on community succession in stream biofilms. Applied and Environmental Microbiology 73 (15), 4966–4974.

Bohn, A., Zippel, B., Almeida, J., Xavier, J., 2007. Stochastic modeling for characterisation of biofilm development with discrete detachment events (sloughing). Water Science and Technology 55 (8-9), 257–264.

Böl, M., Möhle, R. B., Haesner, M., Neu, T. R., Horn, H., Krull, R., 2009. 3D finite element model of biofilm detachment using real biofilm structures from CLSM data. Biotechnology and Bioengineering 103 (1), 177–186.

Characklis, W. G., 1981. Fouling biofilm development: A process analysis. Biotechnology and Bioengineering 23 (9), 1923–1960.

Characklis, W. G., 1990. Microbial fouling. In: Biofilms ed. Characklis, W.G. and Marshall, K.C. Wiley, New York, p. 523–584.

Cogan, N. G., 2004. Two-Fluid model of biofilm disinfection. Bulletin of Mathematical Biology 70 (3), 800–19.

Costerton, J. W., Cheng, K. J., Geesey, G. G., Ladd, T. I., Nickel, J. C., Dasgupta, M., Marrie, T. J., 1987. Bacterial biofilms in nature and disease. Annual Review of Microbiology 41 (1), 435–464.

de Beer, D., Stoodley, P., Lewandowski, Z., 1994. Liquid flow in heterogeneous biofilms. Biotechnology and Bioengineering 44 (5), 636–641.

De Kievit, T. R., Gillis, R., Marx, S., Brown, C., Iglewski, B. H., 2001. Quorum-Sensing genes in *Pseudomonas aeruginosa* biofilms: Their role and expression patterns. Applied and Environmental Microbiology 67 (4), 1865–1873.

Deen, W. M., 1998. Analysis of transport phenomena. Oxford University Press, New York.

Dillon, R., Fauci, L., 2000. A microscale model of bacterial and biofilm dynamics in porous media. Biotechnology and Bioengineering 68 (5), 536–547.

Donea, J., Huerta, A., 2003. Finite element methods for flow problems. Wiley.

Drucker, E. G., Lauder, G. V., 2001. Locomotor function of the dorsal fin in teleost fishes: experimental analysis of wake forces in sunfish. Journal of Experimental Biology 204 (17), 2943 –2958.

Duddu, R., Bordas, S., Chopp, D., Moran, B., 2008. A combined extended finite element and level set method for biofilm growth. International Journal for Numerical Methods in Engineering 74 (5), 848–870.

Duddu, R., Chopp, D. L., Moran, B., 2009. A two-dimensional continuum model of biofilm growth incorporating fluid flow and shear stress based detachment. Biotechnology and Bioengineering 103 (1), 92–104.

Eberl, H. J., Picioreanu, C., Heijnen, J. J., van Loosdrecht, M. C. M., 2000. A three-dimensional numerical study on the correlation of spatial structure, hydrodynamic conditions, and mass transfer and conversion in biofilms. Chemical Engineering Science 55 (24), 6209–6222.

Edwards, K. J., Bond, P. L., Gihring, T. M., Banfield, J. F., 2000. An archaeal iron-oxidizing extreme acidophile important in acid mine drainage. Science 287 (5459), 1796 –1799.

Elenter, D., Milferstedt, K., Zhang, W., Hausner, M., Morgenroth, E., 2007. Influence of detachment on substrate removal and microbial ecology in a heterotrophic/autotrophic biofilm. Water Research 41 (20), 4657–4671.

Fish, F., 1998. Imaginative solutions by marine organisms for drag reduction. In: Proceedings of the International Symposium on Seawater Drag Reduction. pp. 443–450.

Flemming, H., 2011. The perfect slime. Colloids and Surfaces B: Biointerfaces 86 (2), 251–259.

Flemming, H., Wingender, J., Griegbe, M., Mayer, C., 2000a. Physico-chemical properties of biofilms. Evans LV, editor. Biofilms: recent advances in their study and control. Amsterdam: Harwood Academic Publishers, 19–34.

Flemming, H. C., Wingender, J., Mayer, C., Korstgens, V., Borchard, W., 2000b. Cohesiveness in biofilm matrix polymers. In: Community Structure and Co-operation in Biofilms: Fifty-ninth Symposium of the Society for General Microbiology Held at the University of Exeter, September 2000. p. 87.

Fux, C., Costerton, J., Stewart, P., Stoodley, P., 2005. Survival strategies of infectious biofilms. Trends in Microbiology 13 (1), 34–40.

Gjaltema, A., Arts, P. A. M., van Loosdrecht, M. C. M., Kuenen, J. G., Heijnen, J. J., 1994. Heterogeneity of biofilms in rotating annular reactors: Occurrence, structure, and consequences. Biotechnology and Bioengineering 44 (2), 194–204.

Gujer, W., Wanner, O., 1984. Competition in biofilms. Water Science and Technology 17, 27–44.

Hall-Stoodley, L., Costerton, J. W., Stoodley, P., 2004. Bacterial biofilms: from the natural environment to infectious diseases. Nature Reviews Microbiology 2 (2), 95–108.

Hammer, B. K., Bassler, B. L., 2003. Quorum sensing controls biofilm formation in vibrio cholerae. Molecular Microbiology 50 (1), 101–104.

Harder, D. L., Speck, O., Hurd, C. L., Speck, T., 2004. Reconfiguration as a prerequisite for survival in highly unstable Flow-Dominated habitats. Journal of Plant Growth Regulation 23 (2), 98–107.

Henze, M., 2000. Activated sludge models ASM1, ASM2, ASM2d and ASM3. IWA Publishing, London, UK.

Hohne, D. N., Younger, J. G., Solomon, M. J., 2009. Flexible microfluidic device for mechanical property characterization of soft viscoelastic solids such as bacterial biofilms. Langmuir 25 (13), 7743–7751.

Horn, H., Hempel, D., 1997. Growth and decay in an auto-/heterotrophic biofilm. Water Research 31 (9), 2243–2252.

Horn, H., Neu, T., Wulkow, M., 2001. Modelling the structure and function of extracellular polymeric substances in biofilms with new numerical techniques. Water Science and Technology 43.

Horn, H., Reiff, H., Morgenroth, E., 2003. Simulation of growth and detachment in biofilm systems under defined hydrodynamic conditions. Biotechnology and Bioengineering 81 (5), 607–617.

Houari, A., Picard, J., Habarou, H., Galas, L., Vaudry, H., Heim, V., Di Martino, P., 2008. Rheology of biofilms formed at the surface of NF membranes in a drinking water production unit. Biofouling 24 (4), 235–240.

Huang, L., James Quinn, S., Ellis, P. D. M., Ffowcs Williams, J. E., 1995. Biomechanics of snoring. Endeavour 19 (3), 96–100.

Jia, L., Li, F., Yin, X., Yin, X., 2007. Coupling modes between two flapping filaments. Journal of Fluid Mechanics 581, 199–220.

Jia, L., Yin, X., 2008. Passive oscillations of two tandem flexible filaments in a flowing soap film. Physical Review Letters 100 (22).

Khan, W. A., Culham, J. R., Yovanovich, M. M., 2005. Fluid flow around and heat transfer from an infinite circular cylinder. Journal of Heat Transfer 127 (7), 785–790.

Kissel, J. C., McCarty, P. L., Street, R. L., 1984. Numerical simulation of Mixed-Culture biofilm. Journal of Environmental Engineering 110 (2), 393–411.

Klapper, I., Dockery, J., 2006. Role of cohesion in the material description of biofilms. Physical Review E 74 (3), 031902.

Klapper, I., Dockery, J., 2010. Mathematical description of microbial biofilms. SIAM Review 52 (2), 221.

Klausen, M., Aaes-J?rgensen, A., Molin, S., Tolker-Nielsen, T., 2003. Involvement of bacterial migration in the development of complex multicellular structures in *Pseudomonas aeruginosa* biofilms. Molecular Microbiology 50 (1), 61–68.

Koehl, M. A. R., 1996. When does morphology matter? Annual Review of Ecology and Systematics 27 (1), 501–542.

Koehl, M. R., 1977. Effects of sea anemones on the flow forces they encounter. Journal of Experimental Biology 69 (1), 87 –105.

Körstgens, V., Flemming, H. C., Wingender, J., Borchard, W., 2001a. Influence of calcium ions on the mechanical properties of a model biofilm of mucoid *Pseudomonas aeruginosa*. Water Science and Technology 43 (6), 49–57.

Körstgens, V., Flemming, H. C., Wingender, J., Borchard, W., 2001b. Uniaxial compression measurement device for investigation of the mechanical stability of biofilms. Journal of Microbiological Methods 46 (1), 9–17.

Kreft, J., Picioreanu, C., Wimpenny, J. W. T., van Loosdrecht, M. C. M., 2001. Individual-based modelling of biofilms. Microbiology 147 (11), 2897–2912.

Kreft, J. U., Booth, G., Wimpenny, J. W., 1998. BacSim, a simulator for individual-based modelling of bacterial colony growth. Microbiology (Reading, England) 144 (Pt 12), 3275–3287.

Küttler, U., Gee, M., Förster, C., Comerford, A., Wall, W. A., 2010. Coupling strategies for biomedical fluid–structure interaction problems. International Journal for Numerical Methods in Biomedical Engineering 26 (3-4), 305–321.

Küttler, U., Wall, W., 2008. Fixed-point fluid–structure interaction solvers with dynamic relaxation. Computational Mechanics 43 (1), 61–72.

Lardon, L. A., Merkey, B. V., Martins, S., Dötsch, A., Picioreanu, C., Kreft, J., Smets, B. F., 2011. iDynoMiCS: next-generation individual-based modelling of biofilms. Environmental Microbiology.

Laspidou, C., Rittmann, B., 2002. A unified theory for extracellular polymeric substances, soluble microbial products, and active and inert biomass. Water Research 36 (11), 2711–2720.

Laspidou, C., Rittmann, B., Karamanos, S., 2005. Finite element modeling to expand the UMCCA model to describe biofilm mechanical behavior. Water Science and Technology 52 (7), 161–166.

Lau, P. C., Dutcher, J. R., Beveridge, T. J., Lam, J. S., 2009. Absolute quantitation of bacterial biofilm adhesion and viscoelasticity by microbead force spectroscopy. Biophysical Journal 96 (7), 2935–2948.

Lewandowski, Z., Stoodley, P., 1995. Flow induced vibrations, drag force, and pressure drop in conduits covered with biofilm. Water Science and Technology 32 (8), 19–26.

Li, Y., Tang, N., Aspiras, M. B., Lau, P. C. Y., Lee, J. H., Ellen, R. P., Cvitkovitch, D. G., 2002. A Quorum-Sensing signaling system essential for genetic competence in streptococcus mutans is involved in biofilm formation. Journal of Bacteriology 184 (10), 2699–2708.

McLean, R. J. C., Barnes, M. B., Windham, M. K., Merchant, M., Forstner, M. R. J., Fuqua, C., 2005. Cell-Cell influences on bacterial community development in aquatic biofilms. Applied and Environmental Microbiology 71 (12), 8987–8990.

Nagaoka, H., Sanda, K., 2005. Simulation of turbulence and dissolved oxygen concentration profiles over biofilm using k turbulence models. Water Science and Technology 36 (1), 147–156.

Nicolella, C., van Loosdrecht, M. C. M., Heijnen, S. J., 2000. Particle-based biofilm reactor technology. Trends in Biotechnology 18 (7), 312–320.

O'Toole, G., Kaplan, H. B., Kolter, R., 2000. Biofilm formation as microbial development. Annual Review of Microbiology 54 (1), 49–79.

O'Toole, G. A., Kolter, R., 1998. Flagellar and twitching motility are necessary for *Pseudomonas aeruginosa* biofilm development. Molecular Microbiology 30 (2), 295–304.

Pamp, S. J., Gjermansen, M., Tolker-Nielsen, T., 2007. The biofilm matrix: a sticky framework. Norfolk, UK: Horizon Scientific Press.

Peskin, C. S., 1977. Numerical analysis of blood flow in the heart. Journal of Computational Physics 25 (3), 220 – 252.

Peskin, C. S., 2003. The immersed boundary method. Acta Numerica 11, 479–517.

Picioreanu, C., van Loosdrecht, M. C. M., Heijnen, J., 1999. Discrete-differential modelling of biofilm structure. Water Science and Technology 39 (7), 115—122.

Picioreanu, C., van Loosdrecht, M. C. M., Heijnen, J. J., 1998. A new combined differential-discrete cellular automaton approach for biofilm modeling: Application for growth in gel beads. Biotechnology and Bioengineering 57 (6), 718–731.

Picioreanu, C., van Loosdrecht, M. C. M., Heijnen, J. J., 2000a. Effect of diffusive and convective substrate transport on biofilm structure formation: A two-dimensional modeling study. Biotechnology and Bioengineering 69 (5), 504–515.

Picioreanu, C., van Loosdrecht, M. C. M., Heijnen, J. J., 2000b. A theoretical study on the effect of surface roughness on mass transport and transformation in biofilms. Biotechnology and Bioengineering 68 (4), 355–369.

Picioreanu, C., van Loosdrecht, M. C. M., Heijnen, J. J., 2001. Two-dimensional model of biofilm detachment caused by internal stress from liquid flows. Biotechnology and Bioengineering 72 (2), 205–218.

Pizarro, G., Griffeath, D., Noguera, D. R., 2001. Quantitative cellular automaton model for biofilms. Journal of Environmental Engineering 127 (9), 782–789.

Ristroph, L., Zhang, J., 2008. Anomalous hydrodynamic drafting of interacting flapping flags. Physical Review Letters 101 (19), 194502–4.

Rothschild, L. J., Mancinelli, R. L., 2001. Life in extreme environments. Nature 409 (6823), 1092–1101.

Rusconi, R., Lecuyer, S., Autrusson, N., Guglielmini, L., Stone, H. A., 2011. Secondary flow as a mechanism for the formation of biofilm streamers. Biophysical Journal 100 (6), 1392–1399.

Rusconi, R., Lecuyer, S., Guglielmini, L., Stone, H. A., 2010. Laminar flow around corners triggers the formation of biofilm streamers. Journal of the Royal Society Interface 7 (50), 1293–1299.

Salta, M., Wharton, J. A., Stoodley, P., Dennington, S. P., Goodes, L. R., Werwinski, S., Mart, U., Wood, R. J. K., Stokes, K. R., 2010. Designing biomimetic antifouling surfaces. Philosophical Transactions of the Royal Society A: Physical, Mathematical and Engineering Sciences 368 (1929), 4729–4754.

Sauer, K., Camper, A. K., Ehrlich, G. D., Costerton, J. W., Davies, D. G., 2002. *Pseudomonas aeruginosa* displays multiple phenotypes during development as a biofilm. Journal of Bacteriology 184 (4), 1140–1154.

Sawada, T., Hisada, T., 2007. Fluid-structure interaction analysis of the two-dimensional flag-in-wind problem by an interface-tracking ALE finite element method. Computers & Fluids 36 (1), 136–146.

Shaw, T., Winston, M., Rupp, C. J., Klapper, I., Stoodley, P., 2004. Commonality of elastic relaxation times in biofilms. Physical Review Letters 93 (9), 098102.

Shelley, M. J., Zhang, J., 2011. Flapping and bending bodies interacting with fluid flows. Annual Review of Fluid Mechanics 43, 449–65.

Shiino, Y., Kuwazuru, O., 2011. Theoretical approach to the functional optimisation of spiriferide brachiopod shell: Optimum morphology of sulcus. Journal of Theoretical Biology 276 (1), 192–198.

Siegrist, H., Gujer, W., 1985. Mass transfer mechanisms in a heterotrophic biofilm. Water Research 19 (11), 1369–1378.

Silby, M. W., Winstanley, C., Godfrey, S. A. C., Levy, S. B., Jackson, R. W., 2011. Pseudomonas genomes: diverse and adaptable. FEMS Microbiology Reviews 35 (4), 652–680.

Singer, G., Besemer, K., Schmitt-Kopplin, P., Hödl, I., Battin, T. J., 2010. Physical heterogeneity increases biofilm resource use and its molecular diversity in stream mesocosms. PLoS ONE 5 (4), e9988.

Singh, R., Paul, D., Jain, R. K., 2006. Biofilms: implications in bioremediation. Trends in Microbiology 14 (9), 389–397.

Sivadas, V., Wickenheiser, A. M., 2011. A study of several vortex-induced vibration techniques for piezoelectric wind energy harvesting. San Diego, California, USA, pp. 79770F–79770F–13.

Stoodley, P., Cargo, Rupp, Wilson, Klapper, 2002. Biofilm material properties as related to shear-induced deformation and detachment phenomena. Journal of Industrial Microbiology & Biotechnology 29 (6), 361–367.

Stoodley, P., Dodds, I., Boyle, J., Lappin-Scott, H., 1999a. Influence of hydrodynamics and nutrients on biofilm structure. Journal of Applied Microbiology 85, 19S–28S.

Stoodley, P., Jorgensen, F., Williams, P., Lappin-Scott, 1999b. The role of hydrodynamics and AHL signalling molecules as determinants of the structure of *pseudomonas aeruginosa* biofilms. In: R. Bayston, et al. (eds), Biofilms: The Good, the Bad, and the Ugly. J.W.T. BioLine, Cardiff, UK, p. 3.

Stoodley, P., Lewandowski, Z., Boyle, J. D., Lappin-Scott, H. M., 1998. Oscillation characteristics of biofilm streamers in turbulent flowing water as related to drag and pressure drop. Biotechnology and Bioengineering 57 (5), 536–544.

Stoodley, P., Lewandowski, Z., Boyle, J. D., Lappin-Scott, H. M., 1999c. The formation of migratory ripples in a mixed species bacterial biofilm growing in turbulent flow. Environmental Microbiology 1 (5), 447–455.

Stoodley, P., Lewandowski, Z., Boyle, J. D., Lappin-Scott, H. M., 1999d. Structural deformation of bacterial biofilms caused by short-term fluctuations in fluid shear: An in situ investigation of biofilm rheology. Biotechnology and Bioengineering 65 (1), 83–92.

Stoodley, P., Wilson, S., Hall-Stoodley, L., Boyle, J. D., Lappin-Scott, H. M., Costerton, J. W., 2001. Growth and detachment of cell clusters from mature Mixed-Species biofilms. Appl. Environ. Microbiol. 67 (12), 5608–5613.

Taneda, S., 1968. Waving motions of flags. Journal of the Physical Society of Japan 24, 392–401.

Towler, B. W., Cunningham, A., Stoodley, P., McKittrick, L., 2007. A model of fluid-biofilm interaction using a burger material law. Biotechnology and Bioengineering 96 (2), 259–271.

van Loosdrecht, M., Eikelboom, D., Gjaltema, A., Mulder, A., Tijhuis, L., Heijnen, J., 1995. Biofilm structures. Water Science and Technology 32 (8), 35–43.

Vo, G. D., Heys, J., 2011. Biofilm deformation in response to fluid flow in capillaries. Biotechnology and Bioengineering, n/a–n/a.

Vogel, S., 1984. Drag and flexibility in sessile organisms. Amer. Zool. 24 (1), 37–44.

Vogel, S., 1989. Drag and reconfiguration of broad leaves in high winds. Journal of Experimental Botany 40 (8), 941 –948.

Vogel, S., 1994. Life in moving fluids, 2nd Edition. Princeton University Press, Princeton, NJ.

Vogel, S., 2003. Comparative biomechanics: Life's Physical World. Princeton Univ Press, Princeton, NJ.

von Mises, R., 1959. Theory of flight. Dover Publications, New York.

Vrouwenvelder, J., Picioreanu, C., Kruithof, J., van Loosdrecht, M., 2010. Biofouling in spiral wound membrane systems: Three-dimensional CFD model based evaluation of experimental data. Journal of Membrane Science 346 (1), 71–85.

Wagner, M., Taherzadeh, D., Haisch, C., Horn, H., 2010. Investigation of the mesoscale structure and volumetric features of biofilms using optical coherence tomography. Biotechnology and Bioengineering 107 (5), 844–853.

Wall, W. A., Rabczuk, T., 2008. Fluid-structure interaction in lower airways of CT-based lung geometries. International Journal for Numerical Methods in Fluids 57 (5), 653–675.

Wall, W. A., Ramm, E., 1998. Fluid-structure interaction based upon a stabilized (ALE) finite element method. CIMNE, Barcelona.

Wanner, O., Gujer, W., 1986. A multispecies biofilm model. Biotechnology and Bioengineering 28 (3), 314–328.

Wanner, O., Reichert, P., 1996. Mathematical modeling of mixed-culture biofilms. Biotechnology and Bioengineering 49 (2), 172–184.

Wäsche, S., Horn, H., Hempel, D. C., 2002. Influence of growth conditions on biofilm development and mass transfer at the bulk/biofilm interface. Water Research 36 (19), 4775–4784.

Williamson, C. H. K., 2003. Vortex dynamics in the cylinder wake. Annual Review of Fluid Mechanics 28 (1), 477–539.

Wimpenny, J. W. T., Colasanti, R., 1997. A unifying hypothesis for the structure of microbial biofilms based on cellular automaton models. FEMS Microbiology Ecology 22 (1), 1–16.

Winstanley, H. F., Chapwanya, M., McGuinness, M. J., Fowler, A. C., 2011. A polymer–solvent model of biofilm growth. Proceedings of the Royal Society A: Mathematical, Physical and Engineering Science 467 (2129), 1449 –1467.

Wood, T. K., González Barrios, A. F., Herzberg, M., Lee, J., 2006. Motility influences biofilm architecture in *Escherichia coli*. Applied Microbiology and Biotechnology 72 (2), 361–367.

Xavier, J. B., Picioreanu, C., van Loosdrecht, M. C. M., 2005a. A framework for multidimensional modelling of activity and structure of multispecies biofilms. Environmental Microbiology 7 (8), 1085–1103.

Xavier, J. B., Picioreanu, C., van Loosdrecht, M. C. M., 2005b. A general description of detachment for multidimensional modelling of biofilms. Biotechnology and Bioengineering 91 (6), 651–669.

Xu, K. D., Stewart, P. S., Xia, F., Huang, C., McFeters, G. A., 1998. Spatial physiological heterogeneity in *Pseudomonas aeruginosa* biofilm is determined by oxygen availability. Appl. Environ. Microbiol. 64 (10), 4035–4039.

Zhang, J., Childress, S., Libchaber, A., Shelley, M., 2000. Flexible filaments in a flowing soap film as a model for one-dimensional flags in a two-dimensional wind. Nature 408 (6814), 835–839.

Zhang, T. C., Bishop, P. L., Gibbs, J. T., 1994. Effect of roughness and thickness of biofilms on external mass transfer resistance. In: Critical Issues in Water and Wastewater Treatment. p. 593–600.

Zhu, L., He, G., Wang, S., Miller, L., Zhang, X., You, Q., Fang, S., 2010. An immersed boundary method based on the lattice boltzmann approach in three dimensions, with application. Computers & Mathematics with Applications In Press.

Zhu, L., Peskin, C. S., 2002. Simulation of a flapping flexible filament in a flowing soap film by the immersed boundary method. Journal of Computational Physics 179 (2), 452–468.

Zhu, L., Peskin, C. S., 2003. Interaction of two flapping filaments in a flowing soap film. Physics of Fluids 15, 1954.

Zhu, L., Peskin, C. S., 2007. Drag of a flexible fiber in a 2D moving viscous fluid. Computers & Fluids 36 (2), 398–406.

A

Fluid-structure interaction model implementation

The fluid-structure interaction model developed in this study was initially implemented in BACI, which is an in-house finite element framwork developed at the Lehrstuhl für Numerische Mechanik, TUM (Wall and Ramm, 1998; Wall and Rabczuk, 2008; Küttler and Wall, 2008; Küttler et al., 2010). In this chapter, a similar model to the one originally developed in BACI will be introduced that is implemented in the commercially available COMSOL MULTIPHYSICS v4.1 (COMSOL, Burlington, MA).

A.1. Fluid flow

Subdomain settings An incompressible formulation of NAVIER-STOKES equations of flow is implemented on the fluid subdomain, Ω_F. Next, the fluid subdomain is discretisized using P1P1 elements, and consistent stabilization technique, streamline diffusion, is applied to the weak formulation of the domain. The boundary conditions are set according to Section 4.1.

Drag and lift coefficients Due to the finite element based approach to PDEs implemented in COMSOL, the forces and gradients at the boundaries are not accurate enough approximation of actual flux and forces; the values of flux and forces are mesh dependant. The more reliable approximation for computing integrals of reaction forces or fluxes is to use the *Lagrange Multipliers* on the boundaries, since the Lagrange multipliers along the constraints optimally balance the finite element projection of the applied loads (reaction forces, see COMSOL MULTIPHYSICS user guide, section "Using Weak Constraints"). Here we use accurate `reacf()` operators in COMSOL; the reaction force operator of a dependent variable corresponds to the Lagrange multiplier of that dependent variable. Hence, drag, and drag coefficient are calculated as:

$$F_D = \oint \texttt{reacf}(\texttt{u\_fluid})\, ds, \quad C_D = \frac{2 \cdot F_D}{\rho^F \cdot U_{avg}^2 \cdot D_H} \tag{A.1}$$

where `u_fluid` (and related `v_fluid`) is the relative liquid velocity variable name, and s is the arc length of streamer perimeter. Lift force, F_L, and lift coefficient, C_L, are calculated similarly with Equation (A.1) but using `v_fluid`.

A.2. Solid mechanics

In COMSOL, the Solid Mechanics interface describes the motion and deformation of solid objects in space. To compute the displacements, stresses, and strains quadratic elements are used to have higher accuracy in computations, specially since the displacements are very small, and there is a tight coupling between the moving mesh, solid displacement and fluid force and velocity calculations.

A.3. Moving mesh

Moving mesh is applied to the Ω_F subdomain, where fluid mesh is freely allowed to move. For simple cases, there are no special treatments for the moving mesh domain. However, for the special case of biofilm streamers, the solution of the model shows large deformation as a result of FSI movement of the tail section.

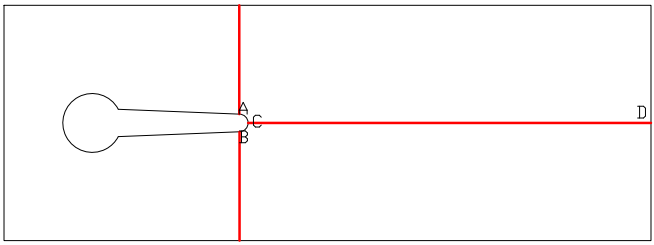

Figure A.1.: Guided mesh boundaries (red lines)

Inverted mesh elements are distorted mesh elements that their nodal order has been changed with respect to the initial/reference numbering of the nodes. As a result, the accuracy of the solution deteriorates and eventually the solvers will diverge due to an ill-conditioned system. Hence, to avoid getting inverted mesh elements a sliding mesh technique is applied on the inner moving mesh domain boundaries.

The red lines in Figure A.1 represent the internal boundaries of moving mesh frame. The displacements of A, B and C points are calculated by integrating the displacement over time, $u_{gmesh,A} = \int u_{solid} dt$, where u_{solid} is the node displacement, and $u_{gmesh,A}$ is the mesh displacement of point A. Then on each boundary segment a prescribed mesh displacement is applied, where at the A, B and C is at maximum displacement, while at the other end of the boundary is the points are fixed to zero.

A.4. Fluid-Structure Interaction Interface

In BACI and earlier versions of COMSOL MULTIPHYSICS the FSI model is setup by applying forces and displacement boundary conditions manually. However, since COMSOL MULTIPHYSICS v4.0 there is a new fluid-structure interaction interface implemented, which combines fluid flow with solid mechanics to capture the interaction between the fluid and the solid structure. Once both the fluid and solid subdomains are defined, the FSI boundaries are automatically marked on the boundaries between the fluid and the solid, and the coupling is applied (see Section 4.1 for details of coupling conditions).

A.5. Solvers and solution procedure

To solve the nonlinear steady-state and transient simulations, PARDISO solver, which is a direct solver (in contrast to iterative solvers) with *Nested Dissection Multithreaded* preordering algorithm is used. For FSI simulations, the resultant equations are solved in a fully coupled arrangement with PARDISO as linear solver, and initial damping of 1×10^{-4} that satisfy the relative tolerance criteria of 1×10^{-5} for stationary solver.

For the transient solver, a scaled relative tolerance of 1×10^{-3}, and non-scaled absolute tolerance of 1×10^{-7} for solid and mesh displacements is applied. Due to higher stability experienced with the GENERALIZED ALPHA (Gen-α) time-stepping method for the FSI case, Gen-α method is selected over the implicit BDF method. The step sizes of Gen-α are set to *free* time-stepping configuration, and limited step size of 5×10^{-4} s. The Jacobians are calculated per step, and a damping factor of 1 is chosen (no damping).

This monolithic formulation of the equations (fully coupled solver) is further solved on a multi-processor servers in parallel.

A.6. Post-processing

The main parameters extracted from the simulations are the lift and drag coefficients, tip position, and von-mises stresses. The tip position is further used to calculate the frequency and amplitudes of the oscillations using FAST FOURIER TRANSFORM (FFT) technique in MATLAB (Mathworks, MA).

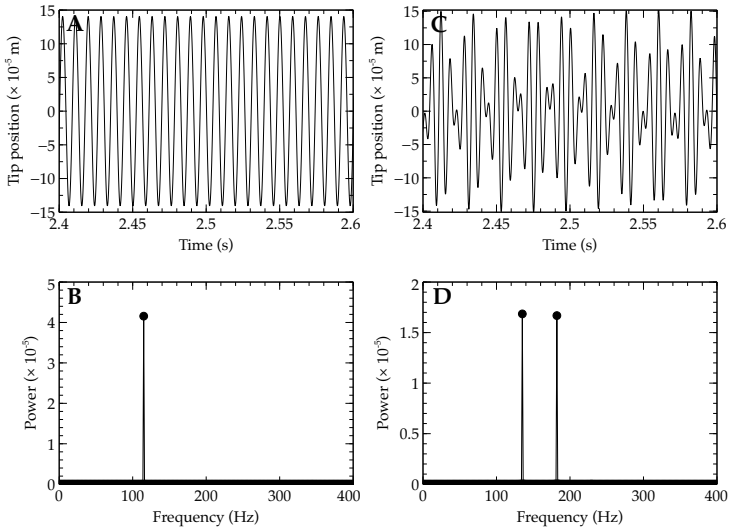

Figure A.2.: Calculating frequencies of oscillations using FFT method. (A) and (C) are the tip displacement in time, and (B) and (D) are the corresponding FFT power diagrams. The peaks in (B) and (D) show the dominant frequencies of oscillations. The simulation conditions are $E = 1000$ Pa, (A) $U_{max} = 0.25\ \mathrm{m \cdot s^{-1}}$ and (C) $U_{max} = 0.30\ \mathrm{m \cdot s^{-1}}$

The Matlab code that is used for calculating the oscillation frequency using FFT is listed below:

```
function dominantFrequeny=findFreq(tt,yy)
% yy: the displacement of the tip vector
% tt: time related to yy
a=find(abs(yy)<1e-5);
x=yy(a(1):a(end));t=tt(a(1):a(end));
Fs = 1/(t(2)-t(1));
N = length(x);                  % length of signal
nfft = N;                       % n-point DFT, by default nfft=length(x)
X = abs(fft(x,nfft)).^2 / nfft;  % square of the magnitude of FFT
cutOff = ceil((nfft+1)/2);      % nyquist frequency
X = X(1:cutOff);                % FFT is symmetric, take first half
X(2:end -1) = 2 * X(2:end -1);  % compensate for the energy of the other half
fr = (0:cutOff-1)*Fs/nfft;      % frequency vector
[v idx] = max(X);
dominantFrequeny = fr(idx);
```

B

Mass transfer model implementation

The transfer of substrate to the biofilm, and the substrate consumption by microorganisms in biofilm are simulated using a convection-diffusion-reaction model in COMSOL Multiphysics. The substrate is transported through the bulk fluid in a convection-dominated processes, and through the boundary layer formed around the biofilm diffuses into the biofilm streamer, where it is consumed following a simple Monod rate with saturation.

B.1. Convection-diffusion subdomains

The conservation of mass of solute enforces the flux continuity on both sides of an inner boundary connecting/separating two sections of a domain without a reaction taking place on that boundary. The case of biofilm streamer with dimensions studied and experimental conditions considered translates to a highly convection-dominated mass transfer problem. The PÉCLET number is a dimensionless number, which quantifies the importance of convection compared to diffusion,

$$\mathrm{Pe}_D = \frac{L_{CH} \cdot u_{fluid}}{D} = \mathrm{Re}_D \cdot \mathrm{Sc} \tag{B.1}$$

where L_{CH} is a characteristic length, u_{fluid} the fluid velocity, D the solute (substrate) diffusion coefficient, Sc the SCHMIDT number ($\mathrm{Sc} = \frac{\mu^F}{\rho^F D}$), and Re_D is the Reynolds number. In current work, the typical Pe_D number varies between 13 000 and 60 000, hence unless refining mesh to very small values — which, practically is not efficient in FSI calculations with large deformation using ALE — application of a numerical stabilization technique is unavoidable. Since, the streamline-diffusion technique used for stabilization relies on the relative speed of the domain, in current model the overall solute domain is segmented into two subdomains: the fluid domain Ω_F, with convection-diffusion, and biofilm domain Ω_B with only diffusion and reaction enabled. Without domains separation one should also move the solute inside the biofilm domain (artificial convective flow) once the tail moves, with a speed identical to the displacement of the biofilm domain. Therefore, a velocity term would have been introduced in the biofilm domain, which would lead to extra numerical diffusion inside biofilm domain Ω_B, where the physical diffusion itself is quite important. The general equation of solute mass balance including transport by diffusion and convection reads:

$$\frac{\partial c}{\partial t} + \nabla(c\,\mathbf{u}) = \nabla \cdot (D \nabla c) + R \tag{B.2}$$

Based on the assumption of incompressible liquid, we can replace the general term $\nabla \cdot (c\,\mathbf{u})$ in Equation (B.2) with $c \cdot \nabla \mathbf{u}$, since $c \nabla \cdot \mathbf{u} = 0$, which leads to the simplified non-conservative form in Equation (4.15). This modification will ensure that our model does not include non-physical terms from the solution of the flow field.

B.2. Coupling fluid-structure interaction with mass transfer

Once the FSI calculations are completed, the velocity fields, pressures and displacements will be available. In coupling of FSI with mass transfer, the relative velocity field is used as the velocity term in convection-diffusion equations. To start, two *Transport of Diluted Species* COMSOL interfaces are created. The *Transport of Diluted Species* interface assumes that all species present are dilute; that is, that their concentration is small in a solvent fluid (here water), so that

the ion activity effects can be neglected. Due to the dilution, mixture properties such as density and viscosity, can be assumed to correspond to those of the solvent. Further, the next step is to connect the two domains in COMSOL: convection-diffusion in the liquid and diffusion-reaction in the biofilm, that is to apply two Dirichlet and Neumann boundary condition on the same boundary. Therefore, concentration equality $\texttt{c1} = \texttt{c2}$ is applied on Γ_{CD} in the biofilm domain, where `c1` and `c2` are the COMSOL concentration variables of solute inside the fluid and biofilm domains. In Fluid domain $-\mathbf{n} \cdot D\nabla c = 0$ is applied on Γ_{CD}. The result of this arrangement ensures the flux continuity along the Γ_{CD} boundary.

B.3. Solvers and solution procedure

The solution procedure is very similar to Section A.5, with the difference that the resultant PDEs are not solved monolithically (fully coupled), but are solved sequentially. First the FSI solver is run for one time step, and the results are fed to the second solver for mass transfer, with one iteration between them. Inside the mass transfer solver, the tolerances determine the termination of the iterations. The maximum number of iterations for each sub-solver is set to 30, since initially the system is quite stiff numerically, but in middle stages usually the solver uses 2-3 iterations internally. The absolute and relative tolerances for concentrations are set to 1×10^{-7} mol/m^3 and 1×10^{-3} , respectively.

B.4. Post-processing

Similar to drag calculations in Section A.1, the average overall Sherwood number, $\overline{Sh}$, is calculated as follow:

$$\overline{Sh} = \frac{\int_s \frac{d_H \cdot \texttt{reacf}(c)}{D \cdot (c - c_0)} \mathrm{d}s}{\int \mathrm{d}s} \tag{B.3}$$

One important point regarding the `reacf()` operator is that it sums the terms on each node (it is actually a Σ operator, as COMSOL stores the reaction terms on nodes), unlike the classic numerical integral operator. Hence, the result of

the integral should be divided by the length to obtain the average.